THE IMPACT OF NATURAL ORGANIC MATTER (NOM) ON PHOTOCATALYTIC PROCESS FOR THE DEGRADATION OF MICROPOLLUTANTS

by

Reza Rezaei

B.Sc., Iran University of Science and Technology, Iran, 2003

M.Sc., Amirkabir University of Technology, Iran, 2007

A THESIS SUBMITTED IN PARTIAL FULFILLMENT OF

THE REQUIREMENTS FOR THE DEGREE OF

DOCTOR OF PHILOSOPHY

in

THE FACULTY OF GRADUATE AND POSTDOCTORAL STUDIES

(Chemical and Biological Engineering)

THE UNIVERSITY OF BRITISH COLUMBIA

(Vancouver)

March 2017

ABSTRACT

Photocatalytic oxidation process has been demonstrated as an effective technology for the removal of micropollutants in water. This process, however, is greatly affected by the presence of natural organic matter (NOM) in natural water, which interferes with treatment process by absorbing UV radiation and scavenging oxidant species. This research focused on investigating the effect of NOM on the photocatalytic oxidation of 2,4-dichlorophenoxy acetic acid (2,4-D), as target contaminant at different pH. Experiments were performed in fluidized photocatalytic reactor using template free photocatalyst spheres.

Changes in solution pH were used to decouple the effects of NOM on adsorption and major oxidative mechanisms, e.g., reactions on the surface of the photocatalytic spheres via positive hole mediation and in the solution via hydroxyl radicals ($^{\bullet}$OH) reaction. At pH 3, due to electrostatic attraction between solutes (2,4-D and NOM) and photocatalyst surface, photocatalytic oxidation mostly occurred via charge transfer on the surface of the photocatalyst. At pH 7, on the other hand, electrostatic repulsion between solutes and photocatalyst surface reduced adsorption and the process was primarily driven by hydroxyl radical reactions. The removal of 2,4-D reduced from 49% in the absence of NOM to 7% in the presence of 5 mgL^{-1} TOC NOM in neutral pH. At pH 3, this reduction was from 88% to 58%. It was observed that at neutral pH, due to higher aromatic moieties concentration and lower NOM adsorption, the effect of NOM on scavenging $^{\bullet}$OH was considerable. This effect substantially decreased at low pH due to high adsorption of NOM.

Higher 2,4-D removal at low pH was also due to the effect of pH on the kinetic of photocatalytic oxidation. Photocatalytic oxidation at pH 7 followed first order kinetic model. At pH 3, on the other hand, the rate of oxidation was a combination of first order and L-H models. Furthermore, the dependence of rate constants on UV intensity changed with pH; the rate constant

was directly proportional to UV intensity at pH 3; whereas it is proportional to the square root of intensity at pH 7.

PREFACE

This dissertation is submitted for the degree of Doctor of Philosophy at The University of British Columbia. The research described herein was conducted under the supervision of professor Madjid Mohseni in Chemical and Biological Engineering department of The University of British Columbia.

The following is the list of manuscripts that have been published in academic journals and in conference proceedings.

Journals:

- **Reza Rezaei**, Madjid Mohseni, 2017, Impact of natural organic matter on the degradation of 2,4 dichlorophenoxy acetic acid in a fluidized bed photocatalytic reactor, Chemical Engineering Journal, 310, part 2, 457-463.

  This manuscript is a version of chapter 7.

- **Reza Rezaei**, Madjid Mohseni, 2017, Impact of pH on the kinetic of photocatalytic oxidation of 2,4-dichlorophenoxy acetic acid in a fluidized bed photocatalytic reactor, Applied Catalysis B: Environmental, 205, 302-309.

  This manuscript is a version of chapter 6.

- In addition, two other manuscripts, other versions of chapters 4 and 5, are currently under preparation.

Conference podium presentation:

- **Reza Rezaei**, Gustavo E. Imoberdorf and Madjid Mohseni, Study of the co-adsorption of natural organic matter (NOM) and target micropollutants on photocatalytic TiO_2 spheres, 62nd CSCHE Conference, Vancouver, Canada, 2012

- **Reza Rezaei** and Madjid Mohseni, Study of the co-adsorption of Natural Organic Matter (NOM) and target micropollutants on photocatalytic TiO_2 spheres, 248th ACS National Meeting, San Francisco, USA, 2014
- **Reza Rezaei** and Madjid Mohseni, Effect of natural organic matter (NOM) on photocatalytic oxidation of a target micropollutant in fluidized bed photoreactor, 64nd CSCHE Conference, Niagara Falls, Canada, 2014
- **Reza Rezaei** and Madjid Mohseni, Photocatalytic oxidation of a target micropollutant in fluidized bed photoreactor; The effect of natural organic matter (NOM), National water and Wastewater Conference, Whistler, Canada, 2015
- **Reza Rezaei** and Madjid Mohseni, Photocatalytic oxidation of a target micropollutant in fluidized bed photoreactor; The effect of natural organic matter (NOM), IUVA World Congress and Exhibition, Vancouver, Canada, 2016

Conference poster presentation:

- **Reza Rezaei**, Gustavo E. Imoberdorf, and Madjid Mohseni, Fluidized Bed Photocatalytic Reactor Activated with VUV/UV, National water and Wastewater Conference, Kelowna, Canada, October 2012.

TABLE OF CONTENTS

LIST OF TABLES

LIST OF FIGURES

NOMENCLATURES

Arabic

$1/n$	Freundlich exponent
Ar	Archimedes number, dimensionless
a_c	Illuminated photocatalytic spheres area, m^2
a_s	Photocatalytic spheres surface area, m^2
C	Reactant concentration, mgL^{-1}
$C_{2,4\text{-}D0}$	2,4-D initial concentration, mgL^{-1}
$C_{2,4\text{-}D}$	2,4-D concentration, mgL^{-1}
C_e	2,4-D equilibrium concentration, mgL^{-1}
C_s	2,4-D concentration on the surface of photocatalyst, mgL^{-1}
$D_{2,4\text{-}D,W}$	Diffusivity of 2,4-D in water, 6.57×10^{-10} m^2/s (Duran et al., 2011)
DAX-8	Supelite resin using for hydrophobic NOM fractionation
d	TiO_2 sphere diameter, 0.0009 m
g	gravity force, m min^{-2}
I	UV intensity, einstein. m^{-2}. min^{-1}
k	Reaction rate constant, min^{-1}
k_F	Fickian diffusion constant
k_f	Freundlich isotherm constant
k_s	Sips isotherm constant
K	Equilibrium adsorption constant, m^3g^{-1}
K_l	Lagergren constant, min^{-1}

K_m	Mass transfer coefficient
n	integer exponent in power law rate expression
q_e	Solute equilibrium adsorption per unit weight of adsorbent, $mg.g^{-1}$
q_t	Solute adsorption per unit weight of adsorbent at time, $mg.g^{-1}$
q_m	Monolayer adsorption capacity introduced by Sips isotherm model, $mg.g^{-1}$
q_{max}	Maximum adsorption capacity introduced by Langmuir isotherm model, $mg.g^{-1}$
r_{sp}	Photocatalyst sphere radius, m
Re	Reynold number, dimensionless
S	Photocatalyst specific area, $m^2.gr^{-1}$
Sc	Schmidt number, dimensionless
Sh	Sherwood number, dimensionless
t	Time, min
XAD-4	Amberlite resin using for transphilic NOM fractionation

Greek

α	Proportionality constant
β	Kinetic parameter
θ_{O_2}	Oxygen equilibrium coverage
θ_R	Reactant equilibrium coverage
λ	Wavelength, nm
κ	Kinetic parameter, m^3g^{-1}
μ_w	Water viscosity, 0.86 Kg m^{-1} s^{-1} (Crittenden et al., 2012)

ξ	Exponential constant to calculate the reaction rate constant based on the UV flux
ρ_w	Density of water, 997 Kg m^{-3} (Crittenden et al., 2012)
ρ_{sp}	Density of sphere, 3571 Kg m^{-3}
ω	Damköhler number, dimensionless

Subscripts

Arabic numbers refer to the reactions number

aq indicates that the parameter or species is non-adsorbed

ads indicates that the parameter or species is adsorbed on the surface of photocatalyst

cal indicates calculated value

ex refers to electron hole pair generation

exp indicates experimental value

obs Refers to overall observed kinetic coefficient rate

rec Refers to electron hole pair recombination

r Refers to observed kinetic rate coefficient

LIST OF ABBREVIATIONS

2,4-D	2,4-dichlorophenoxy acetic acid
AMW	Apparent molecular weight
AOPs	Advanced Oxidation Processes
As (III)	Arsenic ion
As (IV)	Arsenic ion
BET	Brunauer–Emmett–Teller analysis
CB	Conduction band
CFD	Computational fluid dynamics
CSG	Composite sol-gel
Da	Dalton
DOC	Dissolved organic carbon
e^-	Exited electron generated by activated photocatalyst
E_0	Reduction potential
E_{CB}	Conduction band energy
E_g	Energy gap
FBPR	Fluidized bed photocatalytic reactor
Fe^{2+}/H_2O_2	Fenton advanced oxidation process
$Fe^{3+}H_2O_2/hv$	Photo-Fenton advanced oxidation process
FTIR	Fourier Transform Infrared
GAC	Granular Activated Carbon
h^+	Positive hole

HCHD•	Hydroxycyclohexadienyl radical
HCl	Hydrogen chloride
HO_2•	Perhydroxyl radical
HPLC	High-performance liquid chromatograph
HPSEC	High-performance size exclusion chromatograph
HPI	NOM hydrophilic fraction
HPO	NOM hydrophobic fraction
JCPDS	Joint Committee on Powder Diffraction Standards
L-H	Langmuir-Hinshelwood
MF	Microfiltration
M	Molar
NaOH	Sodium Hydroxide
NF	Nanofiltration
NH_4OH	Ammonia solution
NOM	Natural Organic Matter
•OH	Hydroxyl radicals
PCO	Photocatalytic oxidation
PSFG	Photocatalyst spheres first generation
pH	Decimal logarithm of the reciprocal of the hydrogen ion activity
pH_{zpc}	pH of photocatalyst zero point charge
pK_a	Acid dissociation constant
PSs	Photocatalyst spheres

PSS	Polysulfonate standard
RO	Reverse Osmosis
SEM	Scanning electron microscopy
SR	Suwannee River
SRNOM	Suwannee River NOM
SSE	Sum of error squared
SUVA	Specific UV-absorbance
$TiOH_2^+$	Hydrolyzed TiO_2 positively charged
TiO^-	Hydrolyzed TiO_2 negatively charged
TiO_2	Titanium dioxide
TiO_6	Titanium dioxide octahedron
TOC	Total Organic Carbon
TPI	NOM transphilic fraction
TTIP	Titanium tetraisopropoxide
UF	Ultrafiltration
UV	Ultraviolet
UV_{254}	UV absorbance at 254 nm
UV/H_2O_2	UV hydrogen peroxide advanced oxidation process
VB	Valence band
VUV	Vacuum Ultraviolet
XRD	X-ray diffraction

ACKNOWLEDGEMENTS

I would like to express my sincere gratitude to my supervisor, Dr. Madjid Mohseni, for his continuous guidance, support, encouragement, and valuable feed-back throughout this research work.

I also thank Dr. Kevin Smith and Dr. Gustavo Imoberdorf for serving on my PhD committee and for all their valuable comments.

I am truly thankful to Keyvan Maleki and Heidi Backous from RES'EAU-WaterNET for their inspiration and unconditional help during my PhD program.

My special thanks also go to all my fellow researchers, particularly to Ataollah Kheyrandish, Dr. Mehdi Bazri, Dr. Clara Duca, Dr. Muhammad Umar, Dr. Mehdi Bagheri, Adel Hajimalayeri, Adrian Serrano Mora, Sonia Rahmani, Pranav Chintalapati, Sean McBeath and Kai Song who offered countless hours of assistance and companionship during my time in UBC.

This research was privileged with superb dedication and excellent assistance of Kiara Allen, Farbod Rahimi-Nejad, and Chaoran Luo who significantly contributed to this work through experimental and analytical work.

Also, I would like to thank Dr. Tom Troczynski from Material Engineering department of UBC for sharing facilities of his lab and to all his graduate students for the help in conducting the photocatalyst preparation.

Dr. Anita Lam in Chemistry Department, Derrick Horne in Bioimaging Facility, and Haiyan Wang and Mehr Negar Mirvakili in Chemical and Biological Engineering Department of UBC are cordially thanked for the help in conducting the XRD, SEM, BET and catalyst surface charge analysis.

Finally, I would like to acknowledge the financial support received from the Natural Sciences and Engineering Research Council of Canada (NSERC) and RES'EAU-WaterNET NSERC Strategic Network.

To my beloved sister

Chapter 1: INTRODUCTION

Chemical contamination of natural water sources has become one of the major environmental concerns around the world. Industries and municipalities generate large amounts of wastewater containing numerous chemicals (Schwarzenbach et al., 2010). While much of wastewater is treated for many harmful chemicals, micropollutants such as pharmaceuticals, surfactants, pesticides, and herbicides at very low concentration can remain untreated and may pose harm to the environment and human health. These compounds are very persistent in natural water and may quite readily enter drinking water systems (Cunningham et al., 2009; Schwarzenbach et al., 2006). Human exposure may then occur either directly from water consumption or indirectly by consuming aquatic species such as fish which contain accumulated chemical residues (Cunningham et al., 2009). Major concerns of micropollutant exposure in humans are endocrine disrupting effects, chemo-sensitizing effects, possible interactions of contaminant mixtures, and chronic effects of long-term exposure (Musolff et al., 2010).

The removal of these contaminants has been shown to be very difficult due to their physico-chemical properties (low concentration in water and often poor biodegradability). Conventional treatment processes consisting of coagulation with rapid mixing followed by flocculation, sedimentation, granular media filtration, and chlorine disinfection has been demonstrated to be ineffective at removing micropollutants (McGivney and Kawamura, 2008). Studies indicate that coagulation and sedimentation achieve a minimal level of pesticides and pharmaceutical residue removal (Adams et al., 2002; Ternes et al., 2002; Zhang and Emary, 1999). Furthermore, some of these methods generate concentrated waste streams requiring further treatment and/or disposal.

Hence, conventional water treatment systems on their own, cannot remove all pollutants, especially micropollutants present at low concentrations in natural water.

Advanced treatment techniques such as ozonation, granular activated carbon (GAC) adsorption, and membrane filtration processes, occasionally used in conjunction with conventional treatment, have been considered as promising technologies for the removal of micropollutants. While effective at removing micropollutants, these processes bring additional problems of their own. For example, ozone will lead to the formation of bromate when bromide is present in water (O'Shea and Dionysiou, 2012). GAC, on the other hand, brings the problem of transferring contaminants from one phase to another, thereby requiring expensive regeneration and/ or disposal of spent carbon (Adams et al., 2002). High pressure membrane processes such as nanofiltration (NF) and reverse osmosis membranes (RO) that are incorporated in some drinking water treatment plants, are also expensive and generate waste streams that require further treatment.

Advanced oxidation processes (AOPs) are considered as an alternative for the removal of micropollutants. Through a high yield of hydroxyl radicals (•OH), AOPs have been shown to be effective technologies in mineralizing micropollutants leading to the formation of relatively harmless and inorganic molecules (Ameta et al., 2012; Parsons, 2004). Hydroxyl radical is the most powerful oxidizing species after fluorine and is short-lived (10^{-9} s), non-selective, and able to oxidize almost every organic molecule yielding CO_2, water and inorganic ions (Mills et al., 2006; Parsons, 2004; Xiang et al., 2011).

$$Organic\ compound \xrightarrow{hv,\ TiO_2} CO_2 + H_2O + mineral\ acids \qquad (1\text{-}1)$$

Different AOPs vary according to the type of chemical or catalyst used to generate hydroxyl radicals. Some processes use ozone, usually in combination with hydrogen peroxide (O_3/ H_2O_2) (Wojcicka et al., 2009). Fenton (Fe^{2+} / H_2O_2), photo-Fenton (Fe^{3+} H_2O_2 / hν) have also been studied

as AOPs. Other processes make use of ultraviolet (UV) irradiation as part of the process, such as UV/H_2O_2 and Vacuum UV (VUV) and some use photocatalysts such as titanium dioxide (TiO_2). Each of these processes have advantages and disadvantages, and as a result have their niche application areas.

The focus of this thesis is on photocatalysis as a treatment for the removal of micropollutants. Photocatalysis is a widely studied UV-based AOPs that has shown great potential for the effective removal of pollutants from water (de Lasa et al., 2005a; Guzsvány et al., 2012; O'Shea and Dionysiou, 2012). The following are some of the potential advantages of photocatalysis:

- It is chemical free process, which does not require continue addition of chemical oxidants (e.g., H_2O_2, ozone)
- Photocatalysis has high capability to mineralize organic pollutants,
- The most commonly used photocatalysts are cheap, non-toxic, stable, biologically, and chemically inert, and insoluble under most conditions and reusable
- In most cases, the catalyst needs a low energy UV source to be activated

Further to the above, photocatalysis is an effective process against a broad range of pollutants such as herbicides, pesticides, pharmaceuticals, surfactants, dye stuff etc., which are not biodegradable and also easily removed by conventional water treatment processes (Byrne and Fernández-Ibáñez, 2012). However, the performance of photocatalytic process is affected by water matrix and any constituents and hence, any effort to implement this technology in real condition should consider such impacts. The primary objective of this thesis is to address this challenge and evaluate of water matrix, in particular natural organic matter (NOM), on the efficiency of photocatalysis.

1.1 Photolcatalysis

Photocatalysis is an effective process against a broad range of pollutants that are not easily removed by conventional water treatment processes (Byrne and Fernández-Ibáñez, 2012). In this process, UV radiation activates a semiconductor photocatalyst to generate hydroxyl radicals (see Eq. (1-2) to Eq. (1-7)).

Photocatalytic process can be described as photo-driven catalytic process where a semiconductor is activated by light with energy equal or greater than the band gap energy (*Eg*). Unlike conductors with continuum electronic states, semiconductors possess a void energy region where electron is promoted from high energy level (conduction band) to no energy level (valence band) by photoactivation in the solid (Linsebigler et al., 1995). The energy of photons excites electrons from the valence band (VB) to the conduction band (CB) generating e^- -h^+ pairs. These electron-hole pairs migrate to the surface of the semiconductor where they initiate redox reactions with adsorbed molecules such as organic pollutants, water or oxygen (Vega, 2009).

$$Photocatalyst \xrightarrow{h\nu} Photocatalyst\ (e_{cb}^- + h_{vb}^+) \quad (1\text{-}2)$$

$$h^+ + H_2O \rightarrow {}^\bullet OH + H^+ \quad (1\text{-}3)$$

$$h^+ + RX \rightarrow RX^+ \quad (1\text{-}4)$$

$$e^- + O_2 \rightarrow O_2^- \quad (1\text{-}5)$$

$$O_2^- + H^+ \rightarrow HO_2^\bullet \quad (1\text{-}6)$$

$$O_2^- + H^+ + HO_2^\bullet \rightarrow H_2O_2 + O_2 \quad (1\text{-}7)$$

$$H_2O_2 \xrightarrow{h\nu} 2\ {}^\bullet OH \quad (1\text{-}8)$$

$${}^\bullet OH + RX \rightarrow Intermediate \rightarrow CO_2 + H_2O + inorganic\ ions \quad (1\text{-}9)$$

Excited electrons and holes can get trapped in metastable surface states, or react with adsorbed electron donors (e.g., water) and electron acceptors (e.g., oxygen) on the semiconductor surface. Suitable electron and hole scavengers prevent the recombination of electron-hole pairs, and leads the redox reactions to remove organic molecules. Organic molecules can be oxidized either directly via positive holes on the surface of photocatalyst or indirectly by hydroxyl radicals attack in the solution (see Figure 1-1).

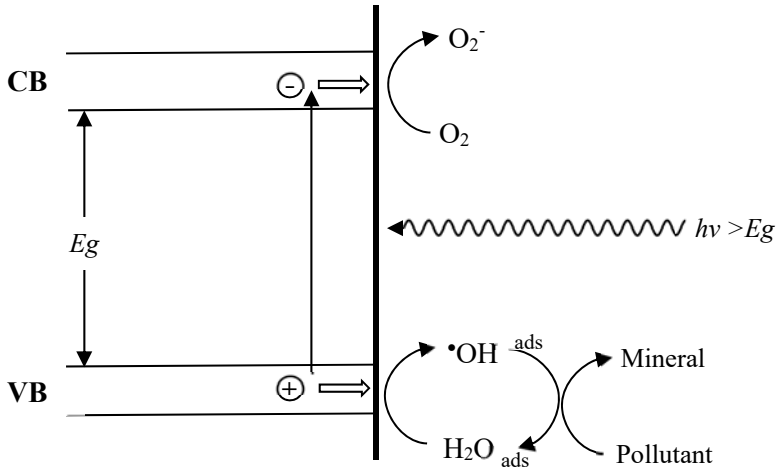

Figure 1-1. A semiconductor photo-electrochemical mechanisms

1.1.1 Titanium dioxide (TiO_2) as photocatalyst

TiO_2 is the most common and widely studied photocatalyst that has been employed for environmental applications and water purification. There is a general consensus that TiO_2 is superior because it is cheap, easy to produce, has high chemical stability, and its photogenerated holes are highly oxidizing (Dalrymple, 2011; Haarstrick et al., 1996; Vega et al., 2011). TiO_2 band gap Energy (E_g) is 3.0-3.2 eV, thereby it requires an excitation light wavelength range shorter than 400 nm ($E_g = hc/\lambda \cong 1240/\lambda$) (Boschloo et al., 2006; Park et al., 2013). Moreover, the band edge positions of TiO_2 ($E_{CB} = -0.51$ V at pH 7) are suitable for achieving the redox transformation of

environmental pollutants. It lies below the reduction potential of oxygen ($E_0(O_2/O^{\bullet}{}_2^-) = -0.33$ V) used as an electron scavenger in aqueous media. (Hernández-Ramírez and Medina-Ramírez, 2015; Park et al., 2013).

The efficiency of a photocatalyst depends on the competition between charge transfer reactions and the recombination of e^--h^+ pairs. In this context, TiO_2 surface properties as an intrinsic parameter along with extrinsic parameters such as pH of solution, initial pollutant concentration, light intensity, catalyst dosage, and flowrate affect the kinetic and mechanism of photocatalytic reaction in aqueous media (Hernández-Ramírez and Medina-Ramírez, 2015; Nosaka, 2010).

1.1.1.1 TiO_2 crystalline characteristics

Titanium dioxide exists in three crystallographic forms: rutile, anatase and brookite. Rutile and anatase structures are the two most common and widely used polymorphs of TiO_2; brookite transforms to rutile at quite low temperatures (Diebold, 2003). Since the anatase type is the most active form of TiO_2 it has been widely used for photocatalytic application (Wetchakun and Phanichphant, 2008). Anatase has a body centered tetragonal crystalline structure while rutile has a symmetrically tetragonal crystalline structure and is more stable (Kosmulski, 2002). The octahedron (TiO_6) is the fundamental structure of TiO_2 in crystal form. Ti^{4+} is surrounded by an octahedron of six O^{2-}. Each Ti atom is coordinated with the six neighboring oxygen via two longs (1.976 A^o in anatase and 1.979 A^o in rutile) and four shorts (1.946 A^o in anatase and 1.932 A^o in rutile) bonds. The anatase phase is 9% less dense than rutile, and has a tetragonal unit cell containing four TiO_2 units (Diebold, 2003). These different lattice structures cause different electronic band structures, the band gap of anatase is 3.2 eV while it is 3.0 eV for rutile (Hernández-Ramírez and Medina-Ramírez, 2015). Anatase, due to the position of oxygen and titanium ions on

the exposed crystal surface, is the most active phase but thermodynamically is less stable; it is formed at temperatures above 600ºC (Hernández-Ramírez and Medina-Ramírez, 2015; Thiruvenkatachari et al., 2008). Upon increasing the calcination temperature (from 600ºC to 700ºC) the anatase gradually transforms to the rutile phase (Vega et al., 2011).

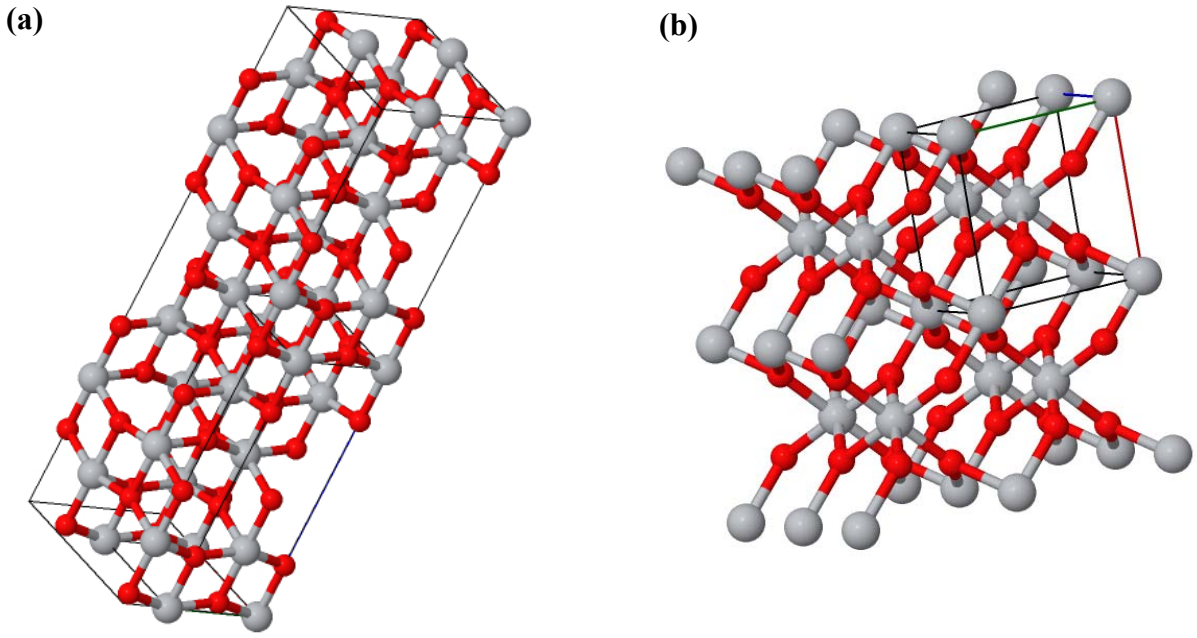

Figure 1-2. (a) Anatase Structure (b) Rutile structure (University of Liverpool)

While anatase is the most active phase in the photocatalytic process, the presence of the rutile phase causes a wider pore size distribution and high surface area which may be responsible for the increased catalytic activity (Bacsa and Kiwi, 1998; Thiruvenkatachari et al., 2008). Furthermore, increasing the calcination temperature improves the mechanical strength of the photocatalyst which is a crucial factor in reducing fines production (Vega et al., 2011). These might be the reasons why commercial TiO_2 (Degussa- P25) with the mixture of 80% anatase and 20% rutile is introduced as reference for getting better degradation efficiency compared to other crystalline ratios (Bacsa and Kiwi, 1998; Mir et al., 2013).

1.1.2 Photocatalytic reactors

The successful application of photocalytic processes hinges on the use of a proper reactor that provides efficient contact between photons, photocatalysts, and reactants. Given the involvement of radiation sources and the need for optimum configuration of light sources, photocatalytic reactor engineering is much more complicated than the common chemical reactor engineering (Parsons, 2004). To achieve a successful commercial implementation, several reactor design parameters such as geometry of the reactor, type of photocatalyst, and optimum utilization of radiation energy, must be considered (de Lasa et al., 2005b). Photocatalytic reactors can be classified in terms of the irradiation source such as artificial UV light or solar radiation, or based on the state of catalyst in the reactor. However, classification of photocatalytic reactors based on the state of catalyst, that is, suspended or immobilized, is more common.

Photocatalytic slurry reactors, with the photocatalyst suspended in liquid phase, are the most widely studied photoreactors (Mazierski et al., 2016). The use of suspended photocatalyst provides high total surface area which brings improved photocatalytic activity (de Lasa et al., 2005b; Mazierski et al., 2016). However, the use of suspensions requires separation of the ultrafine photocatalyst from the treated liquid and recycling of the photocatalyst back into the reactor. This can be an inconvenient, time-consuming and expensive process. In addition, the penetration of UV light is limited in slurry reactors due to strong light absorptions by catalyst particles.

These problems can be avoided by having the photocatalyst immobilized in layers to a photoreactor. The use of immobilized photocatalyst eliminates the need of photocatalyst recovery and improves the UV radiation penetration. In stationary photocatalytic reactor, however, the overall degradation rate is affected by mass transfer limitation and low surface area (Mazierski et al., 2016; Parsons, 2004; Serrano and de Lasa, 1997).

1.1.2.1 Fluidized bed photocatalytic reactor (FBPR)

Fluidized bed photocatalytic reactor (FBPR) is an alternative to slurry and stationary photocatalytic reactors. It presents many advantages, such as efficient contact between reactants and catalysts, efficient UV distribution and low mass transfer resistance (Haarstrick et al., 1996; Kabir, 2006; Vega et al., 2011). However, attrition of photocatalysts, which are usually immobilized on support materials, is a serious concern in utilizing FBPRs. Because of inter-particle collisions and bed-to-wall impacts, catalysts as small particles may detach from the support. Attrition causes a significant loss of the catalyst mass, with the subsequent activity decay, and the need for downstream separation of the fine particles.

Braham and Harris (2009) reviewed different photocatalytic reactors and showed that attrition of supported photocatalyst is the main concern in the photocatalytic processes. Pozzo et al. (2005) evaluated photocatalyst TiO_2-P25 in two different forms of operations, finely powder in a slurry photocatalytic reactor and immobilized on quartz sand in FBPR. The results showed attrition to be the main issue in FBPRs, reducing the efficiency of the process. Also, Qiu and Zheng (2007) showed poor adherence of TiO_2 on hydroxylated glass beads, prepared via thermal and sol-gel coating method, leading to significant attrition in FBPR. To address the issues of attrition, Chen and Dionysiou (2006) introduced a modified technique, involving the loading of TiO_2-P25 in sol derived TiO_2, to coat the photocatalyst on stainless steel support. The authors reported an improved mechanical integrity for the coated photocatalyst.

Vega (2009) introduced an alternative approach to overcome the reduced photocatalytic activity due to attrition in a fluidized bed photoreactor. He developed a template-free composite photocatalyst, with high attrition resistance. The core of this photocatalyst with a diameter between

0.9-1.1 mm is TiO_2. Studies with this photocatalyst showed superior mechanical integrity and high efficiency in removing model contaminants in water (Vega, 2009).

1.1.3 Photocatalytic oxidation kinetic overview

Analysis of liquid-phase kinetics in photocatalytic systems relied on Langmuir-Hinshelwood (L-H) model for years. This classic kinetic model assumes that a relatively rapid reaction achieving adsorption equilibrium, is followed by a slow surface reaction step (Ollis, 2013).

$$R(liquid) \overset{K_{ads}}{\longleftrightarrow} R(ads) \tag{1-10}$$

$$R(ads) \overset{k}{\rightarrow} Product \tag{1-11}$$

$$K_{ads} = \frac{k_1}{k_{-1}} \tag{1-12}$$

$$\theta = reactant\ equlibrium\ coverage = \frac{K_{ads}C}{1 + K_{ads}C} \tag{1-13}$$

$$-r_A = k\theta_R = k\frac{K_{ads}C}{1 + K_{ads}C} \tag{1-14}$$

where C is solute concentration, k is L-H reaction rate constant, and K_{ads} is Langmuir equilibrium adsorption constant. Some key experiments have revealed that this mechanism is not consistent with the observed results(Emeline et al., 2005; Ollis, 2005). The dark adsorption equilibrium constant (K_{ads}) was found to differ from the apparent adsorption constant (K_{ads}^{app}) achieved through experimental results. According to the experimental results that assessed the influence of concentration and intensity on the photocatalytic reaction, the rate constant k and the apparent adsorption (K_{ads}^{app}) depend on the intensity of UV radiation(Emeline et al., 2000). Accordingly, Ollis (2005) proposed a revised simple model that has the same mathematical form as the L-H model. However, instead of equilibrium adsorption of reactants and, correspondingly a slow rate controlling surface step, the revised model assumes a pseudo steady state hypothesis to the surface coverage ($\frac{d\theta}{dt} = 0$). Under this assumption:

$$-r_A = k\frac{K_{ads}^{app}C}{K_{ads}^{app}C + 1} \quad (1\text{-}15)$$

where

$$K_{ads}^{app} = \frac{k_1}{k_{-1} + k} \quad (1\text{-}16)$$

One important contribution is that *k* is related to intensity based on the following expression (Emeline et al., 2000; Mills et al., 2006; Turchi and Ollis, 1990).

$$k = \alpha I^{\xi} \quad (1\text{-}17)$$

where ξ is a power term and usually varies from 0.5 at high photon flux to unity at low photon flux. While it could address the role of intensity in the kinetic of photocatalytic oxidation, this model did not consider photocatalytic oxidation via •OH attack in the solution. Studies (Fu et al., 2006; Hoffmann et al., 1995) have demonstrated the contribution of •OH in oxidizing contaminants far from the surface of photocatalyst.

A number of studies (Fox and Dulay, 1993; Gaya, 2014a; Herrmann, 2010; Pelaez et al., 2011; Rengifo-Herrera et al., 2013) have demonstrated that water matrices and natural water condition could also influence the photocatalytic performance. These characteristics of water matrix such as dissolved oxygen, pH, natural organic matter (NOM) concentration, and alkalinity are critical on photocatalysis efficiency. For example, oxygen, adsorbed on the surface of photocatalyst, plays the important role in improving the performance of the process by scavenging electrons from the surface of photocatalyst and subsequently reducing e^-- h^+ recombination rate. The dependence of photocatalytic degradation rate on dissolved oxygen concentration can be interpreted by Langmuir adsorption (Turchi and Ollis, 1990),

$$r \propto \frac{K_{O_2}[O_2]}{1 + K_{O_2}[O_2]} \quad (1\text{-}18)$$

where K_{O_2} is oxygen adsorption rate constant. However, in implementation condition the oxygen coverage at the surface of photocatalyst is constant and can be integrated into the apparent rate constant (Herrmann, 1999). In other words, the apparent rate constant is a function of the intensity and of the oxygen coverage.

$$R + O_2 \rightarrow Product \quad (1\text{-}19)$$

$$r = \frac{-d[R]}{dt} = k\theta_R\theta_{O_2} = k_{app}\theta_R \quad (1\text{-}20)$$

1.1.3.1 Effect of pH on photocatalytic process

pH is another important factor, affecting the efficiency of photocatalytic process. Nonetheless, there is no general consensus over the effect of pH. Some studies showed that the rate of photocatalysis was not dependent upon pH (Duran, 2010; Mills et al., 1993), whereas de Lasa et al. (2005a) and Sakthivel et al. (2003) showed that increasing the pH of medium consistently reduced the rate of photocatalytic process. Pelaez et al. (2011) showed a indirect relationship between the performance of photocatalytic process and the pH of medium. The authors illustrated that the reaction rate decreased from 3.5×10^{-3} $\mu M.min^{-1}$ in acidic condition (pH 3) to 0.54×10^{-3} $\mu M.min^{-1}$ in neutral condition (pH 7.1). Šojić et al. (2009), on the other hand, demonstrated that the effect of pH was dependent on its range. At very low range (pH= 1-3.2) an increase of pH caused a significant increase in degradation rate, a further increase of pH showed a distinct decay in degradation rate. pH effect on photocatalytic process depends on the influence of number of factors such as electrostatic interactions among the semiconductor surface, water, and charged compounds formed during the reaction process.

The impact of pH can be explained based on its role in changing the semiconductor surface charge (Byrne and Fernández-Ibáñez, 2012; Rezaei and Mohseni, 2017a; Sakthivel et al., 2003) and the

energy levels of conductance and valence band (Byrne and Fernández-Ibáñez, 2012; Rothenberger et al., 1985). TiO_2 like any other semiconductor behaves as a simple diprotic acid in water. In an aqueous medium, Ti cations can bond to oxygen atoms of water molecules that are adsorbed on the surface of the catalyst and dissociated to OH groups (Sakthivel et al., 2003). When a water molecule approaches to the surface of TiO_2 , both the H_2O and bridging oxygen disappear and are replaced by OH pairs (Figure 1-3) (Linsebigler et al., 1995).

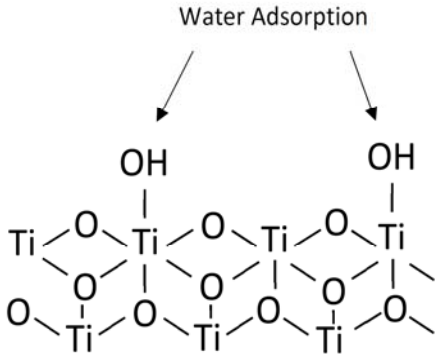

Figure 1-3. Hydrated TiO_2 surface.

Hydrolyzed TiO_2 surface according to medium pH becomes positively or negatively charged (See Eqs (1-21) and (1-22)). The effect of pH on photocatalyst surface charge can be explained basis on the zero point charge pH (pH_{zpc}). pH_{zpc}, a particular pH where the charge of the photocatalyst surface is zero, is the average of pK_a, $\frac{pK_{a1}+pK_{a2}}{2}$ (Eqs (1-21) and (1-22)). In the case of TiO_2 P25 the pH_{zpc} is 6.2 (pK_{a1} =4.5 and pK_{a2} =8) (Park et al., 2013). Nonetheless, different pH_{zpc} of different types of TiO_2, between 5.5 and 6.8, has been reported (Boschloo et al., 2006; Byrne and Fernández-Ibáñez, 2012; Doll and Frimmel, 2005a; Sakthivel et al., 2003; Šojić et al., 2009).

$$TiOH_2^+ \rightleftarrows Ti-OH+H^+ \quad pK_{a1} \tag{1-21}$$

$$Ti - OH \rightleftarrows Ti - O^- + H^+ \quad pK_{a2} \tag{1-22}$$

TiO_2 surface is positively charged ($TiOH_2^+$) in acidic media (pH< pH_{zpc}), whereas it is negatively charged (TiO^-) at pH> pH_{zpc}; This will in turn, influences the micropollutant adsorption and its degradation pathways (Šojić et al., 2009; Tunesi and Anderson, 1991).

Tunesi et al. (1991) attempted to make a connection between pH effect on TiO_2 adsorption capability and photocatalytic mechanism. He showed that due to an increase in the electrostatic repulsion between the micropollutant anion and the oxide surface, the adsorption reduced at high pH. The increased distance between the reactant and the surface of photocatalyst causes reducing direct charge transfer.

It should be emphasized that the effect of pH cannot be limited to its influence on surface charge of photocatalyst. Changing pH also causes a shift in the position of the valence and the conduction bands (Shaham-Waldmann and Paz, 2013). These changes in the position of the band edges may affect the rate of interfacial charge transfer (Duffy et al., 2000). Howe and Gratzel (1985) showed that pH affects the rate of the trapping charge process. In the acidic medium the rate of recombination is very low causing a high rate of oxidation via positive holes on TiO_2 at low pH.

According to Henderson-Hasselbalch (Clugston and Flemming, 2000), pH also influences the protonation state of micropollutants. At pH, higher than its pK_a, the contaminant dissociates into unprotonated species that affects the adsorption and consequently the oxidation performance.

1.1.3.2 Effect of Natural Organic Matter (NOM)

NOM containing organic materials such as largely alphatic, highly coloured, aromatic, hydrophobic, hydrophilic, charged, and uncharged components, is produced from the decomposition of living materials and synthetic activities of microorganisms (Liu et al., 2013;

Matilainen and Sillanpää, 2010). NOM affects the quality of water by causing colour, taste and odour. Moreover, the presence of NOM in raw surface water brings several challenges to drinking water treatment processes. For example, NOM affects the efficiency of GAC adsorption process by competing with target pollutants (Ding, 2010). NOM also has a strong impact on the rate of fouling in microfiltration (MF)/ultrafiltration (UF) water treatment processes (Cho et al., 1998). Although, NOM can reduce the efficiency of UV disinfection by attenuating light as it passes through the water.

NOM can have a pronounced influence on the performance of photocatalytic degradation. NOM may affect the adsorption process by competing with micropollutant for available binding sites or/and altering the surface charge of photocatalysts through adsorption (Liu et al., 2008). Lin and Lin (2007) and Doll and Frimmel (2005b) studied the effect of NOM on photocatalytic removal of organic compounds, such as iomeprol, clofibric acid, carbamazepine, 4-chlorophenol, and 1,2,3-trichlorobenzene. The authors reported that NOM interferes with the adsorption process by competing with organic compounds for active sites on TiO_2. However, they did not elaborate on the extent of competition between NOM and target contaminants as well as the parameters that affect this competition. For example, there was no mention of the effect of pH and its role in the adsorption process. As discussed earlier, the effect of pH can be interpreted in terms of electrostatic interaction between the charged TiO_2 and solutes. The solution pH also affects the degree of dissociation of solutes (which depends on solutes pKa), and consequently the adsorption of their ionized form. Among the few studies investigating the effect of pH, Liu et al. (2008) analyzed the impact of NOM on photocatalytic degradation of arsenic at different pH. The study demonstrated that the presence of NOM, due to competition with As (III) for available binding site, caused a reduction of approximately 40% in adsorption of arsenic (As (III)) at low pH (Liu et al., 2008).

However, the effect of NOM on adsorption cannot be limited to its influence on competition for available binding site. The chemical structure of NOM also plays the major role in performance of contaminants adsorption. For example, adsorbed NOM due to negative charge of phenolic and carboxylic functional groups interferes with TiO_2 surface charge; it reverses the photocatalyst surface charge and consequently reduces the adsorption of contaminants ionic form at low pH (Yang and Lee, 2006). NOM, due to its chemical structure, can also enhance the adsorption of target micropollutants. Drosos et al. (2015) demonstrated that the adsorbed NOM attracts carbamazepine (CBZ) adsorption ontoTiO_2. In this study, π bound attraction between CBZ and aromatic functional group of adsorbed NOM facilitated CBZ adsorption.

Much the same as its impact on UV disinfection process, NOM also plays as inner filter and decreases the efficiency of photocatalytic oxidation, by blocking the UV radiation reaches the photocatalyst surface. Aromatic and olefinic moieties in the NOM structure absorb UV at 254 nm and partially filter the radiation (Matilainen and Sillanpää, 2010). This in turn causes a reduction of photocatalysis efficiency, because the catalyst receives less photons, and fewer oxidant species are generated.

Finally, NOM interferes with the process by scavenging the oxidant species generated in the system. Adsorbed NOM on the surface of photocatalyst acts as a scavenger of positive holes (h^+). NOM is electron-rich and capable of scavenging positive holes from the surface of photocatalyst to reduce the rate of oxidation (Doll and Frimmel, 2005b; Lin and Lin, 2007; Yang and Lee, 2006). Non-adsorbed NOM in the solution, on the other hand, scavenges free hydroxyl radicals in the solution (Doll and Frimmel, 2005b; Rezaei and Mohseni, 2017b). While studies showed negative effects of NOM on photocatalytic oxidation, assessing the effect of NOM on scavenging different oxidant species is still lacking.

According to the above discussion, the exact role of NOM on photocatalytic process is not-well known and very challenging. However, to better understand the efficiency of photocatalytic processes in the presence of NOM, further studies are required to elucidate this complex behavior of NOM in photocatalysis.

1.2 Knowledge gaps

Application of FBPR involving photocatalytic spheres to real world water treatment needs a detailed understanding of the effect of the water matrix, in particular NOM. This is challenging, because of the complexity of the process as well as the complex nature of NOM molecules. To the best of the author's knowledge, there has been no prior comprehensive research evaluating the impact of NOM and its fractions on the photocatalytic oxidation process. In particular, little work has been done to develop an understanding on the effect of NOM on adsorption and oxidation pathways (direct oxidation on the surface of photocatalyst vs. indirect reaction via hydroxyl radicals attack). The specific knowledge gaps around the influence of NOM on photocatalytic process are highlighted below:

1.2.1 NOM impact on micropollutant adsorption

It is well established that adsorption of reactants on the surface of the TiO_2 photocatalyst improves the efficiency of electron transfer during the photocatalytic process (Friedmann et al., 2010). It is hypothesized that NOM interferes with the adsorption process. However, there is no general consensus around the impact of NOM on adsorption process. To et al. (2008) reported that NOM has an adverse effect on micropollutant adsorption efficiency because NOM's large molecular weight blocks adsorbent pores and slows down the diffusion of smaller compounds into the pores. Liu et al. (2008), on the other hand, showed that NOM competes with the target

micropollutant for adsorption sites. The authors asserted that arsenic adsorption reduces because NOM competes with arsenic ion for adsorption on TiO_2 available binding sites. The aforementioned studies, however, are not in agreement with other reports which state that NOM does not have any effect on the adsorption of micropollutants (Faur et al., 2005; Li et al., 2003). For instance, Li et al. (2003) propose that large molecular NOM adsorbs onto the pores larger than those where small molecules of micropollutants are preferentially adsorbed.

Adsorption is a complicated process with several determining parameters such as adsorbent surface properties, adsorbate molecular structure, temperature, inorganic ion strength, and pH of the solution (Newcombe, 1994; Snoeyink and Summers, 1990). The presence of NOM due to its complexity and heterogeneity in aquatic media, makes this process intricate. Investigating adsorption of different NOM fractions and functional groups is necessary to better delineate the effect of NOM adsorption. Therefore, a comprehensive study is required to understand thoroughly the adsorption of NOM on photocatalyst surface and its effect on the overall photocatalytic process.

1.2.2 Impact of NOM on photocatalytic oxidation

While several attempts have been performed to demonstrate the effect of NOM on photocatalytic oxidation, researchers could not separate the impact of NOM on different photocatalytic oxidation mechanisms; direct oxidation on the surface of photocatalyst via positive hole or indirect oxidation via hydroxyl radicals attack in the solution ($^{\bullet}OH_{aq}$). Lin and Lin (2007) and Doll & Frimmel (2005) studied the effect of humic substances and NOM on reducing the efficiency of the photocatalytic process. While the impact of NOM on the overall photocatalytic process was evaluated, these studies did not separate NOM interferes with photocatalytic oxidation

mechanisms. Selli et al. (1999) attempted to examine the influence of NOM through a complicated approach of analyzing all the reaction pathways affected by NOM. The results showed that this effect is dependent upon the source of NOM and chemical structure of micropollutants. Drosos et al. (2015) studied the effect of adsorbed humic acid, as a model NOM, on photocatalytic oxidation of micropollutant CBZ. Nonetheless, a comprehensive analysis of adsorbed humic acid on the surface oxidation was performed, this study could not analyze the effect of humic acid on scavenging hydroxyl radicals in the solution.

Attributable to the complexity of the photocatalytic oxidation process, separating the influences of NOM is a major challenge. Hence, based on the existing literature on prior research, a comprehensive study is needed to assess NOM interferences on photocatalytic oxidations.

1.3 Thesis scope and objectives

The overall goal of this research is to assess the impact of NOM on the photocatalytic degradation of micropollutant in FBPR. In particular, this research aims to contribute substantially to the understanding of the NOM effect on adsorption and photocatalytic oxidation of 2,4-D during the process of photocatalysis. 2,4-D is an inexpensive and common herbicide used for the control of broadleaf weeds in agriculture, forestry and lawn care practices. Because of its poor biodegradability, 2,4-D remains active for very long and can easily spread within the environment (Trillas et al., 1995). 2,4-D was selected as a target micropollutant in this research due to its propensity for being adsorbed on the surface of catalysts at different pH. The adsorption of 2,4-D on the surface of photocatalyst can be controlled and consequently the impacts of NOM on each photocatalytic oxidation pathways can be quantified.

To achieve the aforementioned overall goals, the following specific tasks are pursued:

1. Study the impacts of NOM and its various fractions on the adsorption of 2,4-D on the photocatalytic spheres used in FBPR,
2. Investigate the kinetics of different mechanisms involved in the photocatalytic oxidation of 2,4-D using the effect of pH,
3. Examine the effect of NOM on photocatalytic oxidation of 2,4-D on the surface of photocatalyst and in the solution, separately by,
    i. evaluating the effect of NOM on different photocatalytic oxidation mechanisms,
    ii. developing a method to separate the effect of NOM on scavenging different oxidant species involved in photocatalytic oxidation at low pH,
    iii. measuring NOM removal during different photocatalytic oxidation mechanism.

1.4 Thesis layout

This dissertation compiles the results achieved throughout the course of research, and discusses them in the form of five chapters following introduction and experimental methods chapters. Not all the research results are included main body of the thesis, so complementary data are presented in the appendices. The following is a description of how each of the above objectives has been met with respect to their presentation in the following chapters;

Chapter 2 provides a detailed description of the experimental plan and research methodology, as well as analytical techniques employed in this study.

Chapter 3 provides comprehensive information about the characteristics of the photocatalyst used in this research.

Chapter 4 contributes primarily to present the results related to objective 1, that is adsorption of 2,4-D and the impact of NOM on the adsorption process.

Chapter 5 provides an in depth look into the adsorption of NOM, contributing objective 1. It discusses the adsorption of NOM and its fractions in terms of hydrophobicity and molecular weight. The effect of different NOM functional groups and their contribution to the adsorption, is also studied in this Chapter.

Chapter 6 contributes primarily to meeting objective 2. It provides a detailed discussion around the kinetics of photocatalytic oxidation and the impact of pH on the photocatalytic oxidation mechanisms and kinetics.

Chapter 7 contributes to meeting objective 3. It presents a method to separate the photocatalytic oxidation mechanisms to evaluate the impact of NOM on each oxidation process. It also demonstrates the impact of NOM on the photocatalytic oxidation of 2,4-D.

Chapter 8 presents an overall conclusion, a summary of key findings, and recommendation for future research.

Chapter 2: EXPERIMENTAL METHODOLOGY

2.1 Water sample preparation

The synthetic water was prepared by diluting a NOM stock solution in milli-Q water to make different dissolved organic carbon (DOC) concentrations. The NOM stock solution was made by dissolving Suwannee River (SR) NOM, purchased from the International Humic Substances Society, in milli-Q water to make 100 mgL^{-1} DOC following filtration by 0.45µm. The stock solution was stored in dark at 4°C. The pH of the synthetic water samples was adjusted using HCl and NaOH (0.1 N).

2.1.1 NOM fractionation

The experimental method and apparatus used for NOM fractionation were based on the fractionation technique proposed by Chow et al. (2004). Two resins, Supelite DAX-8 (Supelco) and Amberlite XAD-4 (Supelco) were used in series to fractionate the NOM. Water was filtered (0.45 µm) and acidified to pH 2 using HCl. The solution was pumped through DAX-8 column. Samples were taken for DOC, UV absorbance at 254 nm and, HPSEC analysis. The hydrophobic (HPO) fraction was defined as the fraction of NOM that was adsorbed on DAX-8. The rest of the sample was pumped through the XAD-4 column, and similar samples were taken for the same analytical measurements termed Transphilic fraction (TPI). The fraction of NOM that was not adsorbed on either DAX-8 or XAD-4 is termed as hydrophilic (HPI). NaOH (0.1 N) and HCl will be used to adjust the pH.

$$\%\text{HPO} = \frac{TOC_{initial} - TOC_{after\ DAX-8}}{TOC_{initial}} \times 100$$

$$\%TPI = \frac{TOC_{after\ DAX-8} - TOC_{after\ XAD-4}}{TOC_{initial}} \times 100$$

$$\%HPI = \frac{TOC_{after\ XAD-4}}{TOC_{initial}} \times 100$$

In general, this method has an error (TOC instrument and fractionation procedure errors) around 0.25 mgL^{-1} when measuring the DOC concentration after and before exposure to resins. Therefore, the fractionation of NOM was performed for NOM concentration higher than 3 mgL^{-1} to eliminate or minimize the potential error.

2.1.2 NOM analytical measurement

The concentration of NOM was measured using total organic carbon (TOC) analyzer (Shimadzu TOC- VCPH). The UV absorbance at 254 nm (UV_{254}) was employed to measure NOM aromatic moieties using a UV–vis spectrophotometer (Agilent Technologies UV-Vis Cary 100) with a cell path length of 1 cm.

The apparent molecular weight (AMW) distribution of NOM in untreated and treated waters were measured using high-performances size exclusive chromatograph (HPSEC). Following the method described by Sarathy & Mohseni (2007), HPLC Waters 2695 separation module equipped with a Waters Protein-Pak$_{TM}$125 Å column and a 2998 photodiode array detector, set to detection at 260 nm, was used as the instrument for HPSEC analysis. The carrier solution was phosphate buffer (0.02 M), pH 6.8, (Laboratory grade, Fisher Scientific) adjusted to 0.1 M ionic strength using sodium chloride (certified A.C.S, Fisher Scientific). The flow rate of the carrier solution was set at 0.7 $mL.min^{-1}$. AMW was correlated to retention time using polysulfonate standards (15 kDa PSS15K, 7 kDa PSS7K, 4 kDa PSS4K, 3 kDa PSS3K, American Polymer Standards Corporation) for making a the calibration curve.

Fourier Transform Infrared (FTIR) analysis was performed to identify the inorganic and organic functional groups using Perkin Elmer Frontier FTIR Spectrometer. The sample was pressed under a pressure of about 12 MPa to produce a thin film. FTIR spectra of the sample was recorded from 1000 to 4000 cm^{-1} with a 4 cm^{-1} resolution operated at scan speed of 50 scans. The spectra of adsorbed species on the surfaces of titanium dioxide were obtained following the protocol by Gong (2001).

2.2 2,4-D sample preparation

2,4-D solution was prepared by diluting 2,4-D stock solution in synthetic or milli-Q water to make different 2,4-D concentrations (1 mgL^{-1}, 4 mgL^{-1} and, 7 mgL^{-1}). The 2,4-D stock solution was made by dissolving 2,4-D solids purchased from Sigma–Aldrich, Canada, in milli-Q water to make 180 mgL^{-1} 2,4-D. The solution was filtrated by 0.22 μm before being used. The stock solution was stored in the dark at 4ºC.

2.2.1 2,4-D measurement

Concentration of 2,4-D was quantified using a high-performance liquid chromatograph (HPLC, Dionex 2695) equipped with C-18 column (4-micronmeter particle diameter) and a UV detector. Methanol/water/acetic acid (58%:40%:2%v/v) were used as mobile phase. The injected sample volume was 100 μL. The flow rate of the mobile phase was 1 mL min^{-1} using λ=280 nm UV detection.

2.3 Photocatalyst

2.3.1 Photocatalyst preparation

The template free photocatalytic spheres (PSs) are made of sol-gel derived composite TiO_2 as described in (Vega et al., 2011). Titanium tetraisopropoxide (TTIP) is used as the precursor and slowly added to a solution of denatured ethyl alcohol (81% v/v), water (5% v/v) and HCl (14%v/v). Ethyl alcohol is used as a solvent for the sol-gel reaction and HCl is used to control the rate of condensation, eliminating the fast gelation and precipitate formation due to uncontrolled hydrolysis reactions. The mixture is magnetically stirred for 2 hrs, resulting in a clear and stable alkoxide-based solution. Pre-calcined TiO_2 powder, Degussa P-25, is used as a filler material. The powder is added to the sol-gel solution (0.3 g P-25 per mL TTIP) and the resulting composite sol-gel (CSG) is vigorously stirred overnight (16 hrs) to form a homogenous mixture.

One part of CSG is mixed with two parts of a polymeric solution made of chitosan (10 gL^{-1}) and milli-Q water at pH 4.5 (used glacial acetic acid to acidify milli-Q water) to create a suspension with desirable viscosity (135 cp) needed for sphere formation. The solution is added drop-wise to a basic solution, (pH 12) NH_4OH/water (20:80% v/v), to produce the spheres. On contact with the basic solution, the droplets are instantly hardened into spherical particles due to the fast gelation of the chitosan polymer. The spheres are then dried at 85^o C for 45 hours before calcination. The calcination process is carried out at 600^o C for 3 hours. The ramping temperature is regulated at approximately 3.5^o C min^{-1} during the calcination process.

2.3.2 Attrition resistance determination

Titanium dioxide fine particles generated due to attrition in the fluidized bed photocatalytic reactor were quantified through a spectrophotometric method initially proposed by (Sandell and

Ōnishi, 1978) and later updated by Jackson et al. (1991). In this technique, 10 mL of a sample containing TiO_2 particles is added to a solution of 0.85 mL $(NH_4)SO_4/H_2SO_4$ (40% w/v) and boiled until the TiO_2 is fully dissolved. 6 mL H_2O is added to the cooled solution followed by diluting with concentrated H_2SO_4 (95%) reached to 25 mL. 10 mL of this solution is then transferred to a beaker into which 2-3 drops of H_2O_2 (30%) is added. The amount of Ti^{+4} present in the solution is then determined using spectrophotometer at λ=410 nm.

Figure 2-1. Template free photocatalyst spheres.

2.3.3 Photocatalyst characterization

Microstructural characteristics of the photocatalyst were analyzed using Hitachi S2600 Variable Pressure-SEM. An X-ray diffraction (XRD) diffractometer (Bruker D8-Advance X-ray, 40 kV,40 mA) was used to determine the crystallinity of produced photocatalyst. X-ray diffraction patterns were recorded using $CoK\alpha_1$ (λ_1= 1.5406A˚) and $CoK\alpha_2$ (λ_2= 1.54439A˚) over the range 2θ from 5º to 90º, with a scanning speed of 0.016º min^{-1}. Diffraction patterns of both anatase and rutile TiO_2 powders were compared with reference to Joint Committee on Powder Diffraction Standards (JCPDS) database. The Rietveld refinement method was used to determine the amount of anatase and rutile phases.

Specific surface areas of PSs were measured by nitrogen adsorption at 77K, and based on the multipoint Brunauer-Emmet-Teller (BET) method using Micromeritics ASAP 2020. The pore size distributions (average pore diameter and mean pore volume) were measured from the N_2 desorption isotherm using the method proposed by Barrett, Joyner and Halenda (BJH).

Zeta potential charges of PSs were determined using a Malvern Zetasizer 2000. The spheres were first ground to form a colloidal suspension (0.002 wt% in water) before analysis.

2.4 Photocatalytic process

2.4.1 Experimental setup

Photocatalytic experiments were conducted in a fluidized bed photoreactor (FBPR) consisting of a quartz tube (150 mm height and 26 mm internal diameter) as the body of the reactor, held by two polycarbonate pieces at the top and the bottom. The flow passed through the photocatalytic spheres bed in the quartz tube to fluidize them. The conical shape of the bottom piece helped to fluidize the spheres and expand them thoroughly in the reactor. Photocatalytic spheres inside the quartz tube (the photoreactor) were irradiated by three UV lamps placed surrounding the reactor. The reactor and UV lamps were placed in a wooden box to avoid any direct contact with UV radiation.

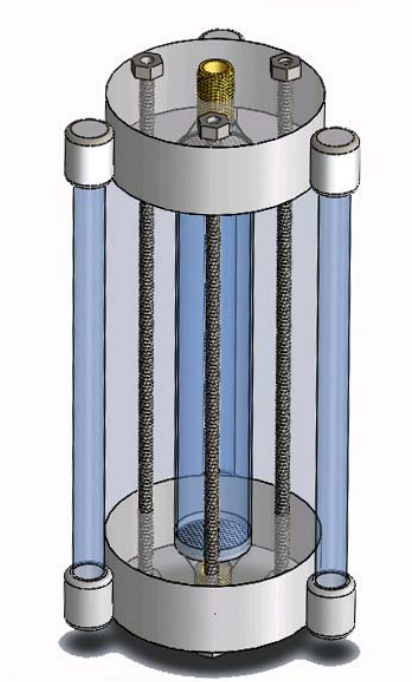

Figure 2-2. Fluidized bed photocatalytic reactor.

2.4.2 Experimental procedure

The reactor was filled with 25 g PSs and the system was operated at a flowrate of 3.6-3.9 $L.min^{-1}$, corresponding to a bed expansion of about 400%. The storage tank was equipped with a diffuser to sparge air through the solution in order to provide a constant concentration of dissolved oxygen, which is required as an electron acceptor for photocatalytic oxidation reactions. Two liters of water contaminated with different concentrations of 2,4-D and NOM was re-circulated in the reactor, first with the lamps being turned off to ensure the adsorption of solutes on the surface of spheres reached equilibrium. The lamps were then turned on after 90 min and samples were taken at different intervals with a total reaction time of 30 min. The samples were filtered through 0.2 μm filter prior to analysis.

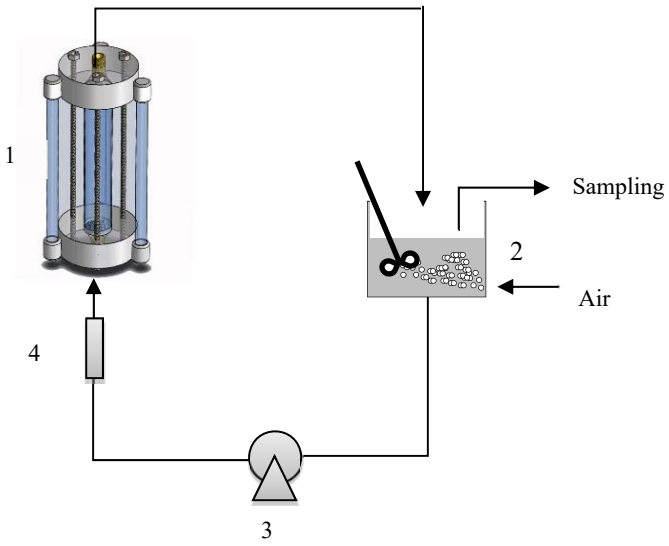

Figure 2-3. Experimental setup: (1) FBPR, (2) storage tank, (3) pump, (4) flowmeter.

2.5 Photocatalyst spheres reactivation

Photocatalytic spheres were reactivated by desorption of organic molecules at high pH. Used 25 g photocatalysts were fluidized by NaOH solution (pH 11) in FBPR. Two liters of NaOH solution was recirculated in the reactor in the absence of UV radiation and at the same condition used for photocatalytic experimental procedure for 30 min to desorb 95±2% of organic molecules from the surface of photocatalyst spheres.

2.6 Adsorption process

2.6.1 2,4-D adsorption

Adsorption experiments were performed in the FBPR at 25º C. The reactor was filled with 25 g photocatalytic spheres and two liters of the solution was recirculated in the reactor in the absence of light at the same condition used for photocatalytic experiments.

Adsorption kinetic experiments were performed for 90 min and samples were taken at different intervals to monitor the change in 2,4-D concentrations. For the isotherm experiments, the solution was recirculated through the reactor for over 8 hrs to ensure an equilibrium condition was reached before taking samples. Samples were filtered through a 0.22 μm syringe filter before being analyzed by HPLC.

2.6.2 NOM adsorption

Adsorption experiments were performed in a shaker incubator (Lab Companion SI-600) protected from light, at 25° C and 70 rpm (the optimum rate to minimize the fine production of the photocatalyst). Adsorption isotherms were studied through a series of experiments involving different initial concentrations of NOM exposed to a constant amount of photocatalyst spheres (1.5 g) and mixed over 48 hrs to ensure equilibrium condition. The equilibrium samples were taken and filtered with 0.22 μm syringe filter before analysis.

Adsorption kinetics study was carried out to evaluate the time course of the adsorption of NOM on photocatalytic spheres. The experiments were performed in the shaker incubator at 25°C and 70 rpm. Photocatalyst spheres of 1g were placed into 100 mL solution (in Erlenmeyer) and mixed for a period of 300 min. Samples were taken at different intervals to monitor the change in the concentrations of NOM in the solution.

Chapter 3: TEMPLATE FREE PHOTOCATALYST SPHERES CHARACTERISTICS

This Chapter reviews the intrinsic properties of the photocatalyst used in this research, template free photocatalyst spheres (PSs). PSs various analysis such as XRD, SEM and BET were performed and compared with the PSs previous generation synthesized by Vega et al. (2011) and pre-calcined commercial photocatalyst (TiO_2 Degussa P25) characteristics. Analytical results showed that PSs provided relatively high surface area (35.27 m^2g^{-1}) and good percentage of anatase (71.5%). The charge of photocatalyst surface was also measured at different pH to determine the pH of zero point charge (pH_{zpc}) as the major factor impacting the photocatalytic oxidation pathways.

3.1 Photocatalyst spheres (PSs) crystalline characteristic

Figure 3-1 shows XRD paterns of PSs and pre-calcine TiO_2 P-25. High intensity peaks at $2\theta=25^o$ identify the most intensive peak (101) for the anatase TiO_2. The rutile (110) characteristics peak was found at $2\theta=27^o$. The Rietveld refinement method showed that the weight fraction of anatase is 71.5%, higher than that reported by Vega, et al. (2011) (64.19%) and lower than TiO_2-P25 (80%)(Mir et al., 2013).

PSs low anatase ratio comparison to TiO_2-P25 is due to heat treatment of photocatalyst preparation. Vega et al. (2011) showed that the percentage of anatase was significantly reduced from 64.19% to zero when the calcination temperature rose from 600ºC to 700ºC. Therefore, the calcination temperature of 600ºC was applied to produce PSs with predominant anatase phase. On the other hand, as Zhang et al. (2008) showed that the surface-phase junction between anatase and rutile particles, formed during the calcination process, is responsible for the highest photocatalytic activity; the phase junctions facilitates transfer of the electron from CB of the rutile phase to the

trapping sites on the anatase surface, thereby improving the photocatalytic activity. Studies (Bacsa and Kiwi, 1998; Mir et al., 2013; Thiruvenkatachari et al., 2008; Yamazaki et al., 2001) demonstrated that 70% - 80% of anatase phase gives the best result for degradation of micropollutants. Thus, the ratio of the photocatalyst of this research was improved to place in the ideal range in terms of photocatalytic activity. Reducing the heating rate from 10° C min^{-1} reported by Vega et al. (2011) to 3.5° C min^{-1} in this research improves the heat treatment and increased the anatase percentage. This result is in agreement with Zhang et al. (2008) studies which demonastrated that not only calcination tempreture is responsible for higher anatase persentage on the surface of catalyst but the calcination time process was also a main factor to improve the anatase phase percentage.

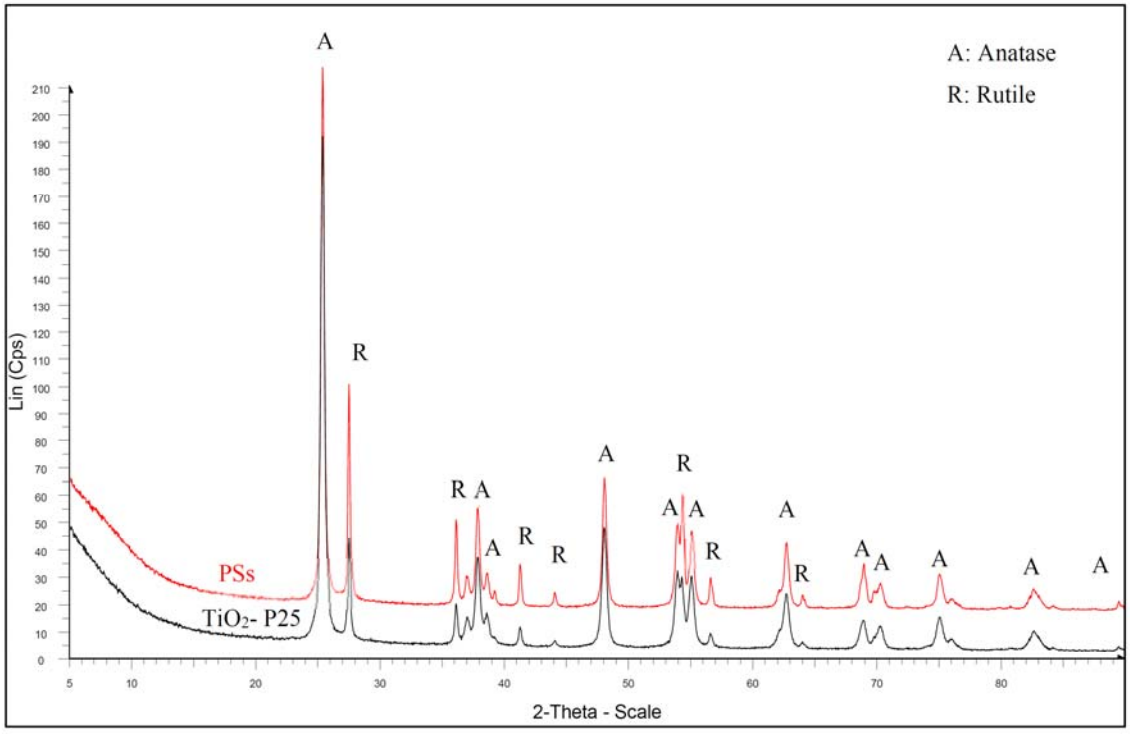

Figure 3-1. XRD diffraction pattern of TiO_2- P25 pre-calcine and photocatalytic spheres.

3.2 PSs surface properties

Table 3-1 shows surface properties information of PSs from this research and that of reported by Vega et al. (2011) as well as pre-calcined TiO_2-P25. The surface area, pore volume and pore size were improved to a higher value compared to those of previously study (Vega et al., 2011). Increasing these parameters may result in an improvement of adsorption and consequently photocatalytic performance. Kim and Kwak (2007) showed that the photocatalyst with larger surface area due to providing more active sites for pollutants adsorption, exhibits better photocatalytic activity. It is clear that TiO_2-P25 in powder form has a higher surface area than the composite photocatalyst spheres. This result indicates that PSs porosity is in the meso-range (Haber, 2009). BET results and XRD analysis of PSs from this study and Vega et al (2011), in agreement with other researches (Bacsa and Kiwi, 1998; González-Reyes et al., 2011; Vega et al., 2011), indicates that the higher percentages of anatase culminate the surface area.

Table 3-1. Different photocatalyst TiO_2 surface properties data

Material	Anatase (%)	Surface area (m^2g^{-1})	Pore volume (cm^3g^{-1})	Pore size (nm)
PSs (this study)	71.5%	35.2	0.30	25.0
PSs (Vega et al., 2011)	64.2%	29.3	0.17	18.2
TiO_2-P25 (Vega et al., 2011)	87.8%	54.0	0.23	16.6

3.3 PSs morphology

The Scanning Electron Microscope (SEM) is commonly used to analyze the morphology (size and shape), topography (surface features) and crystallographic features (atomic arrangements) of a photocatalyst. Photocatalytic spheres showed a consistency in size and shape with the average diameter of 0.90 mm, as shown in Figure 3-3. PSs had a relatively smooth surface

despite the presence of some roughness along the surface of the catalyst. No cracks were present, indicating there were no extreme stresses during the catalyst production process. Figure 3-2 also shows SEM micrographs of the catalyst after 10 hrs of continuous use. The surface of the catalyst is smoother than that of the fresh photocatalyst.

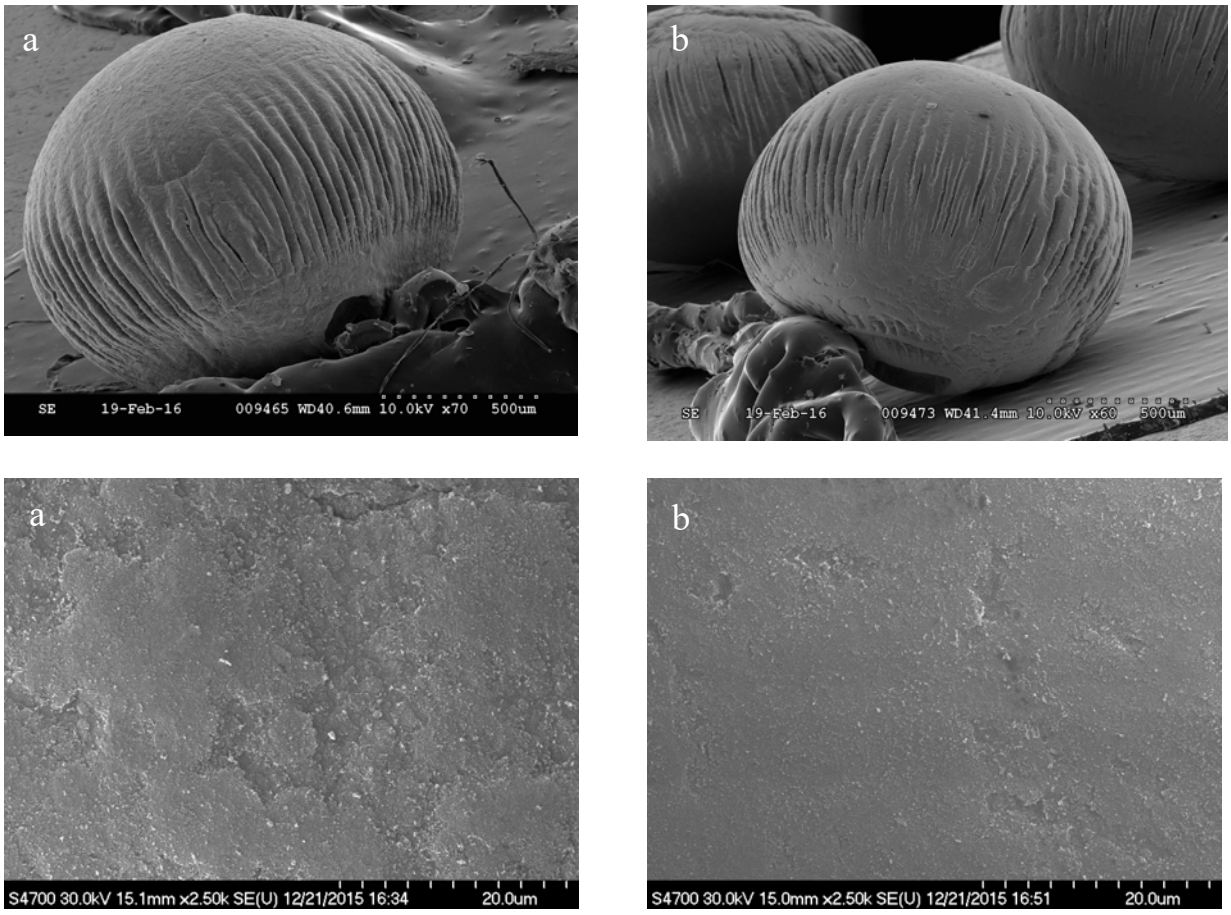

Figure 3-2- SEM micrograph of (a) fresh photocatalyst (b) used photocatalyst.

3.4 Attrition

Figure 3-3 shows the amount of TiO_2 detached from the spheres and released into the water after 90 min of operation for the modified PSs developed in this research and that of made by the previous procedure, suggested by Vega et al. (2011). The results demonstrate that the attrition resistance of the PSs made in this study improved by nearly %80, reducing the amount of TiO_2

fines from 15.6 mg. L^{-1} to 3.3 mg. L^{-1}. This improvement can be because of the more consistent geometry/shape and smaller size of the photocatalyst from this study, compared to that made by the previous procedure. According to the literature (Hatzantonis et al., 1998; Yang, 2003) several factors such as particle shape, initial particle size, and particle size distribution affect the attrition of the catalyst in fluidized bed reactors. That is, applying smaller particles with higher consistency in shape and size reduces the attrition.

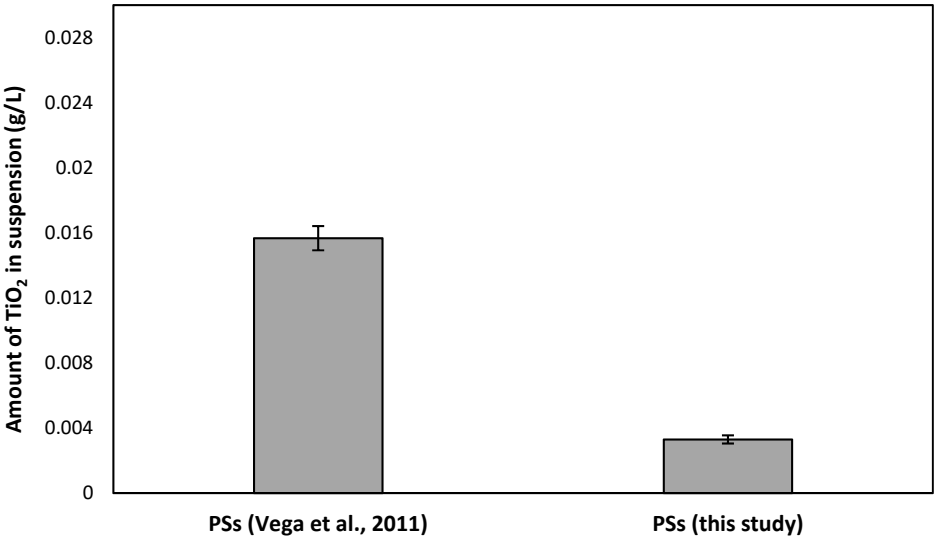

3-3. Amounts of titanium detached from the photocatalyst spheres during fluidization. Error bars represent the standard errors for the four replicate runs.

3.5 The effect of pH on PSs charge surface

Figure 3-3 shows the surface charge of the PSs versus pH of the solution. The results illustrate that pH_{zpc} of PSs is 6, meaning the surface of PSs is positively charged ($TiOH_2^+$) at pH< 6, whereas it is negatively charged (TiO^-) at pH> 6. At pH higher than 6, photocatalyst is favorable for adsorption of positively charged micropollutants, while it is favorable for negatively charged micropollutants at pH lower than 6. Hence, controlling the pH, and consequently controlling the surface charge of PSs, may serve as means toward preferential degradation.

Although changing the pH of the medium primarily affects the contaminant charge. At pH value higher than contaminant pK_a, it dissociates into unprotonated species that affects the adsorption and consequently the oxidation performance. It should be emphasized that understanding the effect of pH is complex and important. This dissertation will present a detailed discussion in following chapters of the impact of pH on adsorption and photocatalytic oxidation performance.

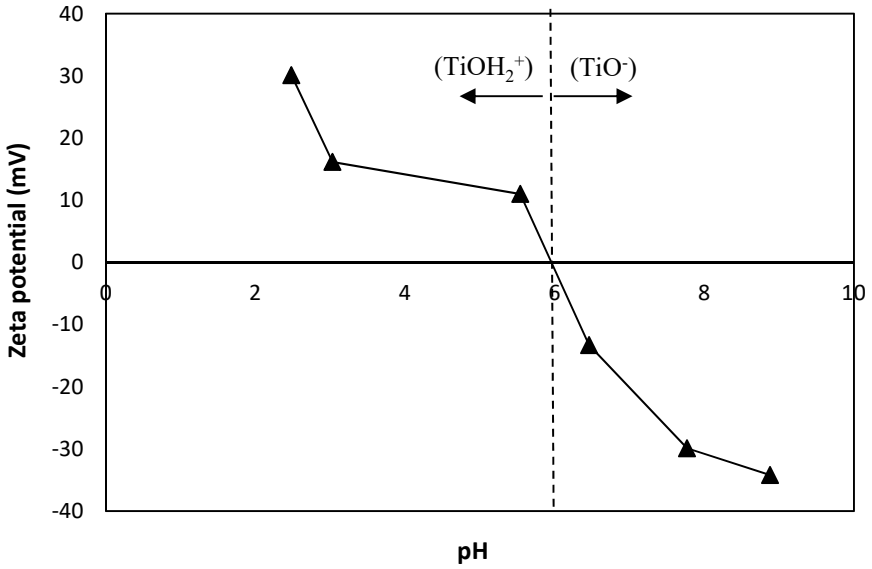

Figure 3-4. Influence of pH on zeta potential of TiO_2 in aqueous medium.

Chapter 4: ADSORPTION OF 2,4-D ON THE SURFACE OF PHOTOCATALYST SPHERES

4.1 Introduction

Thorough investigation of 2,4-D interaction with the photocatalyst surface is an essential prerequisite to the study of photocatalytic process. Adsorption affects the photocatalytic reaction rate by bringing molecules such as water, oxygen and organic solute (in the case of this work 2,4-D), together and within a quasi-liquid layer on the surface of the photocatalyst (Satterfield, 1980). Moreover, since hydroxyl groups or water molecules in an aqueous medium can serve the role of forming hydroxyl radical, initial adsorption is a prerequisite to highly efficient detoxification (Fox and Dulay, 1993).

This Chapter presents the effect of pH and NOM on 2,4-D adsorption on the surface of photocatalyst spheres. It reports on the research involving detailed isotherm experiments and assessment of different isotherm models to determine the nature of the adsorption process and the role of pH. Also, it presents the results of kinetic experiments performed to provide detailed insights into the mechanism of adsorption. The interference of NOM on 2,4-D adsorption is investigated in detail and the results are presented.

4.2 Results and discussion

4.2.1 The effect of pH

Figure 4-1 shows the results obtained from adsorption experiments conducted in FBPR at different pH. The amount of 2,4-D adsorbed by photocatalytic spheres increased by ~ 60% with decreasing pH from 7 or 5 to pH 3. 2,4-D adsorption is limited (~10%) at pH 5 and pH 7.

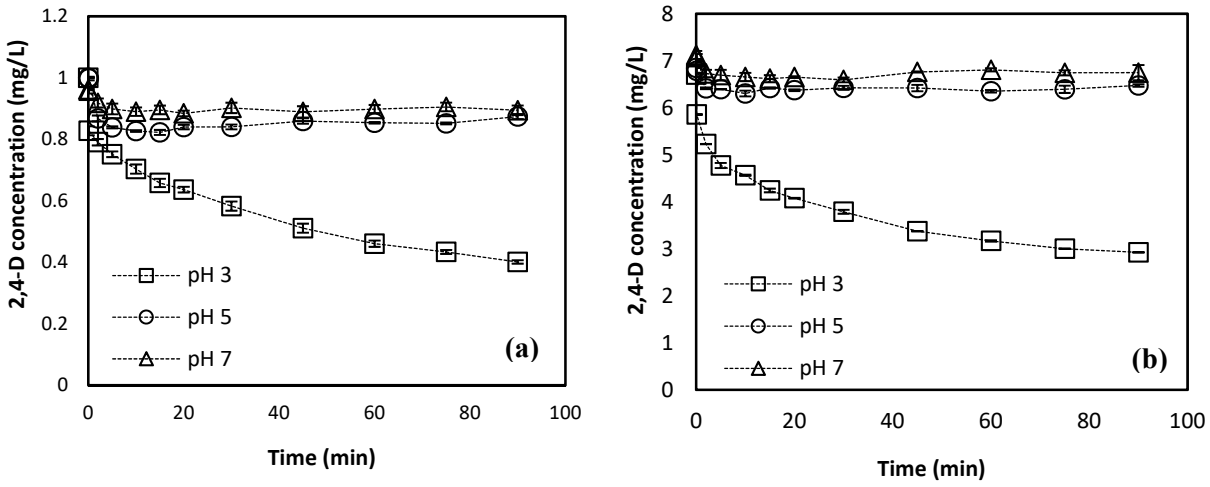

Figure 4-1. 2,4-D adsorption in FBPR with different initial concentration of 2,4-D; (a) 1 mgL^{-1} and (b) 7 mgL^{-1}. Error bars represent the standard errors for the triplicate runs.

According to the results shown in Figure 4-1, the loading capacity of photocatalyst spheres in 90 min can be evaluated; it increases from 0.05 mg. g^{-1} to 0.32 mg. g^{-1} with increasing the initial concentrations of 2,4-D from 1 mgL^{-1} to 7 mgL^{-1} 2,4-D.

Difference in the amount of 2,4-D adsorbed at different pH can be explained based on the effect of pH on the photocatalyst surface charge. The photocatalyst surface is positively charged when pH is below pH_{pzc} (i.e., pH 3), whereas it is negatively charged at pH above pH_{pzc} (i.e., pH 7). Moreover, the pK_a of 2,4-D is 2.64 (Avdeef, 2012). This means that 2,4-D is negatively charged at pH above 2.64 (Eq. 4-1). This causes high adsorption of deprotonated 2,4-D on positively charged photocatalyst surface. However, 2,4-D adsorption reduces markedly because of the electrostatic repulsion at pH above 3.

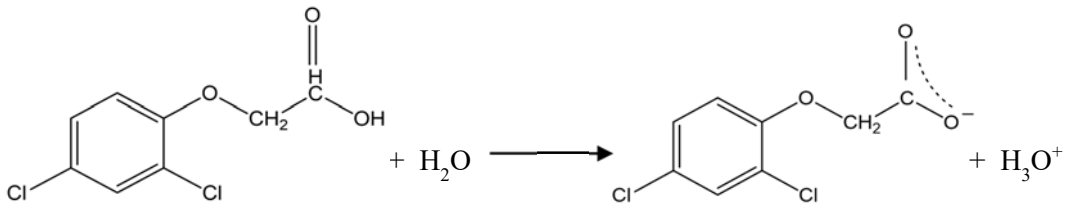

(4-1)

Figure 4-2 shows that the photocatalyst pH_{pzc} changed from 6 for fresh catalyst to less than 5 after 2,4-D adsorption of 0.31 mg per gram of photocatalyst. It means the photocatalyst surface is negatively charged at pH 5 after some initial adsorption of 2,4-D which causes an overall low adsorption of 2,4-D, the same that occurs at pH 7.

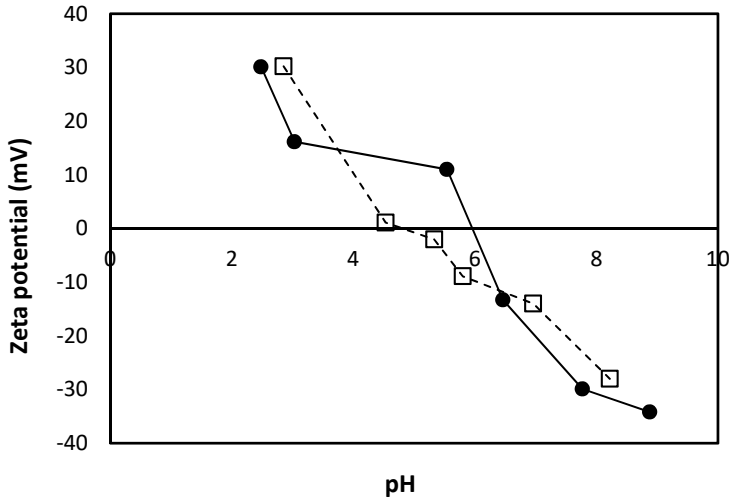

Figure 4-2. The influence of the medium pH on zeta potential of, (●) bare photocatalyst and (□) photocatalyst with adsorbed 2,4-D of 0.31 mg.g^{-1} photocatalyst.

4.2.2 Adsorption Equilibrium

Adsorption isotherm equilibrium of 2,4-D was studied applying known isotherm models, Langmuir and Freundlich. In agreement with the literature (Doll and Frimmel, 2005a; Liu et al., 2008), the results show that Freundlich model fits experimental data very well at pH 3 where 2,4-D adsorption is high due to electrostatic attraction (see Figures 4-3 and 4-4). However, the equilibrium adsorption of 2,4-D at pH 5 and pH 7 due to repulsion between the photocatalyst's negative charge and deprotonated 2,4-D, are very low and not considerable.

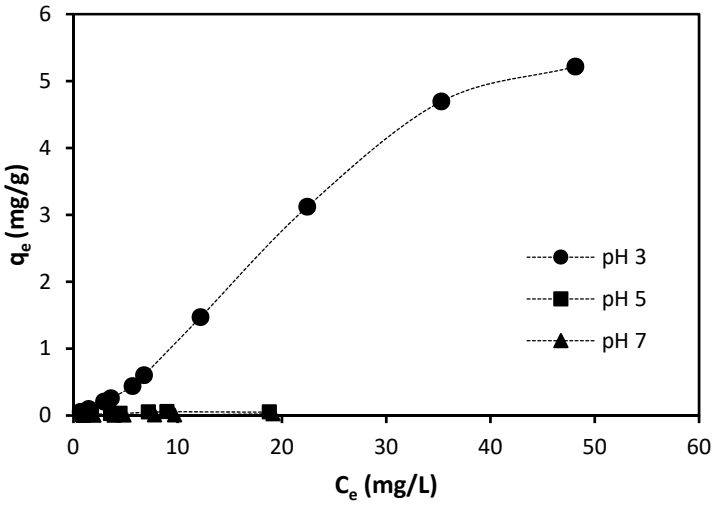

Figure 4-3. 2,4-D isotherm adsorption at different pH.

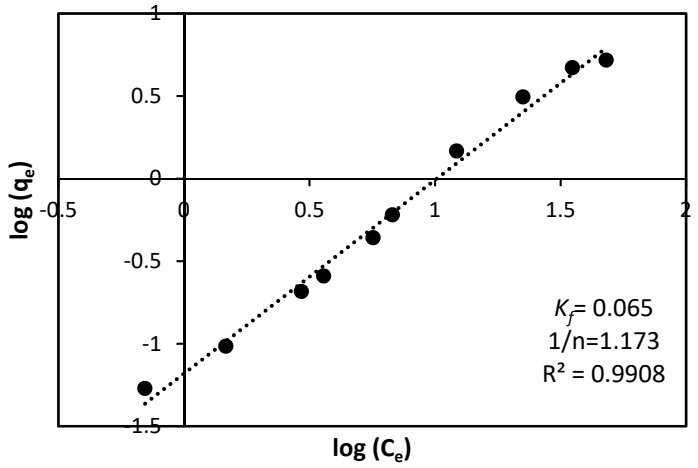

Figure 4-4. Freundlich fitting of adsorption of 2,4-D on photocatalytic spheres at pH 3.

The Freundlich isotherm is widely used to explain the multilayer adsorption, with non-uniform distribution of adsorption and affinities over the heterogeneous surface (Foo and Hameed, 2010). The Freundlich isotherm model is shown in the following equation:

$$q_e = k_f C_e^{\,1/n} \tag{4-2}$$

where C_e (mg/L) is equilibrium concentration of 2,4-D, and q_e (mg/g) is the amount of 2,4-D adsorption per unit weight of photocatalyst at adsorption equilibrium, 1/n represents the Freundlich

exponent and unitless, and k_f is the Freundlich constant. The Freundlich constant (k_f) is related primarily to the capacity of the adsorbent for the adsorbate, and $1/n$ is a function of the strength of adsorption (Snoeyink and Summers, 1990).

A sigmoidal isotherm shape (Figure 4-3) indicates that the sorption-promoting effect starts only after a certain loading of the adsorbent (Schwarzenbach et al., 2002).

According to the literature (Diebold, 2003b; Schmidt and Steinemann, 1991; Thomas et al., 2007), it can be assumed that 2,4-D adsorption mostly occurs through binding of deprotonated carboxylic group with Ti_{c5} on the surface of TiO_2 (see Figure 4-5). Based on some other studies (Liu et al., 2008; Pang et al., 2008), it can be hypothesized that 2,4-D adsorption on hydroxylated TiO_2 releases protons (see Eq (4-3)) which promote 2,4-D adsorption at the first layer. Furthermore, studies of organic adsorption onto TiO_2 (Johansson et al., 2010; Thomas et al., 2007) shows that multilayer adsorption is governed by hydrogen binding may lead to multilayer adsorption for 2,4-D.

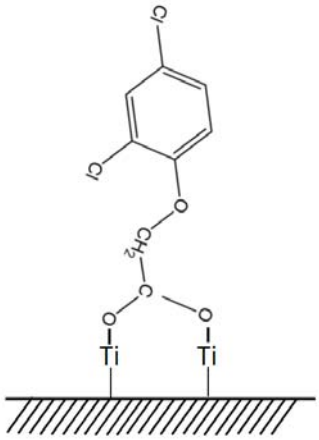

Figure 4-5. Adsorption of 2,4-D on the surface of TiO_2.

$$TiOH_2^+ + RCOO^- \rightarrow Ti - OOCR + H_3O^+ \qquad (4\text{-}3)$$

4.2.3 2,4-D adsorption kinetics

Figure 4-6 shows time course adsorption of 2,4-D on the surface of photocatalyst with different initial concentration of 2,4-D at pH 3. 2,4-D adsorption reached plateau within approximately 90 min for all initial concentrations, indicating that the rate of C/C_0 of 2,4-D adsorption is independent of its initial concentration and falls rapidly during the initial uptake. Weber and Morris (1963) demonstrated that the adsorption initial rate is directly proportional to the solute concentration if external mass transfer is rate-limiting step. For this reason, the external mass transfer coefficients of different initial concentrations of 2,4-D were calculated (refer to Appendix A) and the results demonstrate that the mass transfer coefficients are similar and independent of 2,4-D initial concentrations. This indicates that external mass transfer is a not rate-controlling step in this process.

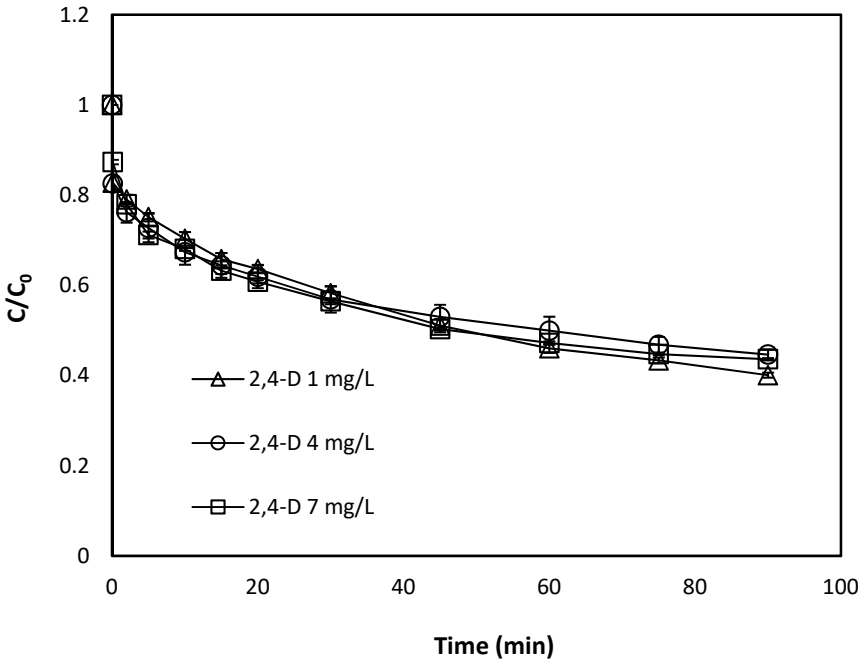

Figure 4-6. Time course adsorption of 2,4-D on the surface of photocatalytic spheres at pH 3. Error bars represent the standard errors for the triplicate runs.

To better understand 2,4-D adsorption behaviour, the kinetics of 2,4-D adsorption was modeled using Lagergren pseudo-first order model (See Eq. (4-4) and Eq. (4-5)) (Hameed et al., 2008; Lee et al., 2007).

$$\frac{dq_t}{dt} = K_1(q_e - q_t) \tag{4-6}$$

$$q_t = q_e(1 - e^{-K_1 t}) \tag{4-7}$$

where K_1 is the Lagergren's first order rate constant (min^{-1}) and q_e (mg. g^{-1}) and q_t (mg. $g^{-1}.min^{-1}$) are the amounts of solute adsorption per unit weight of photocatalyst at equilibrium and at time t, respectively.

The pseudo-first order rate constant, K_1, was obtained by plotting $\ln[(q_e - q_t)/ q_e]$ vs. time (Figure 4-7). A good linear correlation coefficient indicates an appropriate fit of Lagergren's equation to 2,4-D adsorption data in the range from 2 to 90 min.

Snoeyink and Summers (1990) described that the adsorption rate initially is controlled by intraparticle diffusion. A deviation from Lagergren model observed during the first 2 minutes can be due to the diffusion that governs the adsorption at the beginning of the process. Akasu and Kabasakal (2005) showed that intraparticular diffusion is a function of time squared and control the adsorption rate before uptake of 2,4-D on the sorption sites.

The Lagergren's first-order rate constant (K_1) determined from the model, is presented in Table 4-1 along with the corresponding correlation coefficients. The similar rate constants for different initial concentrations of 2,4-D indicate high adsorption capability of the photocatalyst spheres.

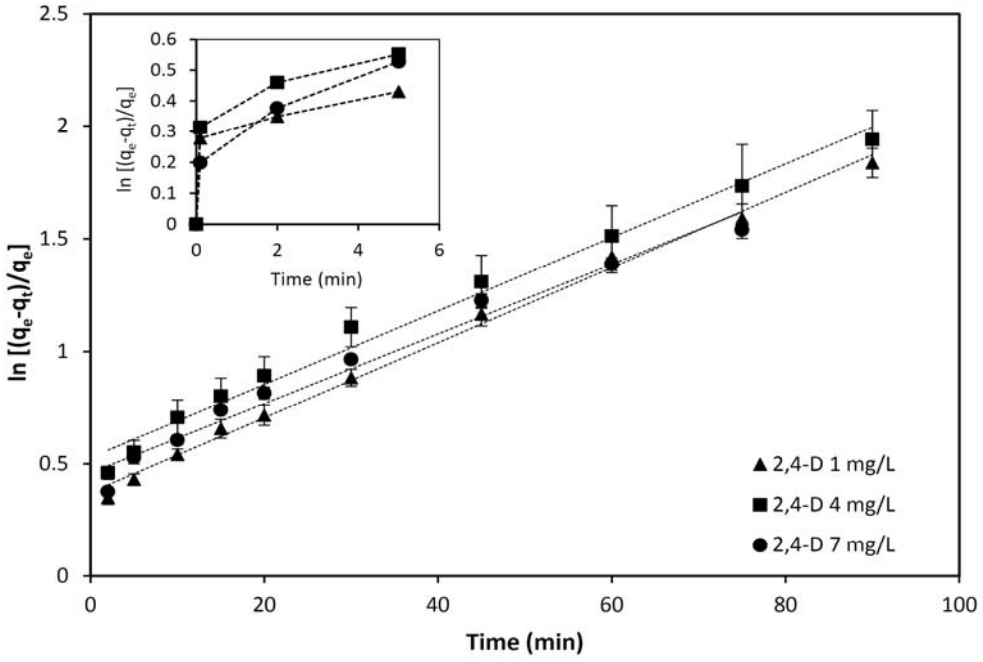

Figure 4-7- Lagergren pseudo-first order fitting of 2,4-D adsorption at different concentration on photocatalytic spheres at pH 3. Error bars represent the standard errors for the triplicate runs.

Table 4-1. Lagergren pseudo-first order adsorption rate constant obtained at different 2,4-D initial concentrations.

2,4-D initial concentration (mgL^{-1})	q_e ($mg.\ g^{-1}$)	K_l (min^{-1})	R^2
1	0.046	0.016 ± 0.001	0.99
4	0.171	0.016 ± 0.002	0.98
7	0.274	0.014 ± 0.001	0.97

4.2.4 2,4-D adsorption in the presence of NOM

Figure 4-8 presents the effect of NOM on 2,4-D adsorption at different initial concentration at pH 3. The experimental results suggest that NOM irrespective of its initial concentration, does not have any impact on 2,4-D adsorption. This result is in agreement with the observation of Pelekani and Snoeyink (1999) who demonstrated the negligible effect of NOM on adsorption of

different micropollutants. The negligible effect of NOM on 2,4-D adsorption is most likely due to the high capacity of photocatalyst spheres for adsorption and the relatively larger molecular size of NOM in comparison with that of 2,4-D.

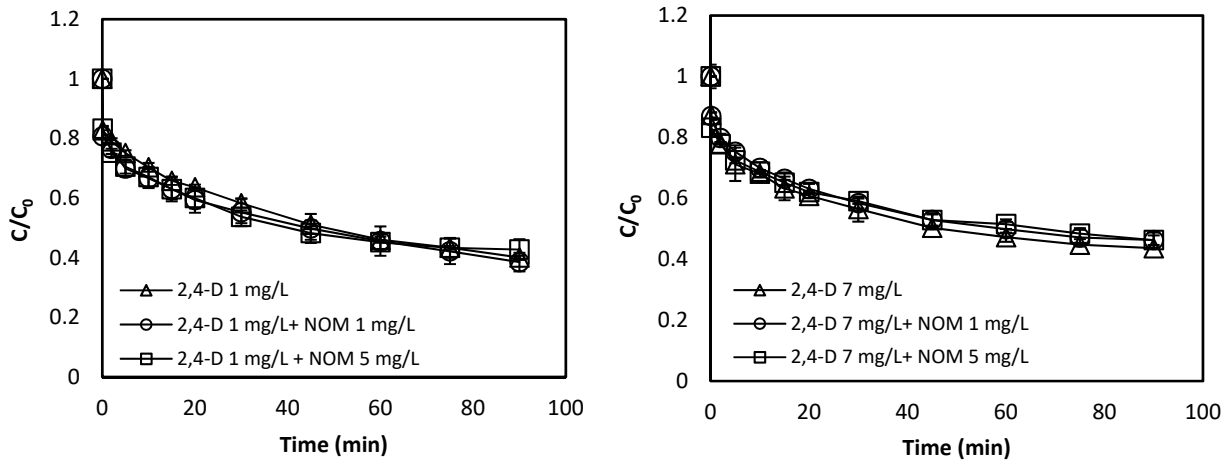

Figure 4-8. Time course adsorption of 2,4-D onto photocatalytic spheres in the presence and absence of NOM at pH 3. Error bars represent the standard errors for the triplicate runs.

Figure 4-9 shows the adsorption of NOM in the presence of different concentrations of 2,4-D at pH 3. This result shows that irrespective of the concentration of 2,4-D, a significant NOM adsorption takes place (~ 95%), confirming that the adsorptions of NOM and 2,4-D takes place independently.

NOM with large molecular chains is adsorbed on larger pores (mesospores) (Newcombe and Drikas, 1997) and dose not interfere with 2,4-D adsorption (Snoeyink and Summers, 1990). 2,4-D adsorption, on the other hand, relies on crystalline and chemical structure of adsorbent. Therefore, photocatalyst spheres with specific crystalline structure and porosity make a good condition for high adsorption of 2,4-D and NOM.

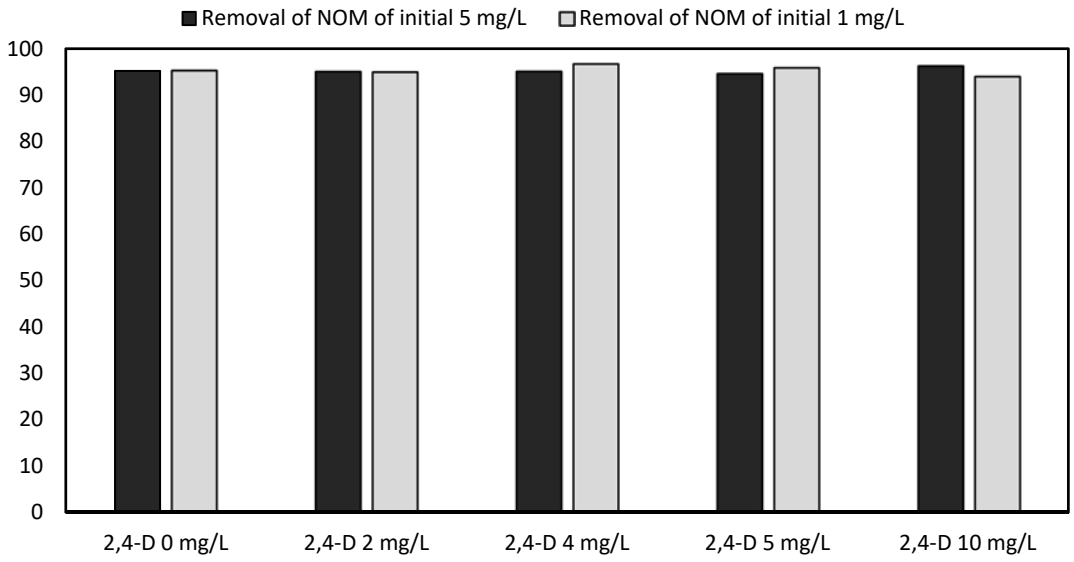

Figure 4-9. NOM removal in the presence of different concentrations of 2,4-D.

NOM, because of its functional groups such as carboxylic, phenolic, etc. (Bai and Zhang, 2001; Thurman, 1985a; Tipping et al., 1990), prevalently has negative charge. Hence, adsorbed NOM may affect the adsorption of organic molecules by changing the photocatalyst surface charge. Figure 4-10 shows the effect of NOM on photocatalyst surface charge. After NOM adsorption, the photocatalyst was found to have lower pH_{zpc}; the pH_{zpc} reduced to 3.3. Nevertheless, this result shows that the photocatalyst surface is still positive at pH 3 even after high NOM adsorption. In other words, adsorbed NOM cannot affect 2,4-D adsorption at pH 3 even by changing photocatalyst surface charge.

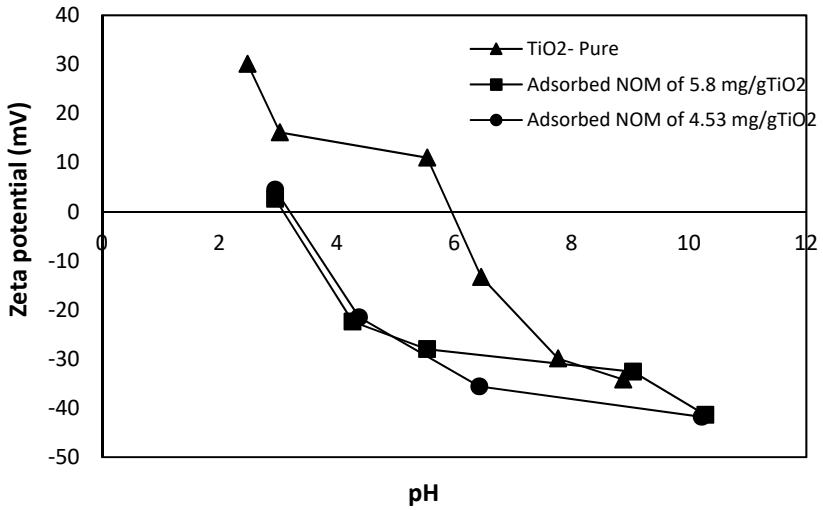

Figure 4-10. The influence of NOM on zeta potential of the photocatalyst spheres.

4.3 Conclusions

The adsorption kinetics and isotherm of 2,4-D on the surface of photocatalytic spheres were studied. 2,4-D adsorption kinetics showed relatively high adsorption (~ 60%) at pH 3. The amount of adsorbed 2,4-D, however, dropped to 10% at pH>3. Adsorption of 2,4-D on photocatalyst, due to low mass transfer resistance, was independent of the initial concentration. Also, 2,4-D adsorption isotherm Freundlich model indicated multilayer adsorption of 2,4-D on the photocatalyst surface.

2,4-D adsorption in the presence of NOM showed that NOM did not have any effect on adsorption performance. Since the photocatalyst has a high adsorption capacity and the adsorption mechanism of NOM is different from that of 2,4-D, none of these adsorbates can interfere with one another when it comes to their adsorption. Regardless of the initial concentration of 2,4-D, NOM is adsorbed by up to ~95% in the presence of different concentrations of 2,4-D.

Chapter 5: ADSORPTION OF NATURAL ORGANIC MATTER ON THE SURFACE OF PHOTOCATALYST SPHERES

5.1 Introduction

Natural organic matter (NOM) represents a complex group of organic compounds with a wide range of chemical structure and molecular sizes which are commonly present in natural surface water. NOM contains largely aliphatic, highly coloured, aromatic, hydrophobic, hydrophilic, charged, and uncharged components. The presence of NOM in raw surface water brings several challenges to drinking water treatment processes such as the photocatalytic process. It significantly affects the efficiency of the photocatalytic degradation of micropollutants (Doll and Frimmel, 2005a) by absorbing UV radiation and scavenging oxidant species formed in the solution and on the surface of photocatalyst (Doll and Frimmel, 2005a; Guojing Liu et al., 2008; Guoj. Liu et al., 2008; Rezaei and Mohseni, 2017b). Hence, investigating the adsorption mechanism of NOM on photocatalyst spheres is crucial for better understanding the impact of NOM on photocatalytic oxidation taken place on the surface of photocatalyst.

In this Chapter, the adsorption of NOM and its fractions at the different pH on photocatalyst spheres are discussed. In particular, the impact of pH on electrostatic and hydrophobic interactions between NOM molecules and photocatalyst surface is presented. A characterization technique such as fractionation, and analytical methods like HPSEC, UV absorption and FTIR are used to analyze the adsorption of NOM and its fractions on the surface of photocatalyst spheres.

5.2 Results and discussion

5.2.1 The effect of pH on NOM adsorption

Figure 5-1 shows the percentage of NOM removed at equilibrium (during adsorption isotherm experiments). At pH 3, the removal of NOM (95%) did not vary significantly with increasing the initial concentration; however, it decreased ~15% as NOM concentration increased from 5 to 20 mg.L^{-1} at pH 5 and 7. High removal of NOM at pH 3 indicates the role of hydrophobic attraction in the process. At pH 3 the charge on NOM is zero or very low (Newcombe and Drikas, 1997) indicating the negligible electrostatic repulsion between adsorbed NOM (NOM_{ads}) and dissolved NOM (NOM_{sol}). In the absence of a strong electrostatic interaction, the adsorption is governed by hydrophobic interaction with high molecular weight compounds. As shown in Figure 4-10, the pH_{zpc} of NOM post-adsorbed photocatalyst is 3.3 and due to electrostatic repulsion between the negative charge of NOM and the photocatalyst surface, the adsorption of NOM is significantly reduced at pH>3. In other words, the adsorption is quite clearly related to the increased repulsive NOM_{ads} -NOM_{sol} electrostatic interactions with increasing pH (Kim et al., 2009; Lee et al., 2007; Newcombe and Drikas, 1997).

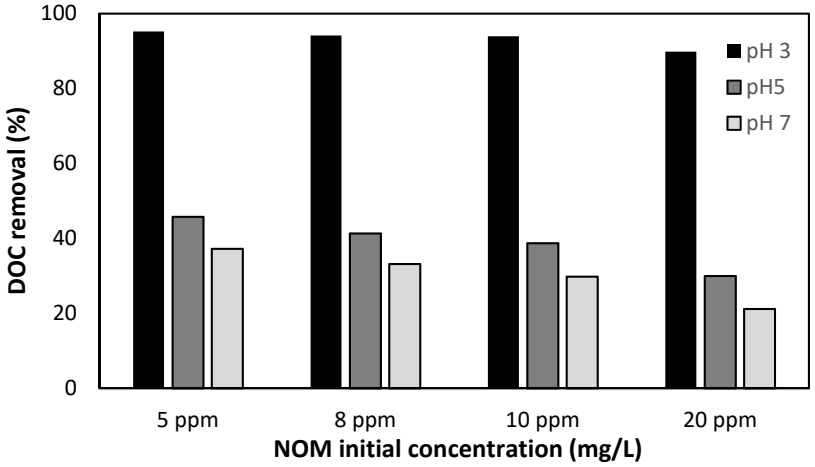

Figure 5-1. The effect of pH on NOM removal in adsorption isotherm process.

5.2.2 NOM equilibrium isotherm

Figure 5-2 shows the adsorption equlibrium of NOM on the surface of the photocatalyst at different pH. Results indicate that NOM adsorption at pH 3 due to lack of electrostatic reputation between NOM_{ads} and NOM_{sol} is substantially higher than that at pH 5 and pH 7. To better understand the behaviour of NOM in the adsorption process, isotherm correlations are utilized. In this study, the NOM equilibrium isotherms have been investigated, by comparing three correlations namely, the Freundlich, Langmuir, and Sips isotherm models. Freundlich and Langmuir are two frequently used isotherm models that have been applied to the experimental data of adsorption studies. Sips is another empirical isotherm model that predicts the heterogeneous adsorption systems, and circumvent the limitation of the rising adsorbate concentration associated with the Freundlich isotherm model (Foo and Hameed, 2010). Langmuir and Freundlich isotherms, were applied on the experimental data using the following equations:

Langmuir:
$$q_e = \frac{q_{max} K C_e}{1 + K C_e} \quad (5\text{-}1)$$

Freundlich:
$$q_e = k_f {C_e}^{1/n} \quad (5\text{-}2)$$

Experimental results (Figure 5-3) show that NOM equilibrium adsorption was fitted well to the Freundlich isotherm model at pH 3. At pH 5 and pH 7, on the other hand, due to the electrostatic repulsion between negatively charged NOM and photocatalyst spheres, the monolayer adsorption process probably dominated the adsorption process.

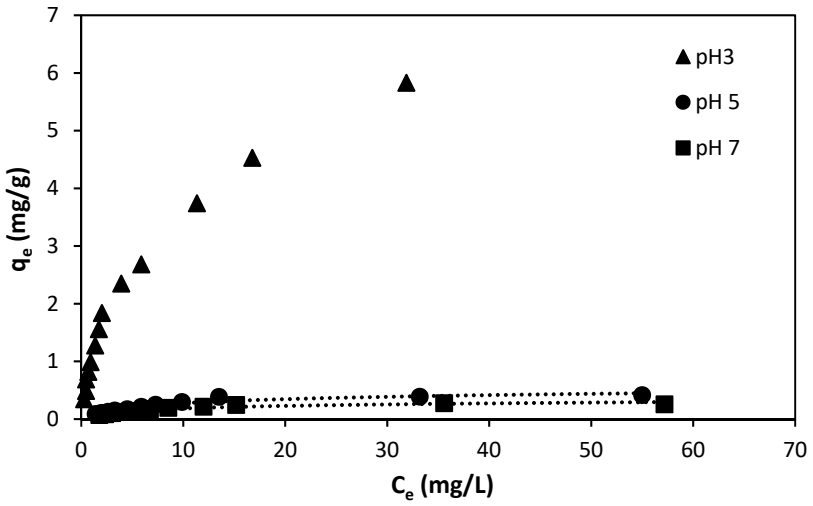

Figure 5-2. Adsorption Isotherm of NOM on the surface of photocatalytic spheres at different pH.

Sips (1948) introduced a modified model of the Freundlich equation that could very well describe the adsorption of NOM on the surface of the photocatalyst spheres at different pH.

$$q_e = \frac{q_m k_s {C_e}^{1/n}}{1 + k_s {C_e}^{1/n}} \tag{5-3}$$

where q_m is monolayer adsorption capacity (mg.g^{-1}) and k_s is Sips constant related to the energy of adsorption (Günay et al., 2007).

As shown in Figure 5-3, the Sips isotherm model could very well interpret the different NOM adsorption behaviours at pH 3 from Freundlich at low concentration to Langmuir at high concentration and also the monolayer adsorption of NOM at pH>3.

The results of the models parameters as well as the sum of error squared (SSE) between the predicted values and the experimental data with the correlation coefficient are summarized in Table 5-1. As can be seen, the Sips isotherm model had a maximum coverage to experimental data and the lowest SEE in comparison to other isotherm models applied to NOM adsorption isotherm at different pH. SEE was analyzed using the following equation:

$$SEE = \sqrt{\sum \frac{\left(q_{e,exp} - q_{e,est}\right)^2}{N}} \quad (5\text{-}4)$$

where the subscripts "exp" and "cal" are the experimental and estimated values of q_e from model, respectively, and N is the number of measurements (Günay et al., 2007).

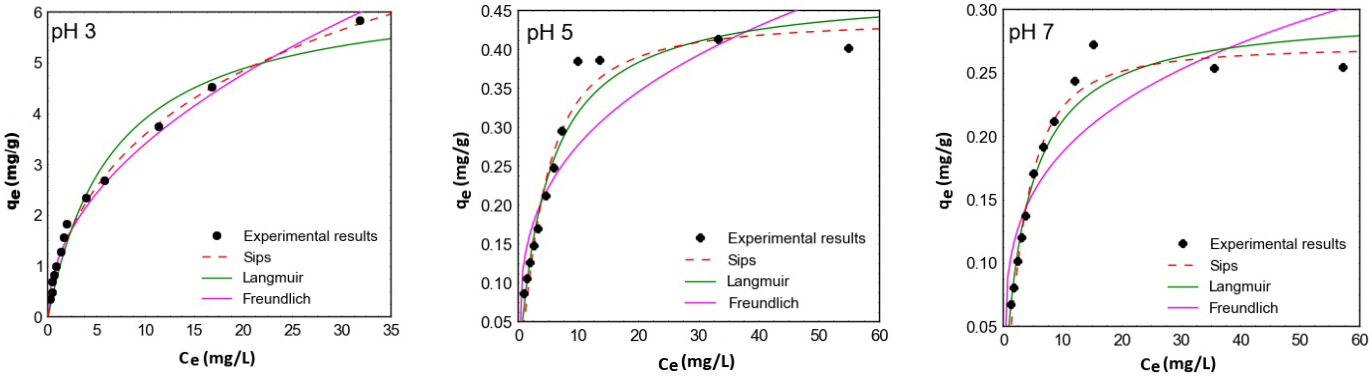

Figure 5-3. Different isotherm equation plots for the adsorption of NOM on the TiO_2 photocatalytic spheres.

Table 5-1. Freundlich, Langmuir and, Sips isotherm constant for NOM adsorption at various pH.

		pH 3	pH 5	pH 7
Freundlich	k_f	1.12	0.13	0.10
	1/n	0.48	0.31	0.27
	R^2	0.98	0.80	0.76
	SSE	0.163	0.051	0.032
Langmuir	$K\ (L.mg^{-1})$	0.15	0.20	0.251
	$q_{max}(mg.g^{-1})$	6.53	0.47	0.29
	R^2	0.97	0.95	0.95
	SSE	0.252	0.025	0.015
Sips	k_s	0.091	0.154	0.173
	$q_m\ (mg.g^{-1})$	12	0.44	0.27
	1/n	0.64	1.32	1.43
	R^2	0.99	0.96	0.97
	SSE	0.111	0.021	0.010

5.2.3 NOM adsorption kinetics

Figure 5-4 shows the effect of pH on the kinetics of adsorption of NOM on photocatalytic spheres. As expected, the adsorption of NOM was significantly reduced at pH >3.

The results show that adsorption of NOM is related to the square root of time. It can be explained by Fickian diffusion model which was used to express the adsorption process controlled by diffusion process (Lee et al., 2007).

$$q_t = 2C_0 S\sqrt{Dt/\pi} = k_F t^{0.5} \quad (5\text{-}5)$$

where q_t is the amount of adsorbed NOM per unit weight of photocatalytic spheres ($mg.g^{-1}.min^{-1}$), C_0 is the initial concentration of NOM in the bulk solution ($mg\ L^{-1}$), D is the diffusion coefficient, and S is the specific area of photocatalytic spheres (m^2g^{-1}). As shown in Figure 5-5, the Fickian diffusion model fits the experimental data well, indicated that diffusion controlled the adsorption process during the first 360 min. It could be due to high capacity of photocatalyst spheres for adsorbing NOM, mentioned in previous chapter. Table 5.2 also presents the estimated values for k_F, which shows a decrease with increasing pH. This can be described based on the effect of pH on diffusion coefficients. Wang et al. (2001) studied the effect of pH on humic substances diffusivity and showed that the value of diffusion coefficients increased by decreasing the pH. According to the authors' explanations, the shape of humic molecules changes due to neutralization of functional groups (e.g., carboxylic and phenolic groups) at different pH. The effect of pH on the size and shape of humic molecules was studied by Schnitzer and Kodama (1975) who showed that humic molecules are transformed from small spheroidal aggregates to flat sheet perforated by voids of various dimensions by increasing pH.

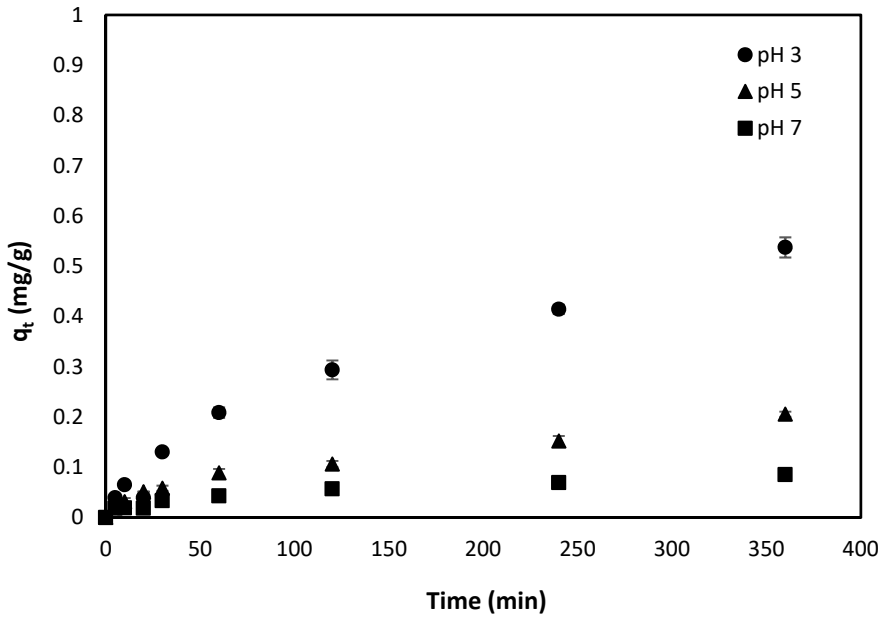

Figure 5-4. NOM adsorption of 10 mg L^{-1} initial concentration on the surface of photocatalytic spheres at different pH. Error bars represent the standard errors for the triplicate runs.

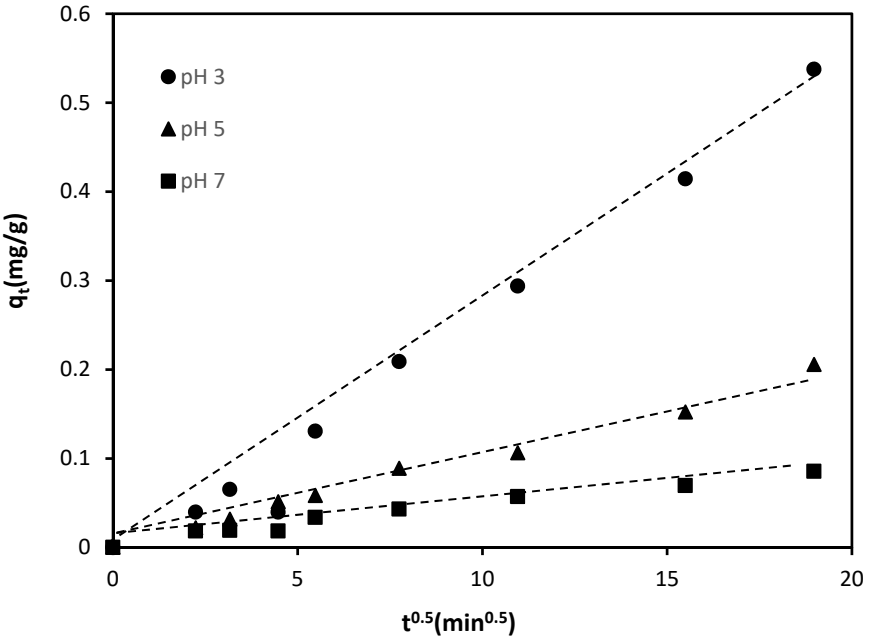

Figure 5-5. NOM adsorption of 10 mgL^{-1} initial concentration on the surface of photocatalyst spheres at different pH; Fickian diffusion.

Table 5-2. Experimental Fickian diffusion constants (k_F) of NOM at different pH

pH	$k_F \times 10^2$ (mg. $g^{-1}min^{-3/2}$)	R^2
3	2.92 ± 0.10	0.990
5	1.03 ± 0.05	0.995
7	0.43 ± 0.06	0.987

5.2.4 NOM fractionation analysis

To further delineate NOM adsorption mechanism, a hydrophobicity fractionation technique was employed to investigate the adsorption of different fractions of NOM. The results showed that Suwannee River NOM (SRNOM) mostly contains hydrophobic (HPO), 76.3%, molecules, while transphilic (TPI) and hydrophilic (HPI) fractions account for about 5.2% and 18%, respectively (Table 5-3). HPO that is adsorbed by DAX-8, contains more aromatic carbons and less hetroaliphatic carbon such as alcohols, esters ethers and carboxylates, while HPI fraction that remains from DAX-4 fraction, has high aliphatic carbon and mostly alcohols (Aiken et al., 1992; Thurman and Malcolm, 1981).

Table 5-3. SRNOM fractionations (post-DAX).

%HPO	%TPI	%HPI
76.31	5.21	18.46

Figure 5-6 shows the adsorption isotherm of 10 mg L^{-1} NOM and its fractions at different pH. By analysing the results, shown in Figure 5-6 and Table 5-3, and subtracting the removal of TPI and HPI fractions from the NOM removal, the percentage of the HPO removal in adsorption isotherm at different pH can be achieved. All (100%) of HPO removes at pH 3, but the removal of the HPO fraction dropps remarkably to 34% and 18% for pH 5 and pH 7, respectively. This significant change is because of the role of electrostatic interaction in adsorption isotherm at pH

higher than 3. HPO contains aliphatic carboxylic acids of 5-9 carbons, one and two-ring aromatic carboxylic acids and, aquatic fulvic acids (Aiken et al., 1992) that are deprotonated and negatively charged at pH>3. At pH 3 the hydrophobic attraction plays a major role in the adsorption process (Newcombe and Drikas, 1997), while at pH>3 the electrostatic repulsion, generally attributed to carboxylic acid and phenolic groups, controls the adsorption (Newcombe and Drikas, 1997).

Likewise, the results (in Figure 5-6) show the removal of HPI at different pH. The removal of HPI fraction reduces from 76% at pH 3 to 30% at pH 5 and pH 7. HPI includes polyfunctional organic acids and aliphatic acids with five or fewer carbon atoms. Compared with the hydrophobic fraction, the HPI molecules have lower molecular weight, with greater hetero-atom and carboxyl content (Aiken et al., 1992). A marked difference between HPI and HPO fractions is not only in different molecular structures, but also in the different sizes of the hydrocarbon chain. HPO fraction includes a hydrocarbon chain higher than 6 carbon atoms (Thurman, 1985b) while a small hydrocarbon chain with the same functional group is categorized as HPI. The considerable adsorption of HPI fraction at pH 3 can be interfered based on the weak electrostatic repulsion. However, higher adsorption of HPI fraction compared to HPO adsorption at pH 5 and pH 7 is due to the different molecular structure. To better understand the impact of HPO and HPI different molecular structures on adsorption, the adsorption of aromatic moieties of NOM and its different fractions were studied. Figure 5-7 shows the specific UV-absorbance (SUVA) of NOM and its fractions at 254 nm. SUVA defined as the ratio of A_{254} to TOC concentration is used as an aromatic character indicator of NOM (Sarathy, 2009). Figure 5-7 shows that 72% of aromatic moieties removed after XAD-4 contact; it might cause improvement of adsorption of PHI at pH 5 and pH 7 because of the absence of aromatic moieties.

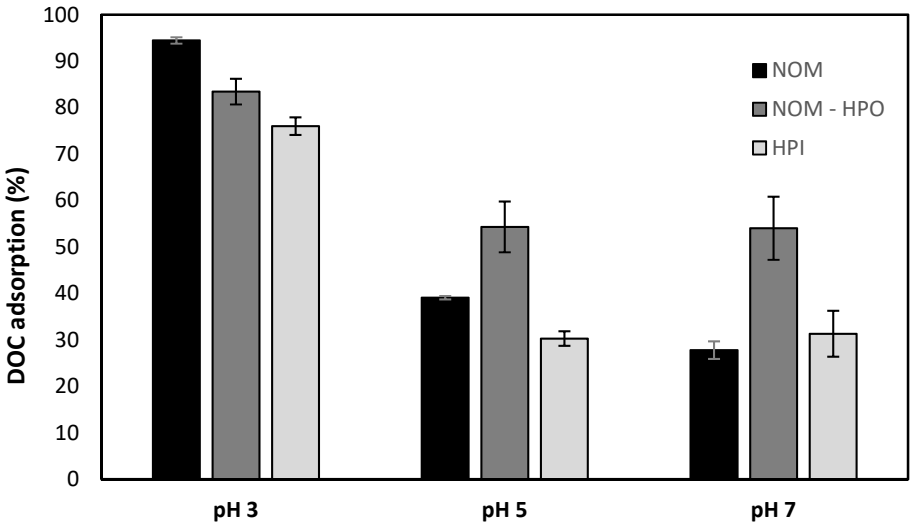

Figure 5-6. Adsorption Isotherm of SRNOM and Post-DAX fractions at different pH. Error bars represent the standard errors for the triplicate runs.

The TPI fraction adsorption behaviour, as shown in Figure 5-6, is similar to HPI fraction. In terms of aromatic moieties concentration, TPI fraction has the same amount as HPI had, as shown in Figure 5-7. However, TPI fraction contains hydrophilic fraction mixed with 5% fulvic and humic acids lost from XAD-8 (Marhaba et al., 2003) that causes an increase in the adsorption at pH>3 compared to HPI fraction.

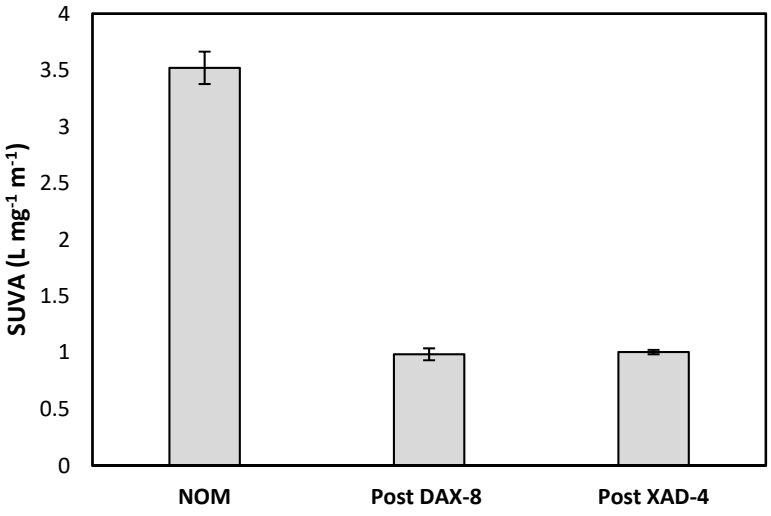

Figure 5-7. SUVA of SRNOM of 10 mg L^{-1} and it fractionations. Error bars represent the standard errors for the triplicate runs.

5.2.5 HPSEC analysis

Figure 5-8 shows (a) the HPSEC chromatograms of NOM and DAX resins effluents (representing HPO, HPI, and TPI fractions) prior to the adsorption process and, (b) the AMW distribution after reaching equilibrium in adsorption process. The HPSEC results indicates a broad molecular weight distribution of different fractions of NOM including HPO (1617 Da), HPI (1230 Da) and, TPI (730 Da). The complete reduction of peak heights at pH 3, as shown in Figure 5-8 (b), confirms the results illustrated in Figure 5-6, indicating high adsorption of NOM at pH 3. However, the removal of NOM is limited at pH>3. At pH 5 and pH 7, the results shows slight preferential removal of HPI and TPI fractions (AMW <1900 Da). In agreement with Figure 5-6, this shows that electrostatic repulsion affects the adsorption of HPO fraction with AMW higher than 1900 Da at pH 5 and 7.

To better understand the pH impact on NOM fractions with different AMW, the HPSEC analysis of NOM during the timewise adsorption at pH 3 was studied. As adsorption progressed, the AMW of NOM decreased as shown in Figure 5-9. Considerable reduction of peak height, specifically for high AMW (>1700) illustrates that the hydrophobic attraction governs the adsorption process.

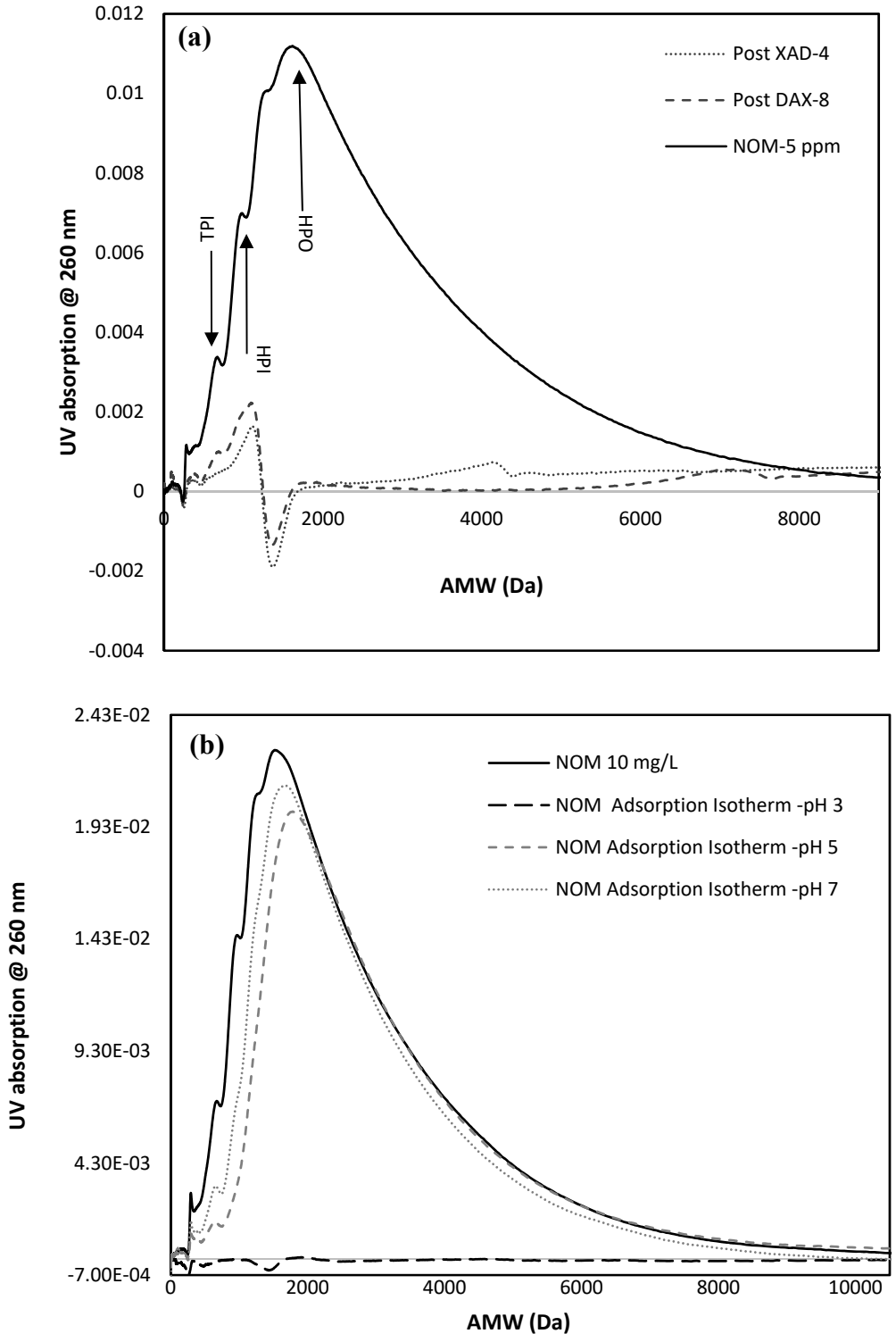

Figure 5-8. HPSEC chromatogram of SRNOM; (a) Post-DAX fractions, (b)after adsorption isotherm of NOM at different pH.

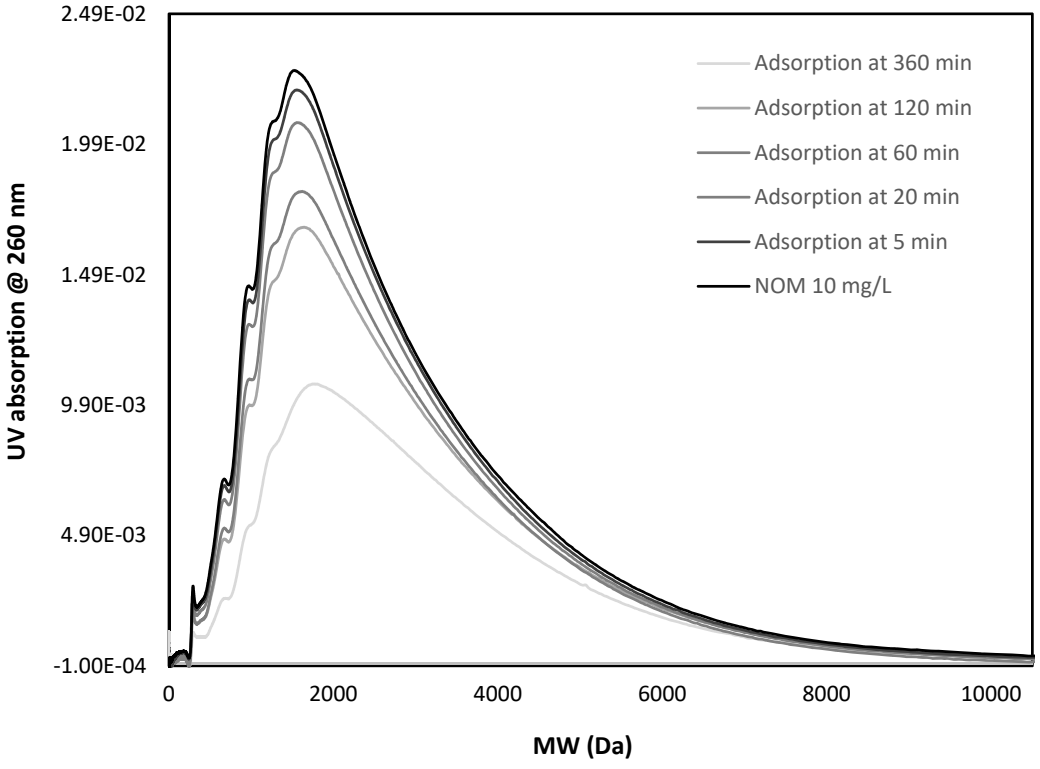

Figure 5-9. HPSEC chromatogram of NOM adsorption at different time at pH 3.

5.2.6 Fourier Transform Infrared (FTIR) analysis

FTIR has been widely used for the characterization of NOM adsorbed on the surface of photocatalyst spheres. FTIR absorption spectrum is a unique fingerprint of compounds, allowing the identification of both inorganic and organic functional groups.

Figure 5-10 shows the FTIR analysis of adsorbed NOM of 60mgL^{-1} COD on the photocatalyst surface at different pH. NOM adsorption at different pH indicates that the NOM bonded via the C-O group (1050 cm^{-1}) associated with alcohols, ethers, and polysaccharides, carboxylic groups (R-COOH) (1253 cm^{-1}, 1400 cm^{-1}, 1707 cm^{-1}), C=C alkenes and aromatic rings structures for the humic substances (1613 cm^{-1}) and, CH_3 and CH_2 groups due to the C–H stretch (2850–2960 cm^{-1}) (Hay and Myneni, 2007; Howe et al., 2002; Rodríguez and Núñez, 2011).

The FTIR results show that the adsorption of NOM from different functional groups at pH 5 and 7, is much lower than that at pH 3. The same peak height of 1613 cm^{-1} and 1707 cm^{-1} at pH 3 indicated the adsorption of C=C alkenes and aromatic rings (1613 cm^{-1}), and C=O stretching vibration from carboxyl group (1707 cm^{-1}) is changed at pH>3, which shows the preferential adsorption of C=O stretching vibration from the carboxyl group. The results also show that the low ratio of adsorption of alcohol or polysaccharides groups (1056 cm^{-1}) to C-O-H of carboxyl groups (1253 cm^{-1}) is changed at pH 3 to pH>3. This indicates the higher adsorption of alcohol or polysaccharides groups than those of the carboxylic group at pH>3.

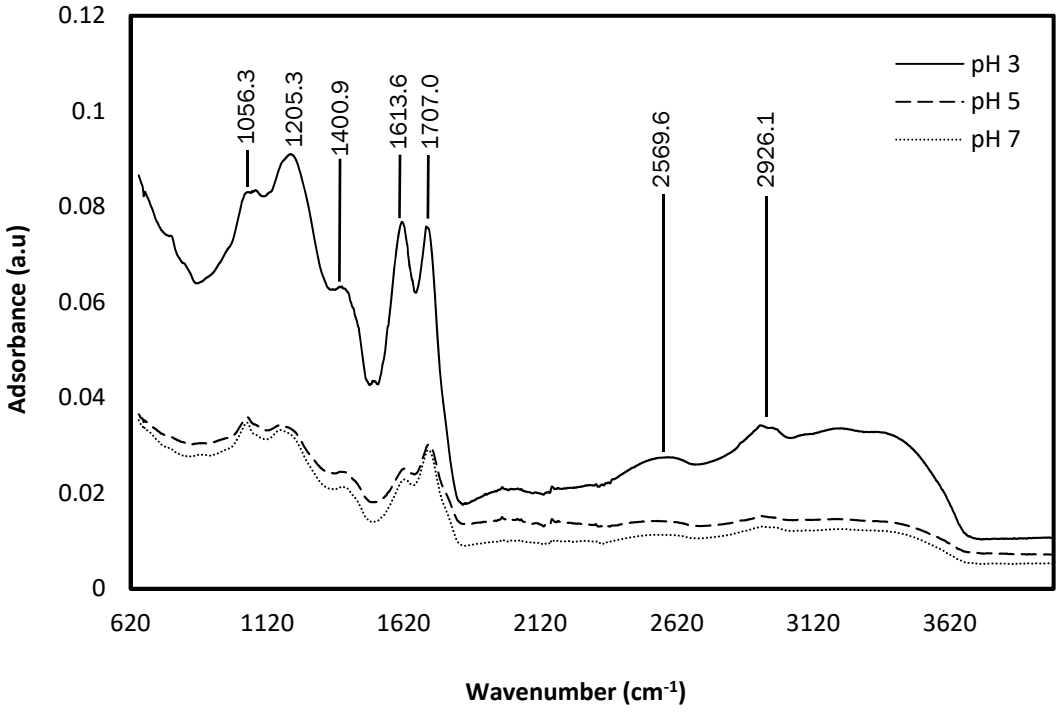

Figure 5-10. ATR-FTIR spectra of SRNOM of 60 mgL^{-1} adsorbed on the surface of photocatalytic spheres

5.3 Conclusions

In this research, the effect of pH on the adsorption of NOM on the surface of TiO_2 photocatalyst spheres was studied. At pH 3, where electrostatic interactions were minimised, the hydrophobic interaction governed the adsorption process. High adsorption at pH 3 indicated that

photocatalytic spheres had a very high capacity for adsorbing NOM under low electrostatic interaction conditions. At pH>3, the electrostatic repulsion between NOM_{ads} and NOM_{sol} remarkably reduced the adsorption of NOM. FTIR analysis and fractionation of NOM showed that aromatic carboxyl groups were deprotonated and played the major role in reducing the adsorption at pH>3. Moreover, the effect of pH on adsorption isotherm models was considerable. It causes exchanging the multi-layer adsorption of Freundlich at pH 3 to monolayer adsorption capacity characteristic of Langmuir isotherm at pH>3.

Supplementary information

Supplementary data related to this chapter are presented in Appendix A.

Chapter 6: PHOTOCATALYTIC OXIDATION KINETICS AND THE IMPACT OF pH

6.1 Introduction

Photocatalysis is a process where a semiconductor is activated by UV radiation to produce hydroxyl radicals. Hydroxyl radicals are bound or diffuse into the solution to act as the primary oxidants in the photocatalytic system. Hoffmann et al. (1995) analyzed the kinetics of photocatalytic oxidation of several acidic and non-acidic organic compounds. Assuming that all reactions take place on the surface of photocatalyst, the authors used the Langmuir-Hinshelwood (L-H) kinetic model to express the photocatalytic oxidation rates. While there was a verification for the presence of hydroxyl radical in the solution ($^{\bullet}OH_{aq}$)(Cunningham and Srijaranai, 1988; Hoffmann et al., 1995; Howe and Gratzel, 1985; Liao and Reitberger, 2013; Ollis, 2005), Hoffmann et al. (1995) did not consider $^{\bullet}OH_{aq}$ oxidation in their kinetics analysis.

There is strong evidence for the contribution of $^{\bullet}OH_{aq}$ in photocatalytic oxidation (Fu et al., 2006; Hoffmann et al., 1995; Turchi and Ollis, 1990), even though $^{\bullet}OH_{aq}$ has been considered equal to adsorbed hydroxyl radical ($^{\bullet}OH_{ads}$) in many kinetic studies. This is probably due to the difficulty in assessing the role of $^{\bullet}OH_{aq}$ given the very short life of hydroxyl radicals and their high activity, resulting in $^{\bullet}OH_{aq}$ diffusing a very short distance from the surface of the photocatalyst before being consumed (Liao and Reitberger, 2013; Pichat, 2007)

Tunesi et al. (1991) studied the photocatalytic oxidation pathways and showed that there is a marked difference between decomposition via charge transfer on the surface of photocatalyst, and oxidation via $^{\bullet}OH_{aq}$ attack in the solution. The different photocatalytic oxidation pathways can be explained on the basis of the solution pH. Tunesi et al. (1991) made a connection between

pH effect on TiO_2 adsorption capability and photocatalytic mechanism but authors could not delineate how the kinetic of the photocatalytic oxidation changes according to the solution pH.

While several studies have been performed around the effect of pH on photocatalytic oxidation (Du and Rabani, 2003; Sakthivel et al., 2003; Tunesi and Anderson, 1991), detailed information on the effect of pH on photocatalytic oxidation kinetics is still lacking. The effect of pH on photocatalytic mechanism needs through analysis in order to gain an understanding of the impact of pH. In this chapter, a new kinetic model will be theoretically developed and experimentally validated to interpret the photocatalytic oxidation at different pH. It will be analyzed and demonstrated that photocatalytic oxidation kinetic models change according to the solution pH. Furthermore, it will be illustrated how pH impacts various kinetic parameters.

6.2 Theory of the pH effect on Photocatalytic mechanism

Photocatalytic removal of contaminants includes two main processes; adsorption and photocatalytic oxidation (Legrini et al., 1993; Turchi and Ollis, 1990; Wang et al., 2011). The photocatalytic oxidation mechanism may be described by the following sequence of elementary reaction steps: excitation, recombination, charge trapping, generation of oxidant species, and organic decomposition. Below are brief analyses of each of the two processes of adsorption and oxidation:

6.2.1 Adsorption

Adsorption encompasses the adsorption of reactant and water (Eq (6-1) and Eq (6-2)). As explained earlier, in an aqueous medium, the surface TiO_2 is readily hydroxylated. Ti cations can bind to oxygen atoms of water molecules which are adsorbed on the surface of the photocatalyst and dissociated to OH^- groups (Eq (6-2)).

$$Site + R_L \rightleftharpoons R_{ads} \qquad (K = k_1/k_{-1}) \tag{6-1}$$

$$TiO_2 + H_2O \rightleftharpoons Ti - OH^- + H_s^+ \qquad (k_2) \tag{6-2}$$

where R_L and R_{ads} are non-adsorbed and adsorbed reactant, respectively. Attributable to TiO_2 amphoteric behaviour, pH plays the main role in the adsorption of reactants. The TiO_2 surface is positively charged ($TiOH_2^+$) at pH< pH_{zpc}, whereas it is negatively charged (TiO^-) at pH>pH_{zpc}; hence, influencing the micropollutant adsorption and its degradation pathways (Šojić et al., 2009; Tunesi and Anderson, 1991).

$$pH < pH_{zpc} \qquad Ti - OH + H^+ \rightleftarrows TiOH_2^+ \qquad (k_3) \tag{6-3}$$

$$pH > pH_{zpc} \qquad Ti - OH + OH^- \rightleftarrows Ti - O^- + H_2O \qquad (k_4) \tag{6-4}$$

The electrostatic repulsion between the reactant anion and the oxide surface reduces the adsorption and increases the distance between reactant and the photocatalyst surface. The increased distance between the reactant and photocatalyst causes reduced direct charge transfer.

6.2.2 Photocatalytic oxidation

Photocatalytic reaction is initiated when UV radiation activates a photocatalyst. UV radiation excites the electrons in the valence band to the conduction band, resulting in the formation of a positive hole (h_{vb}^+) in the valence band and an electron (e_{cb}^-) in the conduction band.

$$TiO_2 \overset{h\nu}{\rightarrow} TiO_2\ (e_{cb}^- + h_{vb}^+) \qquad (k_{ex}) \tag{6-5}$$

The overall rate of photocatalytic reactions in aqueous systems is governed by the capture of electrons and positive holes, and also by the electron–hole re-combination (e^--h^+), Eq (6-6) to Eq (6-10) (Du and Rabani, 2003; Gaya, 2014b; Hoffmann et al., 1995; Ikeda et al., 2003). Charge carrier trapping suppresses re-combination of the electron-hole pair, and increases the lifetime of the separated electron and hole. The electron in the conduction band reduces adsorbed oxygen to produce supper oxide (Eq (6-9)), whereas the positive hole oxidizes either the reactant directly

(see Eq (6-10)), or the adsorbed water to produce hydroxyl radical ($^{\bullet}OH$), as shown in Eq.(6-7) (de Lasa et al., 2005c; Duran, 2010; Hoffmann et al., 1995).

$$e_{cb}^{-} + h_{vb}^{+} \rightarrow heat \qquad (k_{rec}) \qquad (6\text{-}6)$$

$$Ti^{4+}OH + h^{+} \rightleftharpoons Ti^{4+}OH^{\bullet} \qquad (k_7/k_{-7}) \qquad (6\text{-}7)$$

$$Ti^{4+} + e^{-} \rightleftharpoons Ti^{3+} \qquad (k_8) \qquad (6\text{-}8)$$

$$Ti^{3+} + O_2 \rightleftharpoons Ti^{4+} - O_2^{\bullet -} \qquad (k_9) \qquad (6\text{-}9)$$

$$R_{ads} + h^{+} \rightarrow R_{ads}^{\bullet} \qquad (k_{10}) \qquad (6\text{-}10)$$

Rothenberger et al. (1985) indicated that pH affects the rate of charge trapping. It was also shown that the hole trapping occurs on a time scale (nano-second) much longer than that for the electron (pico-second) (Rothenberger et al., 1985). Therefore, we can assume low recombination rate and high oxidation rate via positive holes on TiO_2 at low pH. As will be shown later, this conclusion of the effect of pH on the trapping charge process plays the major role in the kinetic analysis.

pH also impacts the generation of $^{\bullet}OH_{aq}$; at $pH > pH_{zpc}$ hydroxyl radicals can diffuse into the solution (see Eq (6-11)) to produce $^{\bullet}OH_{aq}$. In contrast, at acidic pH (pH 3) the diffusion rate is very low (Liao and Reitberger, 2013).

$$Ti^{4+}OH^{\bullet} \overset{h\nu}{\rightarrow} Ti^{4+} + OH_{aq}^{\bullet} \qquad (k_{11}) \qquad (6\text{-}11)$$

The other oxidant species, which may contribute to the photocatalytic oxidation process, is perhydroxyl radical ($HO_2^{\bullet}$). The reaction for $HO_2^{\bullet}$ formation (see Eq. (6-12)) is largely pH dependent (the pK_a of perhydroxyl radical is 4.8) (Du and Rabani, 2003; Nosaka and Nosaka, 2013; Pichat, 2007). The contribution of perhydroxyl radical oxidation even at pH 3 has not been considered in this research, because the rate constant of perhydroxyl radical reaction with the reactant is 10^3 times lower than that of hydroxyl radical oxidation (Yoon et al., 2009).

$$pK_a = 4.8 \qquad Ti^{4+} - O_2^{\bullet -} + H^+ \rightleftharpoons Ti^{4+}(HO_2^{\bullet}) \qquad (k_{12}) \tag{6-12}$$

This review of the effect of pH on the photocatalytic mechanism will be used in developing and understanding the kinetic of photocatalytic process in this chapter. Reactions were selected based on their contribution at different pH.

6.3 Results and discussion

Figure 6-1 shows the overall removal of 2,4-D at pH 7 and pH 3. In agreement with results demonstrated in chapter 4, adsorption of 2,4-D is not significant at neutral pH, while nearly 60% of initial 2,4-D is adsorbed on the surface of photocatalyst at pH 3. It is, hence, hypothesized that $^{\bullet}OH_{aq}$ attack is the predominant process for oxidization of 2,4-D at pH 7, whereas all oxidant species, positive holes (trapped and un-trapped) and free hydroxyl radicals in the solution, contribute towards the degradation of 2,4-D at pH 3. This hypothesis will be evaluated through a detailed theoretical analysis and further validated by experimental data.

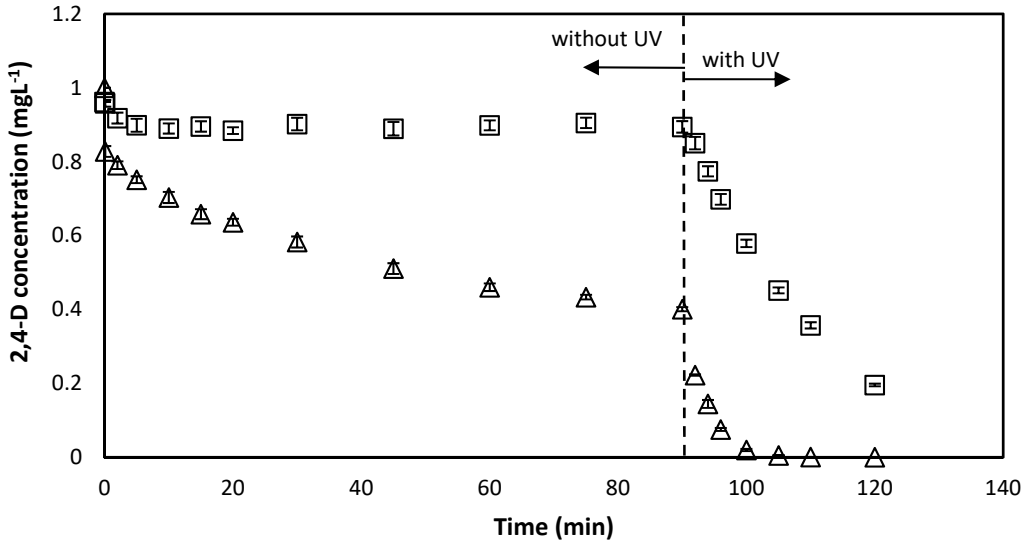

Figure 6-1. Photocatalytic oxidation of 2,4-D with the initial concentration of 1 mgL^{-1} in a fluidized photocatalytic reactor at (Δ) pH 3 and (□) pH 7. Error bars represent the standard errors for the triplicate runs.

6.3.2 Photocatalytic oxidation kinetic analysis at pH 7

Since the adsorption at pH 7 is very negligible, it is assumed that photocatalytic oxidation occurred by the reaction of non-adsorbed reactant and $^{\bullet}OH_{aq}$, Eq (6-13):

$$OH^{\bullet}_{aq} + R_L \rightarrow R^{\bullet}_L \qquad (k_{aq}) \tag{6-13}$$

$$r_{pH7} = k_{aq}[R_L][OH^{\bullet}_{aq}] \tag{6-14}$$

Therefore, reactions presented earlier through Eq (6-4) to Eq (6-9), Eq (6-11), and Eq (6-13) can be considered. Once can denote the trapped positive hole ($[Ti^{4+}OH^{\bullet}]$) as adsorbed hydroxyl radical $[OH^{\bullet}_{ads}]$. Assuming a steady state approximation for the concentration of $OH^{\bullet}_{aq}$ leads to:

$$\frac{d[OH^{\bullet}_{aq}]}{dt} = k_{11}[OH^{\bullet}_{ads}] - k_{aq}[OH^{\bullet}_{aq}][R_L] - \sum_{i=2}^{n} k_{Ri}[OH^{\bullet}_{aq}][R_{Li}] \cong 0 \tag{6-15}$$

$$[OH^{\bullet}_{aq}] = \frac{k_{11}[OH^{\bullet}_{ads}]}{k_{aq}[R_L] + \sum_{i=2}^{n} k_{Ri}[R_{Li}]} \tag{6-16}$$

where R_{Li} and k_{Ri} are 2,4-D intermediates and their rate constants, respectively. To obtain the concentration of $OH^{\bullet}_{aq}$, it is necessary to have the concentration of $OH^{\bullet}_{ads}$, which under steady state condition, can be obtained by:

$$\frac{d[OH^{\bullet}_{ads}]}{dt} = \alpha k_7[h^+][TiOH]a_s - k_{-7}[OH^{\bullet}_{ads}]a_s - k_{11}[OH^{\bullet}_{ads}]a_s \cong 0 \tag{6-17}$$

In this analysis the oxidation of intermediates of 2,4-D on the surface of the catalyst were not considered because intermediates of 2,4-D oxidation possess pK_a higher than 8 (Rezaei and Mohseni, 2017b). 2,4-D intermediates because of high pK_a, are desorbed immediately from the surface of the photocatalyst. This hypothesis was further substantiated by analyzing the

concentration of organics desorbed from the surface of photocatalyst during the reactivation process.

One may assume that the photocatalyst hydrolysis by water and adsorption by oxygen reaches an equilibrium before the photocatalytic oxidation starts and will be constant during the process (Turchi and Ollis, 1990). This means $k_7[TiOH] = k_7'$. Therefore:

$$[OH^{\bullet}_{ads}] = \frac{k_7'[h^+]}{k_{7^-} + k_{11}} \tag{6-18}$$

Similarly, if one uses the steady state approximation for the concentration of h^+, it will lead to:

$$\frac{d[h^+]}{dt} = k_{ex} I a_c - k_{rec}[h^+][e^-]a_s - k_7'[h^+]a_s + k_{7^-}[OH^{\bullet}_{ads}]a_s \cong 0 \tag{6-19}$$

The formation of Ti^{3+} species, in Eq (6-8), is very low in non-acidic solution (Howe and Gratzel, 1985). In other words, the concentration of e^- is supposed to be high at pH 7. On the other hand, Rothenberger et al. (1985) showed that the recombination rate is 10 times faster than h^+ trapping. In conclusion, the concentration of h^+ is high and the recombination rate is fast. Therefore, Eq (6-19) can be modified to Eq (6-21) based on the following assumption:

$$[h^+] = [e^-] \;\; \& \;\; k_{rec}[h^+][e^-]a_s = k_{rec}[h^+]^2 a_s \gg k_7'[h^+]a_s - k_{7^-}[OH^{\bullet}_{ads}]a_s \tag{6-20}$$

$$\frac{d[h^+]}{dt} = k_{ex} I a_c - k_{rec}[h^+]^2 a_s \cong 0 \tag{6-21}$$

Therefore:

$$[h^+] = \sqrt{\frac{k_{ex} I a_c}{a_s k_{rec}}} \tag{6-22}$$

$$[h^+] = \beta\sqrt{I} \quad and \ \beta = \sqrt{\frac{k_{ex}a_c}{a_s k_{rec}}} \tag{6-23}$$

Hence:

$$[OH^{\bullet}_{ads}] = \frac{k'_7\beta\sqrt{I}}{k_{-7} + k_{11}} \tag{6-24}$$

Finally, combining Eq. (6-14), Eq. (6-16) and Eq. (6-24), will provide:

$$r_{pH7} = \frac{\beta k'_7 k_{11} k_{aq}[R_L]}{\left(k_{aq}[R_L] + \sum_{i=2}^{n} k_{Ri}[R_{Li}]\right)(k_{-7} + k_{11})}\sqrt{I} \tag{6-25}$$

Hydroxyl radical is a nonselective and very strong oxidant; the rate constants for •OH is generally in the order of 10^9 $M^{-1}s^{-1}$ (Turchi and Ollis, 1990). Therefore, one can assume that $k_{aq} = k_{Ri}$ simplifying Eq (6-25).

$$r_{pH7} = k_{obs7}[R_L] \tag{6-26}$$

where

$$k_{obs7} = \frac{k'_7 k_{11}\left(\frac{k_{ex}a_c}{s_p k_{rec}}\right)^{1/2}}{(k_{-7} + k_{11})} \times \frac{\sqrt{I}}{[R_{0L}]} \tag{6-27}$$

where R_{0L} is the initial concentration of the reactant, considered equal to the concentration of R_L plus the intermediates present in the system ($[R_L] + \sum_{i=2}^{n}[R_{Li}]$) before CO_2 is formed through complete mineralization.

Eq (6-26) shows that the photocatalytic oxidation at pH>pH_{pzc} followed the first order kinetic equation with respect to the reactant concentration. It should be noted that k_{obs7} is a function of $\sqrt{I}$ and initial concentration of the reactant (See Eq (6-27)).

To validate the kinetic model, an experiment was performed to measure the photocatalytic oxidation rate of 2,4-D at different initial concentrations. Figure (6-2) shows that the apparent rate constant (k_{obs7}) decreases by increasing the initial concentration. To correspond the value of the experimental rate constant to the k_{obs7} obtained from the model, there is an inverse relationship between the experimental k_{obs7} and initial concentration, which is in agreement with Eq (6-27).

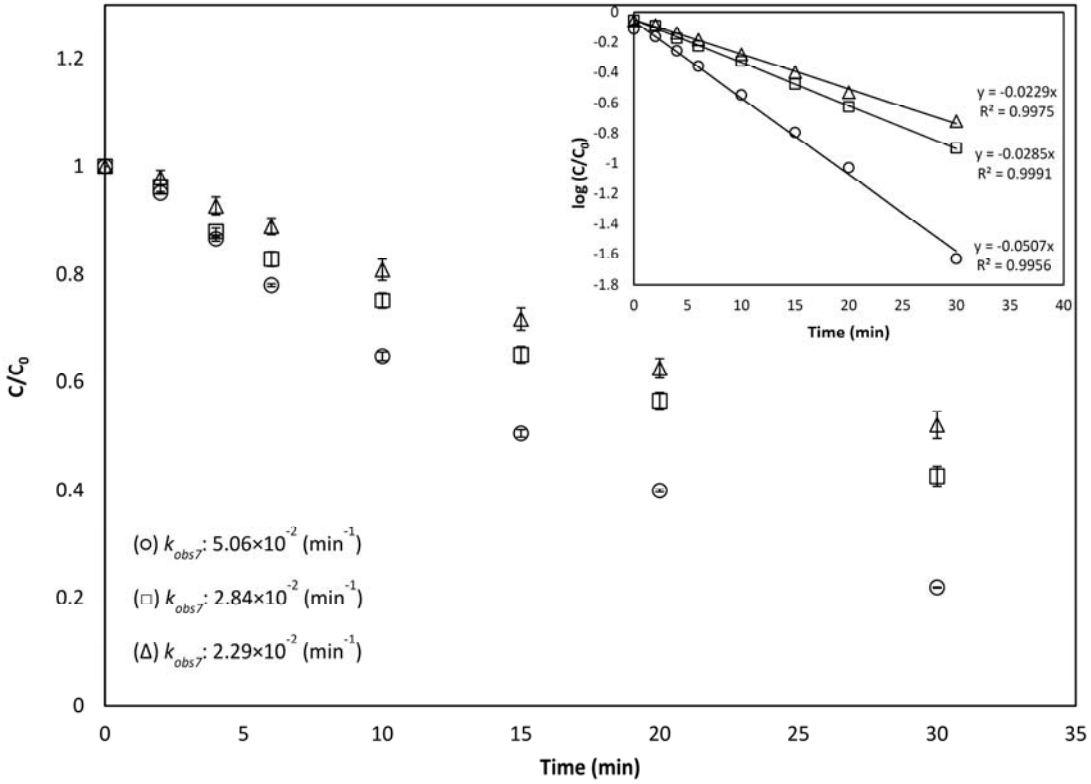

Figure 6-2. Photocatalytic oxidation of 2,4-D in a fluidized photocatalytic reactor at pH 7 with different initial concentration of; (○) 1 mgL^{-1}, (□) 4 mgL^{-1}, and (Δ) 7 mgL^{-1}. Error bars represent the standard errors for the triplicate runs. Full lines represent best-fit lines of first order kinetic model.

6.3.3 The photocatalytic oxidation kinetic analysis at pH 3

At pH 3, due to the high adsorption of the reactant, the oxidation mechanism is more complicated. A series of reactions, i.e., Eq (6-1), and Eq (6-3), Eq (6-5) to Eq (6-11), and Eq (6-13) are involved in oxidizing 2,4-D as target contaminant at pH 3. Reactant can be oxidized

on the surface of photocatalyst via positive holes (Eq (6-10) and Eq (6-28)) or in the solution via hydroxyl radical attack (Eq (6-13)).

$$Ti^{IV}OH^{\bullet} + R_{ads} \rightarrow Ti^{III} + R_{ads}^{\bullet} \qquad (k_{ads}) \qquad (6\text{-}28)$$

$$R_{ads} + h^{+} \rightarrow R_{ads}^{\bullet} \qquad (k_{10}) \qquad (6\text{-}10)$$

$$OH_{aq}^{\bullet} + R_L \rightarrow R_L^{\bullet} \qquad (k_{aq}) \qquad (6\text{-}13)$$

Therefore, three following reactions are considered:

$$r_{ads1} = k_{10}[R_{ads}][h^{+}]a_s \qquad (6\text{-}29)$$

$$r_{ads2} = k_{ads}[R_{ads}][OH_{ads}^{\bullet}]\, a_s \qquad (6\text{-}30)$$

$$r_{aq3} = k_{aq}[R_L][OH_{aq}^{\bullet}] \qquad (6\text{-}31)$$

where the overall photocatalytic oxidation (r_{pH3}) will be the summation of Eq (6-29) to Eq (6-31).

Similarly, a steady state approximation for the concentration of h^+ at pH 3 is assumed:

$$\frac{d[h^{+}]}{dt} = k_{ex}Ia_c - k_{rec}[h^{+}][e^{-}]s_p - k_7[TiOH][h^{+}]a_s + k_{-7}[OH_{ads}^{\bullet}]a_s - k_{10}[R_{ads}][h^{+}]a_s \cong 0 \qquad (6\text{-}32)$$

The positive hole trapping and recombination rate are dependent on the pH; in the acidic medium, the charge transfer occurred very fast (Rothenberger et al., 1985). At pH 3, on the other hand, the high concentration of Ti^{3+} is evidence of a low recombination rate. Therefore, one may assume:

$$k_{rec}[h^{+}]^2 s_p \ll k_7[TiOH][h^{+}]a_s - k_{-7}[OH_{ads}^{\bullet}]a_s + k_{10}[R_{ads}][h^{+}]a_s \qquad (6\text{-}33)$$

The concentration of h^+ will then be:

$$[h^{+}] = \frac{k_{ex}Ia_c + k_{-7}[OH_{ads}^{\bullet}]a_s}{k_7[TiOH]a_s + k_{10}[R_{ads}]a_s} \qquad (6\text{-}34)$$

Since the consumption rate of e^- is faster than the h^+ trapping rate, the reaction in Eq (6-7) is merely on path to generate $OH^{\bullet}_{ads}$. Therefore, one may assume that k_{-7} is very low.

$$[h^+] = \frac{k_{ex} I a_c}{k_7 [TiOH] a_s + k_{10} [R_{ads}] a_s} \tag{6-35}$$

Fujishima et al. (2008) studied electron-hole capturing rates and showed that the rate of positive hole capturing by water (k_7) is almost 40 times greater than that reactant (k_{10}). Moreover, because the number of adsorbed water molecules due to higher water concentration is substantially higher than that of 2,4-D ($[TiOH] \gg [R_{ads}]$) we may assume $k_7[TiOH] \gg k_{10}[R_{ads}]$.

$$r_{ads1} = k_{10}[R_{ads}][h^+]a_s = \frac{k_{10} k_{ex} I a_c [R_{ads}]}{k_7 [TiOH]} \tag{6-36}$$

According to Eq (6-1), $[R_{ads}] = K [R_L][site]$ where $K = k_1/k_{-1}$ and $k_7[TiOH] = k_7'$ Therefore,

$$r_{ads1} = k'[R_L] \tag{6-37}$$

where

$$k' = \frac{a_c k_{10} k_{ex} K [site]}{k_7'} I \tag{6-38}$$

Eqs. (6-37) and (6-38) show that oxidation on the surface of the catalyst via positive holes follows the first order kinetic model and k' as a function of UV intensity, is independent of initial 2,4-D concentration (see Eq (6-38)).

Similarly, using steady state approximation for the concentration of $OH^{\bullet}_{ads}$ gives:

$$\frac{d[OH^{\bullet}_{ads}]}{dt} = k_7 [TiOH][h^+]a_s - k_{11}[OH^{\bullet}_{ads}]a_s - k_{ads}[OH^{\bullet}_{ads}][R_{ads}]a_s \cong 0 \tag{6-39}$$

Therefore,

$$[OH^{\bullet}_{ads}] = \frac{k_7[TiOH][h^+]}{k_{11} + k_{ads}[R_{ads}]} \tag{6-40}$$

Combining Eq (6-35) and Eq (6-40), leads to:

$$[OH^{\bullet}_{ads}] = \frac{k_7[TiOH]k_{ex}Ia_c}{a_s(k_7[TiOH] + k_{10}[R_{ads}])(k_{11} + k_{ads}[R_{ads}])} \tag{6-41}$$

As previously explained, $k_7[TiOH] \gg k_{10}[R_{ads}]$. Thus:

$$[OH^{\bullet}_{ads}] = \frac{k_{ex}Ia_c}{a_s(k_{11} + k_{ads}[R_{ads}])} \tag{6-42}$$

Combining Eq (6-42) and Eq (6-30):

$$r_{ads2} = k_{ads}[R_{ads}][OH^{\bullet}_{ads}]a_s = \frac{a_c k_{ex} k_{ads}[R_{ads}]I}{(k_{11} + k_{ads}[R_{ads}])} \tag{6-43}$$

$$r_{ads2} = \frac{k''[R_L]}{1 + \kappa''[R_L]} \tag{6-44}$$

where

$$k'' = \frac{a_c k_{ex} k_{ads} K[site]}{k_{11}} I \tag{6-45}$$

$$\kappa'' = \frac{k_{ads} K[site]}{k_{11}} \tag{6-46}$$

Eq (6-44) shows that the oxidation via trapped positive holes follows the L-H model. Furthermore, k'' is a function of the intensity and independent of initial 2,4-D concentration.

The concentration of $^{\bullet}OH_{aq}$ at pH 3 can be obtained by combining of $^{\bullet}OH_{aq}$ rate balance and Eq (6-42)

$$[OH^{\bullet}_{aq}] = \frac{a_c k_{ex} k_{11} I}{a_s(k_{11} + k_{ads}[R_{ads}])\left(k_{aq}[R_L] + \sum_{i=2}^{n} k_{Ri}[R_{Li}]\right)} \tag{6-47}$$

By incorporating the above into Eq (6-31), the reaction rate of $^{\bullet}OH_{aq}$ with the target contaminant in the solution will be:

$$r_{aq3} = \frac{k'''[R_L]}{1 + \kappa'''[R_L]} \tag{6-48}$$

$$k''' = \frac{a_c k_{ex}}{a_s[R_{L0}]} I \tag{6-49}$$

$$\kappa''' = \kappa'' = \frac{k_{ads} K[site]}{k_{11}} \tag{6-50}$$

Eq (6-49) shows that while k''' like k'' and k' is a function of intensity, is depends on the initial concentration of the reactant.

Therefore, the overall rate of 2,4-D photocalytic at pH 3 will be:

$$r_{pH3} = r_{ads1} + r_{ads2} + r_{aq3} = k'[R_L] + \frac{k_{obs3}[R_L]}{1 + \kappa''[R_L]} \tag{6-51}$$

$$k_{obs3} = k'' + k''' = (\frac{k_{ads} K[site]}{k_{11}} + \frac{1}{a_s[R_{0L}]}) k'_{ex} \tag{6-52}$$

$$k'_{ex} = a_c k_{ex} I \tag{6-53}$$

The kinetic models at both acidic and neutral pH were compared with experimental results. Figure 6-3 shows that the rate of 2,4-D disappearance at pH 3 is higher than the disappearance rate at pH 7. This difference could be explained based on the different relationships of the rate constants to the intensity at different pH. As is shown in Eqs (6-52) and (6-53), photocatalytic oxidation rate at pH 3 is a function of UV intensity (I), while the rate at pH 7 is related to $(I)^{1/2}$, as shown in Eq (6-27).

Eq (6-51) shows that 2,4-D photocatalytic oxidation kinetic is a combination of L-H and first-order kinetic models at low pH. Oxidation via hydroxyl radicals attack, either on the surface of photocatalyst or in the solution, follows the L-H model, whereas positive hole oxidation is described by the first-order kinetic model. Kinetic parameters introduced in Eq (6-51) were calculated using least-squares optimization technique (See Table 1) and the results, in agreement with Eq (6-52), show that the first order kinetic model can interpret the oxidation of 2,4-D at low concentration.

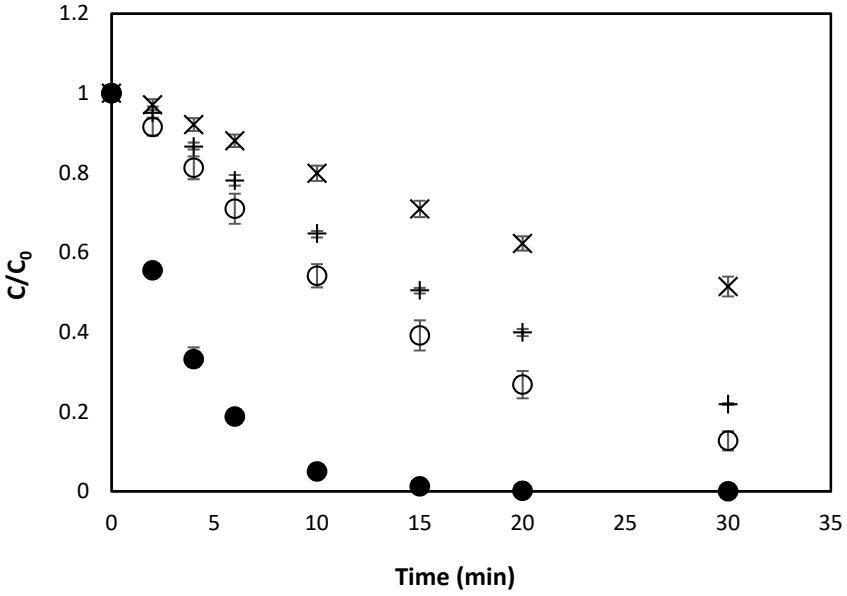

Figure 6-3. 2,4-D degradation in a fluidized bed photocatalytic reactor at different pH and initial concentration; (●) 1 mgL^{-1} 2,4-D at pH 3, (○) 7 mgL^{-1} 2,4-D at pH 3, (+)1 mgL^{-1} 2,4-D at pH 7 and, (×)7 mg/L 2,4-D at pH 7. Error bars represent the standard errors for triplicate runs.

Furthermore, the results (Table 6-1) show that the kinetic parameters are independent of initial concentration at pH 3. However, K_{obs3} which includes $^{\bullet}OH_{aq}$ and $^{\bullet}OH_{ads}$ rate constants, has an inverse relationship with 2,4-D initial concentration. This is because of 2,4-D intermediates that participate in photocatalytic oxidation via $^{\bullet}OH_{aq}$ in the solution.

Table 6-1- Estimated kinetics parameters for the kinetic model described by Eq (6-51) to (6-53). 2,4-D photocatalytic oxidation with different initial concentration at pH 3

Initial concentration (mgL^{-1})	$k' \times 10^3 (min^{-1})$	$k'_{ex} \times 10^3$ (min^{-1})	$\kappa'' \times 10^3$ ($m^3 g^{-1}$)
1	10	227	255
4	11	230	222
7	10	201	233

Figure 6-4 shows the photocatalytic oxidation of 2,4-D with different initial concentration at pH 3 along with the agreement of experimental results with the developed kinetic model. Obviously, results show that the developed model could successfully fit experimental data. Reducing k_{obs3} obtained from the model with increasing 2,4-D initial concentration indicates the effect of 2,4-D initial concentration on k_{obs3} values as estimated in the model.

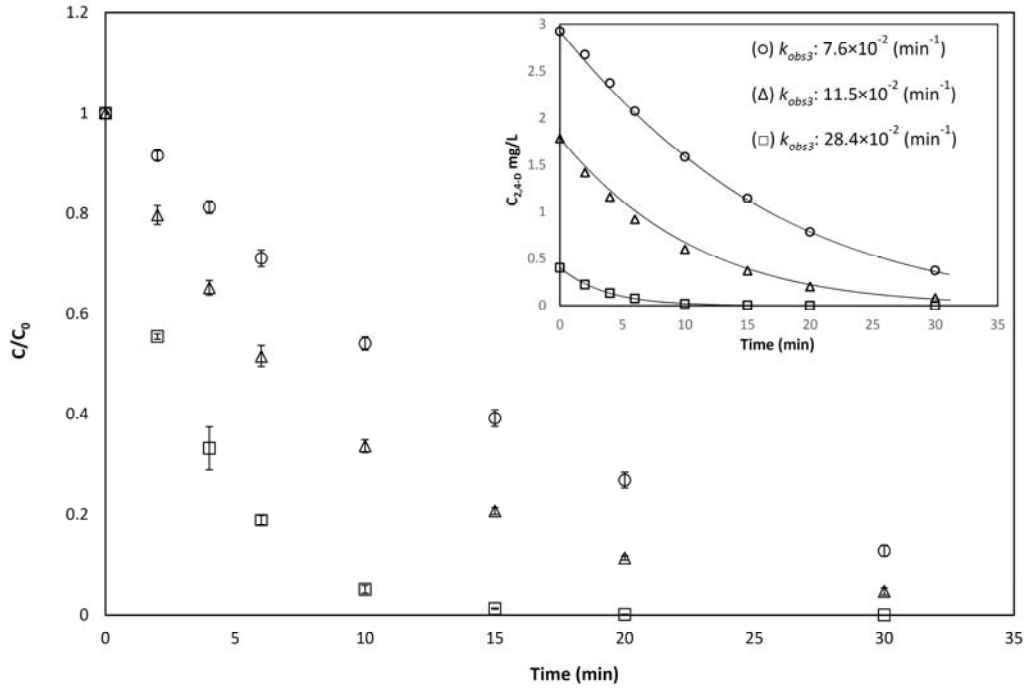

Figure 6-4. Photocatalytic oxidation of 2,4-D in a fluidized photocatalytic reactor at pH 3 with different initial concentration of; (□) 1 mgL^{-1}, (Δ) 4 mgL^{-1}, and (○) 7 mgL^{-1}. Error bars represent the standard errors for the triplicate runs. Full lines represent best-fit curves of the kinetic model developed for photocatalytic oxidation at pH 3

6.4 Conclusion

The effect of pH on the kinetic of photocatalytic oxidation was discussed in this chapter. The photocatalytic oxidation kinetics changed due to the impact of pH on photocatalyst surface charge and the energies of conductance and valence band. Results showed that the photocatalytic oxidation at $pH > pH_{zpc}$ (pH 7) followed first order kinetic model. At $pH < pH_{zpc}$ (pH 3), on the other hand, the rate of oxidation was a combination of the first order and L-H models. Oxidation of 2,4-D intermediates by hydroxyl radicals attack in the solution causes an inverse relationship of observed rate constants with the initial concentration of 2,4-D at low and high pH. Furthermore, the dependence of rate constants to UV intensity changed with pH. The rate constant depended on UV intensity at pH 3; however, this parameter showed a square root functionality with respect to intensity at pH 7.

Supplementary information

Supplementary data related to this chapter are presented in Appendix B.

Chapter 7: IMPACT OF NATURAL ORGANIC MATTER ON THE PHOTOCATALYTIC OXIDATION OF 2,4-D

7.1 Introduction

NOM in raw surface water presents several challenges to photocatalytic processes. It can act as an inner filter to block UV radiation and $^{\bullet}OH$ scavenger to affect the oxidation process. NOM scavenges positive holes (h^{+}) on the surface of photocatalyst and $^{\bullet}OH$ in the solution and consequently slows down the oxidation process. The role of pH as a major influencing factor on adsorption and subsequently on the photocalytic oxidation mechanism was comprehensively discussed. Since pH affects the photocatalytic oxidation pathways, evaluating the impact of NOM on each oxidation mechanism requires to separate the NOM interference at different pH. Based on the existing literature and prior research, a robust and comprehensive study is needed to evaluate interferences of NOM on photocatalytic oxidation of the target micropollutant during the photocatalytic process. This Chapter will analyze the effect of NOM on photocatalytic oxidation mechanisms. The impacts of NOM on scavenging oxidant species, generated on the surface of photocatalyst, and $^{\bullet}OH_{aq}$ in the solution were decoupled and investigated.

7.2 Results and discussion

7.2.1 The effect of NOM on photocatalytic oxidation at pH>pH_{pzc} (neutral pH)

Figure 7-1 shows the effect of NOM on the photocatalytic oxidation of 2,4-D at pH 7. As previously discussed, oxidation via $^{\bullet}OH_{aq}$ attack is the predominant process to oxidize 2,4-D at pH 7. At pH 7, due to the electrostatic repulsion between 2,4-D and the photocatalyst surface, the effect of NOM is considered as $^{\bullet}OH$ scavenger. Moreover, NOM influences the photocatalytic

oxidation of 2,4-D by absorbing UV radiation causes a reduction of •OH production. At neutral pH, the oxidation rate substantially decreased with an increase the presence of NOM to 5 mgL^{-1}. Almost no degradation occurred in the presence of NOM of 5 mgL^{-1} TOC because NOM scavenged almost all $^{\bullet}OH_{aq}$ (See Figure 7-1). Table 7-1 illustrates that NOM reduced the observed rate constant (k_{obs}) from 5.07×10^{-2} min^{-1} to 0.28×10^{-2} min^{-1} for 1 mgL^{-1} 2,4-D initial concentration. This reduction, however, was 2.29×10^{-2} min^{-1} to 0.24×10^{-2} min^{-1} for 7 mgL^{-1} initial concentration of 2,4-D.

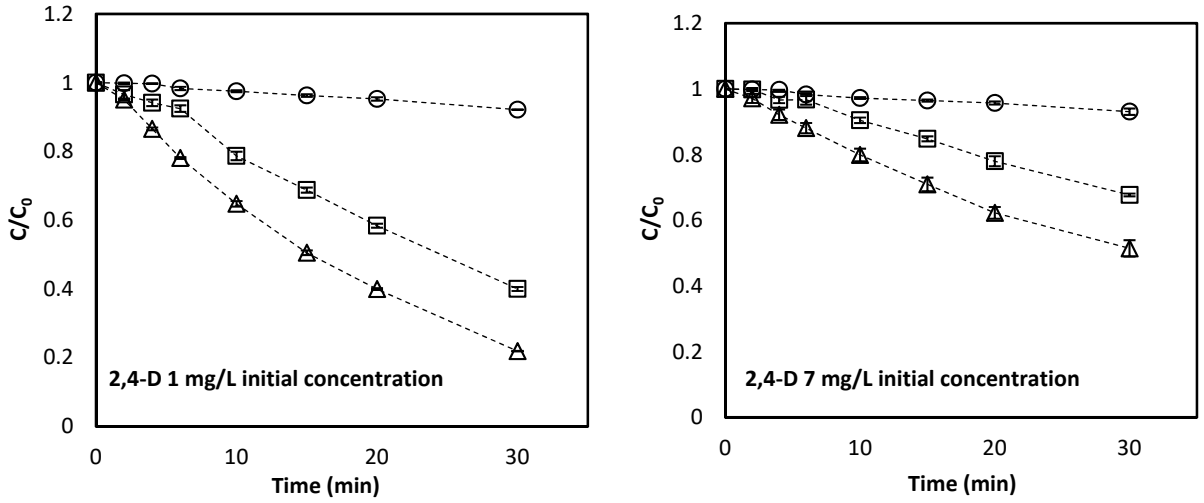

Figure 7-1. Photocatalytic oxidation of 2,4-D at pH 7 in the presence of NOM measured as TOC; (○) 5 mgL^{-1}, (□) 1 mgL^{-1} and, (Δ) 0 mgL^{-1}. Error bars represent the standard errors for the triplicate runs.

Table 7-1. Normalized observed kinetic rate constants (k_{obs}) of 2,4-D photocatalytic degradation at pH 7

NOM (mgL^{-1} DOC)	$K_{obs}\times10^2$ (min^{-1})		
	2,4-D 1 mgL^{-1} initial concentration	2,4-D 4 mgL^{-1} initial concentration	2,4-D 7 mgL^{-1} initial concentration
0	5.07	2.85	2.29
1	3.08	1.69	1.35
5	0.28	0.41	0.24

Figure 7-2 shows the fate of NOM during the photocatalytic process. The results show that the adsorption and photocatalytic oxidation of NOM are almost independent of the concentration of 2,4-D at pH 7; TOC removal of about 8%-10% and 14%-17% was observed for adsorption and oxidation, respectively. As earlier discussed, the negligible effect of 2,4-D on NOM adsorption is most likely due to the high capacity of photocatalytic spheres for adsorption and different mechanism of adsorption between 2,4-D and NOM. Figure 7-2 also shows that initial concentration of 2,4-D does not significantly affect the oxidation of NOM, indicating strong scavenging of $^{\bullet}OH_{aq}$ by NOM.

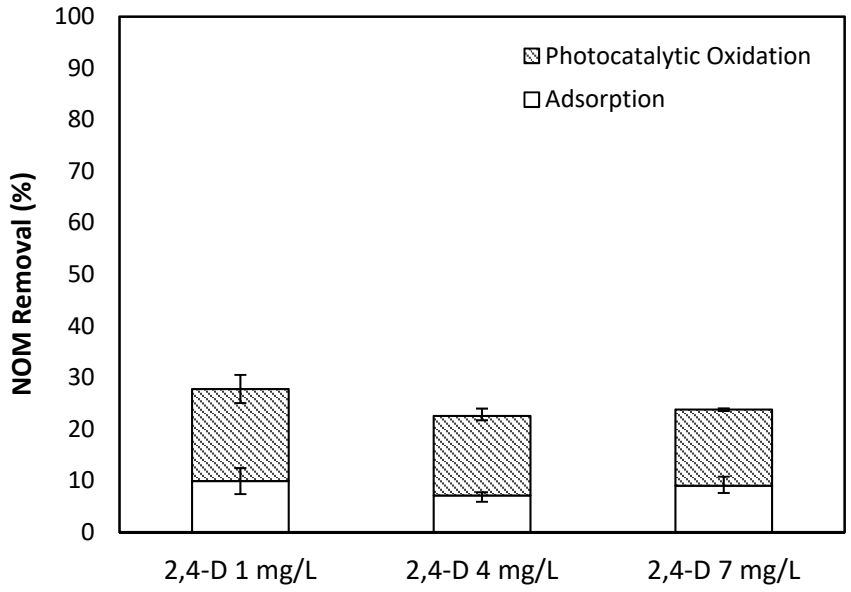

Figure 7-2. The fate of NOM with initial concentration of 5 mgL^{-1} during photocatalytic oxidation in the presence of different initial concentrations of 2,4-D at pH 7. Error bars indicate the standard errors for the triplicate runs.

The free hydroxyl radical oxidation of the different fractions of NOM were studied using a HPSEC chromatogram. Figure 7-3 shows that the total area under HPSEC chromatogram decreased as photocatalytic process progressed. The result illustrated that $^{\bullet}OH_{aq}$ preferentially reacted with larger molecular size resulting in an increase in lower molecular weight. Prior

irradiation, in the first 90 minutes, HPSEC featured a reduction for all molecular weight. As irradiation progressed, the peak indicates that the hydrophobic fraction (1600 Da) decreased. However, the lower molecular weight (<800 Da) seemed to slightly increased in size as irradiation progressed. In agreement with the observation of Liu et al. (2008), •OH due to the complex nature of NOM, is more likely to degrade NOM into smaller fragments.

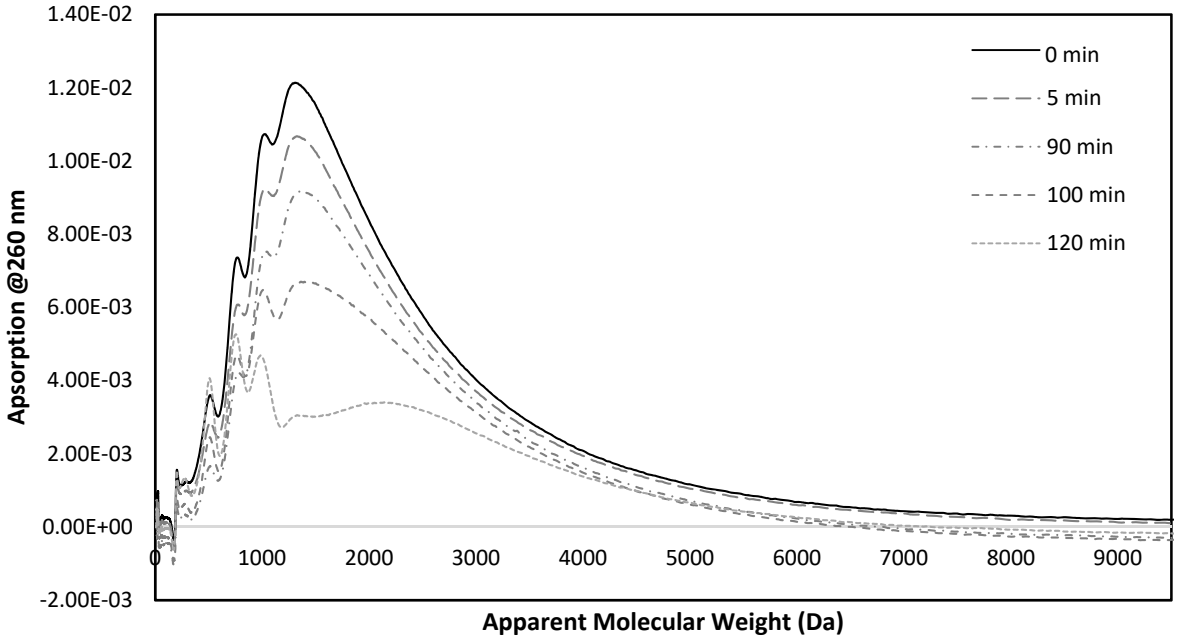

Figure 7-3. HPSEC chromatograms of NOM of 5 mgL^{-1} TOC removal by photocatalytic process.

7.2.2 The effect of NOM on photocatalytic oxidation at pH<pH_{pzc} (pH 3)

To better understand the impact of NOM on photocatalytic oxidation taking place on the surface of photocatalytic spheres, some experiments were performed at pH 3, leading to the photocatalytic oxidation on the surface of the photocatalyst. Results, as shown in Figure 7-4, indicate that there is an inverse relationship between the degradation rate constant and NOM concentration. The effect of NOM on the photocatalytic oxidation rate at pH 3 is less noticeable than its effect at pH 7, likely due to the changes in the oxidation mechanisms (See Table 7-1 and

Table 7-2). At pH 3, the adsorption of NOM on photocatalytic spheres is much higher than that at pH 7 (see Figure 7-5). The results show that more than 70% of NOM is removed because of adsorption during the photocatalytic process at pH 3. This extent of NOM removal dramatically reduces UV absorption and causes the photocatalytic spheres to receive more photons and produce more oxidant species to oxidize 2,4-D. Since NOM does not compete with 2,4-D for adsorption on the other hand, it does not influence the capture of positive holes produced on the surface of the photocatalyst either.

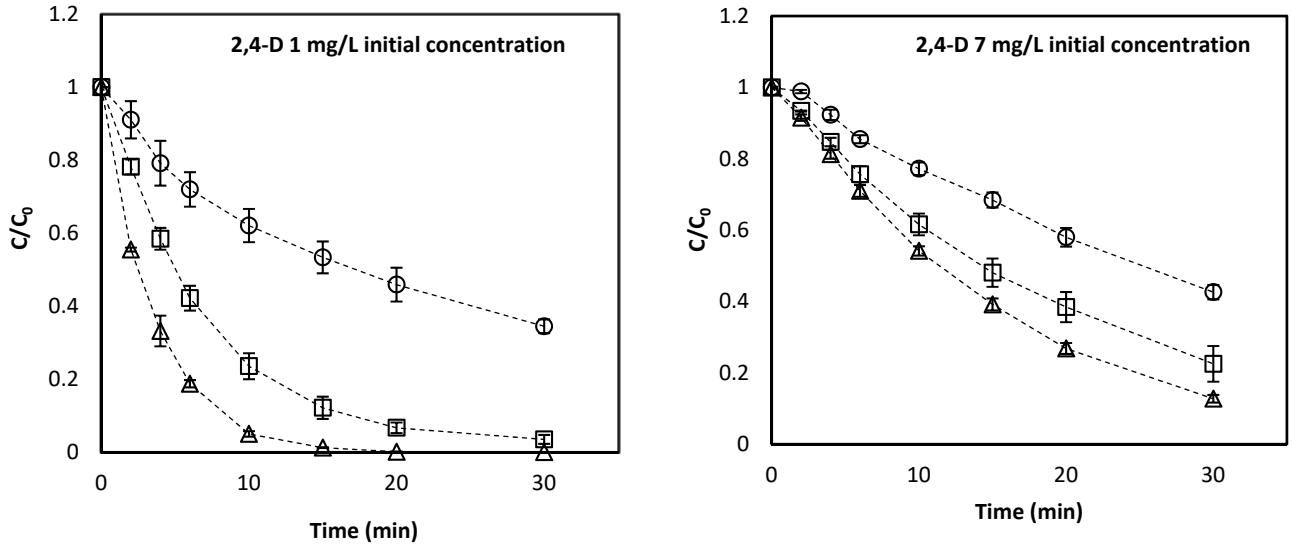

Figure 7-4. Photocatalytic oxidation of 2,4-D at pH 3 in the presence of NOM measured as TOC; (○) 5 mgL^{-1}, (□) 1 mgL^{-1} and, (Δ) 0 mgL^{-1}. Error bars represent the standard errors for the triplicate runs.

Table 7-2. Normalized observed kinetic rate constants (k_{obs}) of 2,4-D photocatalytic degradation at pH 3

NOM (mg L^{-1} DOC)	$K_{obs}\times10^2$ (min^{-1})		
	2,4-D 1 mgL^{-1} initial concentration	2,4-D 4 mgL^{-1} initial concentration	2,4-D 7 mgL^{-1} initial concentration
0	28.59	10.4	6.92
1	11.87	9.24	5.00
5	3.48	2.72	2.89

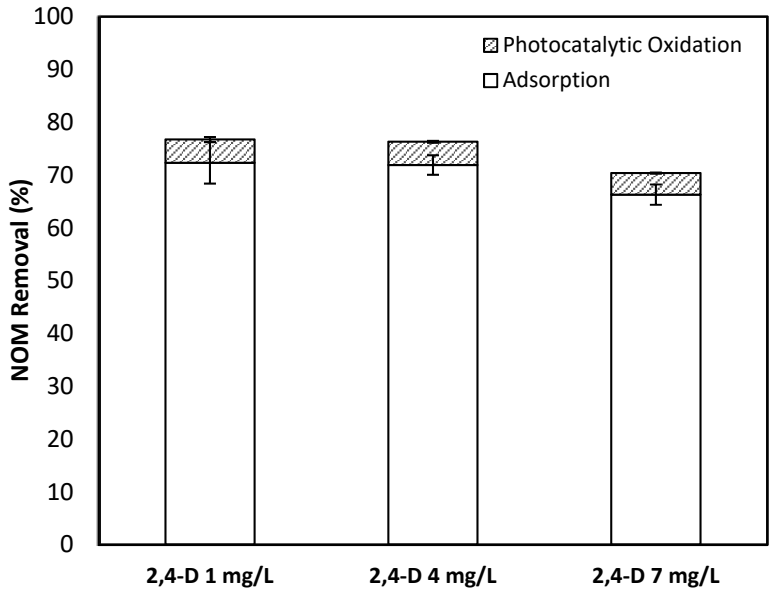

Figure 7-5. The fate of NOM with initial concentration of 5 mgL^{-1} during photocatalytic oxidation in the presence of different initial concentrations of 2,4-D at pH 3. Error bars indicate the standard errors for the triplicate runs.

At pH 3, NOM is both adsorbed on the surface of photocatalyst spheres and present in the solution. Therefore, NOM acts as the scavenger of hydroxyl radicals in the solution and positive holes on the surface of the photocatalyst. To better assess the effect of NOM on different mechanisms, methanol of 0.1 M was used in this experiment as $^{\bullet}OH$ scavenger. Methanol is UV transparent and does not compete with 2,4-D for adsorption sites, but it strongly scavenges $^{\bullet}OH$ (Ilisz and Dombi, 1999; Šojić et al., 2009; Tunesi and Anderson, 1991). Figure 7-6 shows the impact of methanol on the degradation of 2,4-D at different pH values. No degradation occurred in the presence of methanol at pH 7. Given that there is no 2,4-D adsorption taking place at pH 7, the absence of any 2,4-D removal indicates the effectiveness of methanol at scavenging all $^{\bullet}OH$. At low pH, on the other hand, methanol had little effect and significant degradation of 2,4-D

occurred, indicating that photocatalytic oxidation was mostly driven by charge transfer on the surface of the spheres.

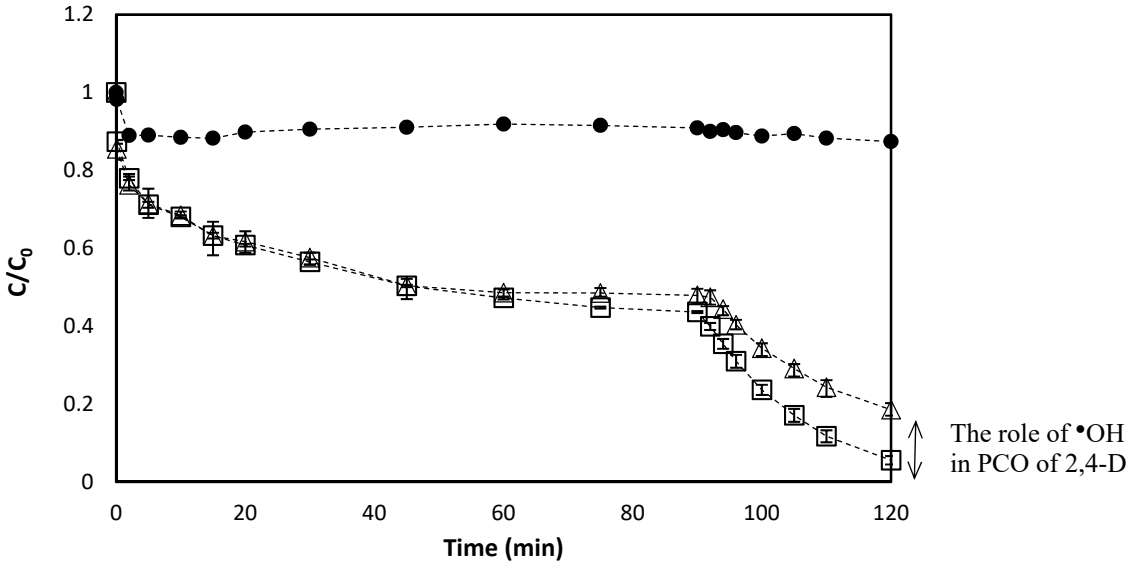

Figure 7-6. Photocatalytic oxidation of 2,4-D with initial concentration of 7 mgL^{-1} in a fluidized photocatalytic reactor, (□) at pH 3, (Δ) in the presence of 0.1 M methanol at pH 3 and, (●) in the presence of 0.1 M methanol at pH 7. Error bars represent the standard errors for the triplicate runs.

The same procedure that was used for the separation of photocatalytic oxidation at pH 3, was carried out in the presence of NOM — with methanol acting as •OH scavenger. Given the absence of hydroxyl radicals, NOM competes with 2,4-D to capture holes produced on the surface of the spheres. As shown in Figure 7-7, increasing the concentration of NOM affected the contribution of direct oxidation on the photocatalyst surface. The 2,4-D removal on the surface of the photocatalyst was reduced from 47% in the presence of 1 mgL^{-1} TOC NOM to 27% in the presence of 5 mgL^{-1} TOC NOM. This was due to the increased amount of adsorbed NOM which in turn increased scavenging of positive holes, and consequently reduced the removal of 2,4-D via this mechanism. The negligible effect of NOM on scavenging $•OH_{aq}$ was due to high adsorption of NOM and the lack of aromatic moieties in the solution.

The effect of aromatic moieties was studied using SUVA analysis at different pH. Figure 7-8 compared SUVA reduction attributed to photocatalytic removal of NOM. At low pH, NOM aromatic adsorption causes a reduction of approximately 50% of SUVA. However, the oxidation via $^{\bullet}OH_{aq}$ did not yield any reduction in SUVA. This result in agreement with the previous result (refer to Figure 5-10) indicated the higher adsorption of carboxylate and aromatic compounds at pH 3 leads to a reduction of 50% SUVA.

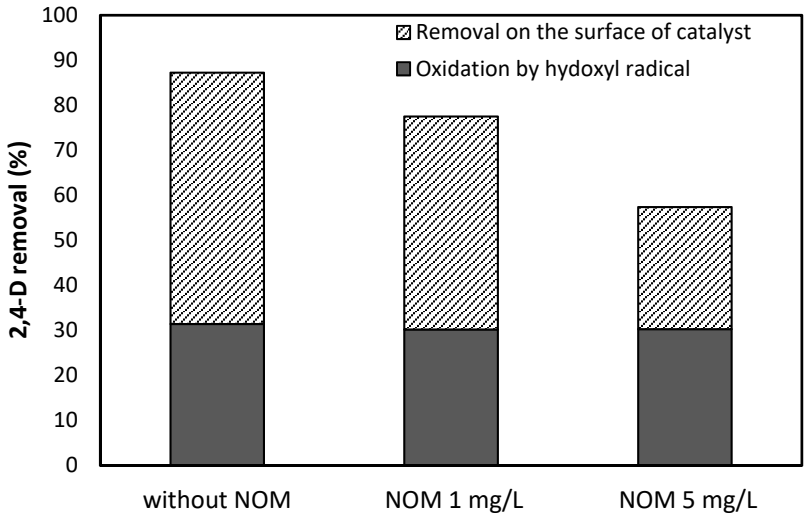

Figure 7-7. The effect of NOM at different concentrations on photocatalytic oxidation mechanisms for the removal 2,4-D with initial concentration of 7 mgL^{-1} at pH 3 in a fluidized photocatalytic reactor.

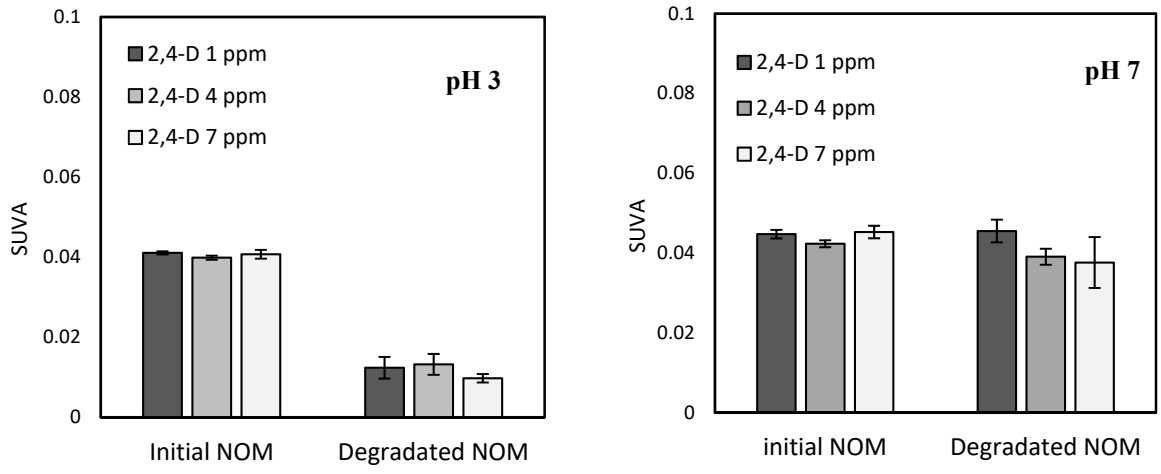

Figure 7-8. Photocatalytic SUVA reduction of 5 mgL^{-1} TOC NOM in presence of 2,4-D different initial concentration at pH 3 and pH 7. Error bars represent the standard errors for the triplicate runs.

7.3 Conclusions

The effect of NOM on photocatalytic oxidation mechanisms was quantified by changing the pH of the medium in this chapter. At pH 7, the impact of NOM was considered as scavenging $^{\bullet}OH_{aq}$ and screening UV radiation. The removal of 2,4-D reduced from 49% in the absence of NOM to 7% in the presence of 5 mgL^{-1} TOC NOM. At pH 3 on the other hand, due to increasing the adsorption of solutes (2,4-D and NOM) NOM mostly affects as a positive holes scavenger; reducing the removal of 2,4-D from 88% in the absence of NOM to 58% in the presence of 5 mgL^{-1} TOC NOM. Results also showed that the effect of NOM on scavenging $^{\bullet}OH_{aq}$ is insignificant at pH 3. NOM photocatalytic oxidation showed that oxidation via $^{\bullet}OH_{aq}$ at pH 7 is more effective than at pH 3; however, the NOM removal due to adsorption at pH 3 is also highly significant. Furthermore, $^{\bullet}OH_{aq}$ preferentially reacts with NOM larger molecular size causing an increase in lower molecular weight during the photocatalytic oxidation at pH 7. High SUVA reduction at pH 3 on the other hand, showed that high adsorption and consequently higher oxidation of NOM aromatic fraction on the surface of photocatalyst.

Supplementary information

Supplementary data related to this chapter are presented in Appendix C.

Chapter 8: CONCLUSIONS AND RECOMMENDATIONS

8.1 Overall conclusions

This research investigated the impact of NOM on photocatalytic removal of micropollutants (with 2,4-D as target contaminant). The experiment was performed in FBPR using template free photocatalyst spheres. Photocatalytic process including adsorption and photocatalytic oxidation is a function of pH. Therefore, the effect of NOM on adsorption and photocatalytic oxidation was separately examined at different pH.

The overall conclusions derived from this research are as follows:

2,4-D adsorption and the effect of NOM

- 2,4-D adsorption is related to the pH of solution. Almost 60% of 2,4-D was adsorbed at pH 3; however, the amount of adsorbed 2,4-D dropped to 10% at neutral pH.
- Adsorption of 2,4-D due to a high number of available site for adsorptions, is independent of the initial concentration.
- The analysis of equilibrium isotherm adsorption suggested that Freundlich fits the experimental data very well.
- NOM does not have any effect on adsorption performance. Since the photocatalyst has a high adsorption capacity and the adsorption mechanism of NOM is different than 2,4-D, none of these adsorbates can interfere with the adsorption performance of the other.
- Regardless of the initial concentration of 2,4-D, the adsorption of NOM is ~95% at pH 3.

Adsorption of NOM

- NOM is prevalently negatively charged and its adsorption is affected by the pH of solution.
- At pH 3, where electrostatic interactions were minimised, the hydrophobic interaction governed the adsorption process. High adsorption of NOM (~95%), irrespective of its initial concentrations indicates that photocatalytic spheres have a very high capacity for adsorbing NOM under low electrostatic interaction conditions at pH 3.
- At pH 7, The electrostatic repulsion between NOM_{ads} and NOM_{sol} remarkably reduced the adsorption of NOM to 37% removal for 5 mg/L TOC initial concentration.
- According to FTIR analysis and fractionation of NOM, carboxyl groups were deprotonated and played the major role in reducing the adsorption at pH>3.
- pH affects the adsorption isotherm models as shown by exchanging the adsorption from multi-layer adsorption of Freundlich at pH 3 to monolayer characteristic of Langmuir isotherm at pH>3.

The effect of pH on Photocatalytic oxidation kinetics

- The photocatalytic oxidation kinetics changed due to the impact of pH on photocatalyst surface charge and the energies of conductance and valence band.
- photocatalytic oxidation at $pH>pH_{zpc}$ (pH 7) followed first order kinetic model.
- The rate of oxidation was a combination of first order and L-H models at $pH<pH_{zpc}$ (pH 3).

- Oxidation of 2,4-D intermediates by hydroxyl radicals attack in the solution, causes an inverse relationship of observed rate constants with the initial concentration of 2,4-D at low and high pH.
- The rate constant depended on UV intensity at pH 3; however, this parameter showed a square root functionality with respect to intensity at pH 7.

Impact of NOM on the photocatalytic oxidation of 2,4-D

- At pH 7, NOM affects the photocatalytic oxidation by scavenging $^{\bullet}OH_{aq}$ and screening UV radiation. The removal of 2,4-D reduced from 49% in the absence of NOM to 7% in the presence of 5 mgL^{-1} TOC NOM.
- At pH 3, due to increasing the adsorption of solutes (2,4-D and NOM), NOM mostly acts as a positive holes scavenger; reducing the removal of 2,4-D from 88% in the absence of NOM to 58% in the presence of 5 mgL^{-1} TOC NOM.
- NOM is mostly oxidized by $^{\bullet}OH_{aq}$ attack at pH 7. However, the NOM removal due to adsorption at pH 3 is also highly significant.
- Free hydroxyl radicals preferentially react with NOM larger molecular size causing an increase in lower molecular weight during the photocatalytic oxidation at pH 7.
- High SUVA reduction at pH 3 showed high adsorption and consequently higher oxidation of NOM aromatic fraction on the surface of the photocatalyst.

8.2 Significance and contributions of this research

While a promising technology for contaminated water purification, photocatalytic process has not yet been successfully developed for commercial systems, since (i) a proper photocatalyst

has not been developed, (ii) a comprehensive study of the effect of water matrix on photocatalytic process has not been performed. This research provided the first step towards applying photocatalytic process in real conditions by modifying template free photocatalyst spheres utilized in FBPR. However, the complexity of the process as well as the complex and none-reliable nature of water matrix is a big challenge for better understanding the effect of water matrix on the photocatalytic process.

This research specifically addressed this need by analyzing the impact of NOM as the main influencing constituent within water matrix on photocatalytic process. This study separately assessed the NOM interference with adsorption and photocatalytic oxidation. Likewise, the approach undertaken in this study could successfully quantify the effect of NOM on each oxidation mechanism. NOM fractionation and analysis of different functional groups could make a unique knowledge of the impact of NOM on photocatalytic process. Moreover, this research provided a significant contribution to understanding of the effect of photocatalytic process on NOM removal.

Changing the pH of the solution was used in this research to decouple the effect of NOM on different oxidation pathways. This research developed a fundamental kinetic study to assess the impact of pH on photocatalytic oxidation pathways and kinetic models.

8.3 Recommendation for future work

- One of the obstacles of using the fluidized bed photocatalytic reactors is catalyst attrition. More studies need to improve the attrition resistance of photocatalyst spheres. Improving the hydrolysis and condensation reactions in the photocatalyst preparation procedure may help to produce a tighter catalyst with higher attrition resistance.

- Another important factor that needs being considered to improve the photocatalyst characteristics, is changing the photocatalyst zero point charge (pH_{zpc}) to desirable pH. pH_{zpc} higher than neutral pH can improve the photocatalyst efficiency in removing micropollutants in ionic form.
- Further study in a large scale fluidized bed photocatalytic reactor is suggested.
- Evaluating the impact of water matrix on the photocatalytic process needs further study to assess the effect of inorganic ions that are present in natural water.

Bibliography

Adams, C., Wang, Y., Loftin, K., Meyer, M., 2002. Removal of Antibiotics from Surface and Distilled Water in Conventional Water Treatment Processes. J. Environ. Eng. 128, 253–260.

Aiken, G.R., McKnight, D.M., Thorn, K.A., Thurman, E.M., 1992. Isolation of hydrophilic organic acids from water using nonionic macroporous resins. Org. Geochem. 18, 567–573.

Akasu, Z., Kabasakal, E., 2005. Adsorption Characteristics of 2,4-Dichlorophenoxyacetic Acid (2,4-D) from Aqueous Solution on Powdered Activated Carbon. J. Environ. Sci. Health Part B 40, 545–570.

Ameta, R., Kumar, A., Punjabi, P., Ameta, S., 2012. Advanced Oxidation Processes, in: Wastewater Treatment. CRC Press, pp. 61–106.

Avdeef, A., 2012. pKa Determination, in: Absorption and Drug Development: Solubility, Permeability, and Charge State. John Wiley & Sons, pp. 31–173.

Bacsa, R.R., Kiwi, J., 1998. Effect of rutile phase on the photocatalytic properties of nanocrystalline titania during the degradation of p-coumaric acid. Appl. Catal. B Environ. 16, 19–29.

Bai, R., Zhang, X., 2001. Polypyrrole-Coated Granules for Humic Acid Removal. J. Colloid Interface Sci. 243, 52–60.

Boschloo, G., Edvinsson, T., Hagfeldt, A., 2006. Dye-Sensitized Nanostructured ZnO Electrodes for Solar Cell Applications - Nanostructured Materials for Solar Energy Conversion, in: Nanostructured Materials for Solar Energy Conversion. Elsevier, pp. 227–254.

Braham, R.J., Harris, A.T., 2009. Review of Major Design and Scale-up Considerations for Solar Photocatalytic Reactors. Ind. Eng. Chem. Res. 48, 8890–8905.

Byrne, J., Fernández-Ibáñez, P., 2012. Solar Photocatalytic Treatment of Wastewater, in: Wastewater Treatment. CRC Press, pp. 37–60.

Chen, D., Li, F., Ray, A.K., 2000. Effect of mass transfer and catalyst layer thickness on photocatalytic reaction. AIChE J. 46, 1034–1045.

Chen, Y., Dionysiou, D.D., 2006. TiO2 photocatalytic films on stainless steel: The role of Degussa P-25 in modified sol–gel methods. Appl. Catal. B Environ. 62, 255–264.

Cho, J., Amy, G., Pellegrino, J., Yoon, Y., 1998. Characterization of clean and natural organic matter (NOM) fouled NF and UF membranes, and foulants characterization. Desalination, Conference Membranes in Drinking and Industrial Water Production 118, 101–108.

Chow, C.W.K., Fabris, R., Drikas, M., 2004. A rapid fractionation technique to characterise natural organic matter for the optimisation of water treatment processes. J. Water Supply Res. Technol. - Aqua 53, 85–92.

Clugston, M., Flemming, R., 2000. Advanced Chemistry. OUP Oxford.

Crittenden, J.C., Trussell, R.R., Hand, D.W., Howe, K.J., Tchobanoglous, G., 2012. Appendix C: Physical Properties of Water, in: MWH's Water Treatment: Principles and Design, Third Edition. John Wiley & Sons, Inc., pp. 1861–1862.

Cunningham, J., Srijaranai, S., 1988. Isotope-effect evidence for hydroxyl radical involvement in alcohol photo-oxidation sensitized by TiO2 in aqueous suspension. J. Photochem. Photobiol. Chem. 43, 329–335.

Cunningham, V.L., Binks, S.P., Olson, M.J., 2009. Human health risk assessment from the presence of human pharmaceuticals in the aquatic environment. Regul. Toxicol. Pharmacol. 53, 39–45.

Dalrymple, O.K., 2011. Mechanistic modeling of photocatalytic water disinfection (Ph.D.). University of South Florida, United States - Florida.

de Lasa, H., Serrano, B., Salaices, M., 2005a. The Energy Efficiency Factors in Photocatalytic Processes, in: Photocatalytic Reaction Engineering. Springer US, pp. 119–131.

de Lasa, H., Serrano, B., Salaices, M., 2005b. Novel photocatalytic reactors for water and air treatment, in: Photocatalytic Reaction Engineering. Springer, pp. 17–48.

de Lasa, H., Serrano, B., Salaices, M., 2005c. Kinetic Modeling of the Photocatalytic Reaction Network: The Parallel-Series Approximation, in: Photocatalytic Reaction Engineering. Springer US, pp. 101–118.

Diebold, U., 2003a. Structure and properties of TiO2 surfaces: a brief review. Appl. Phys. A 76, 681–687.

Diebold, U., 2003b. The surface science of titanium dioxide. Surf. Sci. Rep. 48, 53–229.

Ding, L., 2010. Mechanisms of competitive adsorption between trace organic contaminants and natural organic matter on activated carbon (Ph.D.). University of Illinois at Urbana-Champaign, United States - Illinois.

Doll, T.E., Frimmel, F.H., 2005a. Removal of selected persistent organic pollutants by heterogeneous photocatalysis in water. Catal. Today, Environmental Applications of Photocatalysis, 3rd European Meeting on Solar Chemistry and Photocatalysis: Environmental Applications Environmental Applications of Photocatalysis 101, 195–202.

Doll, T.E., Frimmel, F.H., 2005b. Photocatalytic degradation of carbamazepine, clofibric acid and iomeprol with P25 and Hombikat UV100 in the presence of natural organic matter (NOM) and other organic water constituents. Water Res. 39, 403–411.

Drosos, M., Ren, M., Frimmel, F.H., 2015. The effect of NOM to TiO2: interactions and

photocatalytic behavior. Appl. Catal. B Environ. 165, 328–334.

Du, Y., Rabani, J., 2003. The Measure of TiO2 Photocatalytic Efficiency and the Comparison of Different Photocatalytic Titania. J. Phys. Chem. B 107, 11970–11978.

Duffy, J.E., Anderson, M.A., Hill, C.G., Zeltner, W.A., 2000. Photocatalytic Oxidation as a Secondary Treatment Method following Wet Air Oxidation. Ind. Eng. Chem. Res. 39, 3698–3706.

Duran, J.E., Mohseni, M., Taghipour, F., 2011. Design improvement of immobilized photocatalytic reactors using a CFD-taguchi combined method. Ind. Eng. Chem. Res. 50, 824–831.

Duran, J.E.D., 2010a. Development of a CFD-based model for the simulation of immobilized photocatalytic reactors for water treatment.

Duran, J.E.D., 2010b. Development of a CFD-based model for the simulation of immobilized photocatalytic reactors for water treatment.

Emeline, A.V., Ryabchuk, V., Serpone, N., 2000. Factors affecting the efficiency of a photocatalyzed process in aqueous metal-oxide dispersions: Prospect of distinguishing between two kinetic models. J. Photochem. Photobiol. Chem. 133, 89–97.

Emeline, A.V., Ryabchuk, V.K., Serpone, N., 2005. Dogmas and Misconceptions in Heterogeneous Photocatalysis. Some Enlightened Reflections. J. Phys. Chem. B 109, 18515–18521.

Epstein, N., 2003. Liquid-Solids Fluidization, in: Yang, W.-C. (Ed.), Handbook of Fluidization and Fluid-Particle Systems, Chemical Industries. Marcel Dekker, New York, NY, USA, pp. 705–764.

Faur, C., Métivier-Pignon, H., Cloirec, P.L., 2005. Multicomponent Adsorption of Pesticides onto

Activated Carbon Fibers. Adsorption 11, 479–490. doi:10.1007/s10450-005-5607-2

Foo, K.Y., Hameed, B.H., 2010. Insights into the modeling of adsorption isotherm systems. Chem. Eng. J. 156, 2–10.

Fox, M.A., Dulay, M.T., 1993. Heterogeneous photocatalysis. Chem. Rev. 93, 341–357.

Friedmann, D., Mendive, C., Bahnemann, D., 2010. TiO2 for water treatment: Parameters affecting the kinetics and mechanisms of photocatalysis. Appl. Catal. B Environ., TiO2 photocatalysis-25 years 99, 398–406.

Fu, H., Zhang, L., Zhang, S., Zhu, Y., Zhao, J., 2006. Electron Spin Resonance Spin-Trapping Detection of Radical Intermediates in N-Doped TiO2-Assisted Photodegradation of 4-Chlorophenol. J. Phys. Chem. B 110, 3061–3065.

Fujishima, A., Zhang, X., Tryk, D.A., 2008. TiO2 photocatalysis and related surface phenomena. Surf. Sci. Rep. 63, 515–582.

Garner, F.H., Suckling, R.D., 1958. Mass transfer from a soluble solid sphere. AIChE J. 4, 114–124.

Gaya, U.I., 2014a. Kinetic Concepts of Heterogeneous Photocatalysis, in: Heterogeneous Photocatalysis Using Inorganic Semiconductor Solids. Springer Netherlands, pp. 43–71.

Gaya, U.I., 2014b. Mechanistic Principles of Photocatalytic Reaction, in: Heterogeneous Photocatalysis Using Inorganic Semiconductor Solids. Springer Netherlands, pp. 73–89.

Gong, W., 2001. A real time in situ ATR-FTIR spectroscopic study of linear phosphate adsorption on titania surfaces. Int. J. Miner. Process. 63, 147–165.

González-Reyes, L., Hernández-Pérez, I., Robles Hernández, F.C., 2011. Effect of coarsening of sonochemical synthesized anatase on BET surface characteristics. Chem. Eng. Sci. 66, 721–728.

Günay, A., Arslankaya, E., Tosun, İ., 2007. Lead removal from aqueous solution by natural and pretreated clinoptilolite: Adsorption equilibrium and kinetics. J. Hazard. Mater. 146, 362–371.

Guzsvány, V., Rajić, L., Jović, B., Orčić, D., Csanádi, J., Lazić, S., Abramović, B., 2012. Spectroscopic monitoring of photocatalytic degradation of the insecticide acetamiprid and its degradation product 6-chloronicotinic acid on TiO2 catalyst. J. Environ. Sci. Health Part A 47, 1919–1929.

Haarstrick, A., Kut, O.M., Heinzle, E., 1996. TiO2-Assisted Degradation of Environmentally Relevant Organic Compounds in Wastewater Using a Novel Fluidized Bed Photoreactor. Environ. Sci. Technol. 30, 817–824.

Haber, J., 2009. Manual on catalyst characterization (Recommendations 1991). Pure Appl. Chem. 63, 1227–1246.

Hameed, B.H., Mahmoud, D.K., Ahmad, A.L., 2008. Equilibrium modeling and kinetic studies on the adsorption of basic dye by a low-cost adsorbent: Coconut (Cocos nucifera) bunch waste. J. Hazard. Mater. 158, 65–72.

Hatzantonis, H., Goulas, A., Kiparissides, C., 1998. A comprehensive model for the prediction of particle-size distribution in catalyzed olefin polymerization fluidized-bed reactors. Chem. Eng. Sci. 53, 3251–3267.

Hay, M.B., Myneni, S.C.B., 2007. Structural environments of carboxyl groups in natural organic molecules from terrestrial systems. Part 1: Infrared spectroscopy. Geochim. Cosmochim. Acta 71, 3518–3532.

Hernández-Ramírez, A., Medina-Ramírez, I., 2015. Semiconducting Materials, in: Hernández-Ramírez, A., Medina-Ramírez, I. (Eds.), Photocatalytic Semiconductors. Springer

International Publishing, pp. 1–40.

Herrmann, J.-M., 2010. Fundamentals and misconceptions in photocatalysis. J. Photochem. Photobiol. Chem. 216, 85–93.

Herrmann, J.-M., 1999. Heterogeneous photocatalysis: fundamentals and applications to the removal of various types of aqueous pollutants. Catal. Today 53, 115–129.

Hoffmann, M.R., Martin, S.T., Choi, W., Bahnemann, D.W., 1995. Environmental Applications of Semiconductor Photocatalysis. Chem. Rev. 95, 69–96.

Howe, K.J., Ishida, K.P., Clark, M.M., 2002. Use of ATR/FTIR spectrometry to study fouling of microfiltration membranes by natural waters. Desalination 147, 251–255.

Howe, R.F., Gratzel, M., 1985. EPR observation of trapped electrons in colloidal titanium dioxide. J. Phys. Chem. 89, 4495–4499.

Ikeda, S., Sugiyama, N., Murakami, S., Kominami, H., Kera, Y., Noguchi, H., Uosaki, K., Torimoto, T., Ohtani, B., 2003. Quantitative analysis of defective sites in titanium(IV) oxide photocatalyst powders. Phys. Chem. Chem. Phys. 5, 778–783.

Ilisz, I., Dombi, A., 1999. Investigation of the photodecomposition of phenol in near-UV-irradiated aqueous TiO2 suspensions. II. Effect of charge-trapping species on product distribution. Appl. Catal. Gen. 180, 35–45.

Jackson, N.B., Wang, C.M., Luo, Z., Schwitzgebel, J., Ekerdt, J.G., Brock, J.R., Heller, A., 1991. Attachment of TiO2 Powders to Hollow Glass Microbeads: Activity of the TiO2 - Coated Beads in the Photoassisted Oxidation of Ethanol to Acetaldehyde. J. Electrochem. Soc. 138, 3660–3664.

Johansson, E.M.J., Plogmaker, S., Walle, L.E., Schölin, R., Borg, A., Sandell, A., Rensmo, H., 2010. Comparing Surface Binding of the Maleic Anhydride Anchor Group on Single

Crystalline Anatase TiO2 (101), (100), and (001) Surfaces. J. Phys. Chem. C 114, 15015–15020.

Kabir, M.F., 2006. Fluidized bed photocatalytic reactor system for disinfection and wastewater treatment (Ph.D.). University of Calgary (Canada), Canada.

Kim, D.S., Kwak, S.-Y., 2007. The hydrothermal synthesis of mesoporous TiO2 with high crystallinity, thermal stability, large surface area, and enhanced photocatalytic activity. Appl. Catal. Gen. 323, 110–118.

Kim, J., Shan, W., Davies, S.H.R., Baumann, M.J., Masten, S.J., Tarabara, V.V., 2009. Interactions of Aqueous NOM with Nanoscale TiO2: Implications for Ceramic Membrane Filtration-Ozonation Hybrid Process. Environ. Sci. Technol. 43, 5488–5494.

Kosmulski, M., 2002. The significance of the difference in the point of zero charge between rutile and anatase. Adv. Colloid Interface Sci. 99, 255–264.

Lee, P.F., Sun, D.D., Leckie, J.O., 2007. Adsorption and Photodegradation of Humic Acids by Nano-Structured TiO2 for Water Treatment. J. Adv. Oxid. Technol. 10, 72–78.

Legrini, O., Oliveros, E., Braun, A.M., 1993. Photochemical processes for water treatment. Chem. Rev. 93, 671–698.

Li, Q., Snoeyink, V.L., Mariãas, B.J., Campos, C., 2003. Elucidating competitive adsorption mechanisms of atrazine and NOM using model compounds. Water Res. 37, 773–784.

Liao, H., Reitberger, T., 2013. Generation of Free OHaq Radicals by Black Light Illumination of Degussa (Evonik) P25 TiO2 Aqueous Suspensions. Catalysts 3, 418–443.

Lin, C., Lin, K.-S., 2007. Photocatalytic oxidation of toxic organohalides with TiO2/UV: The effects of humic substances and organic mixtures. Chemosphere 66, 1872–1877.

Linsebigler, A.L., Lu, G., Yates, J.T., 1995. Photocatalysis on TiO2 Surfaces: Principles,

Mechanisms, and Selected Results. Chem. Rev. 95, 735–758.

Liu, Guojing, Zhang, X., Talley, J.W., Neal, C.R., Wang, H., 2008. Effect of NOM on arsenic adsorption by TiO2 in simulated As(III)-contaminated raw waters. Water Res. 42, 2309–2319.

Liu, Guoj., Zhang, X.R., Mcwilliams, L., Talley, J.W., Neal, C.R., 2008. Influence of ionic strength, electrolyte type, and NOM on As(V) adsorption onto TiO2. J. Environ. Sci. Health Part A 43, 430–436.

Liu, S., Lim, M., Amal, R., 2013. Photocatalysis of Natural Organic Matter in Water: Characterization and Treatment Integration, in: Pichat, P. (Ed.), Photocatalysis and Water Purification. Wiley-VCH Verlag GmbH & Co. KGaA, pp. 271–294.

Liu, Sanly, Lim, M., Fabris, R., Chow, C., Chiang, K., Drikas, M., Amal, R., 2008. Removal of humic acid using TiO2 photocatalytic process – Fractionation and molecular weight characterisation studies. Chemosphere 72, 263–271.

Marhaba, T.F., Pu, Y., Bengraine, K., 2003. Modified dissolved organic matter fractionation technique for natural water. J. Hazard. Mater. 101, 43–53.

Matilainen, A., Sillanpää, M., 2010. Removal of natural organic matter from drinking water by advanced oxidation processes. Chemosphere 80, 351–365.

Mazierski, P., Bajorowicz, B., Grabowska, E., Zaleska-Medynska, A., 2016. Photoreactor Design Aspects and Modeling of Light, in: Colmenares, J.C., Xu, Y.-J. (Eds.), Heterogeneous Photocatalysis, Green Chemistry and Sustainable Technology. Springer Berlin Heidelberg, pp. 211–248.

McCune, L.., Wilhelm, R.., 1949. Mass and momentum transfer in a solid-liquid system. Ind. Eng. Chem. 41, 1124–1134.

McGivney, W., Kawamura, S., 2008. Water treatment process, in: Cost Estimating Manual for Water Treatment Facilities. John Wiley & Sons, p. 215.

Mears, D.E., 1971. Tests for Transport Limitations in Experimental Catalytic Reactors. Ind. Eng. Chem. Process Des. Dev. 10, 541–547.

Mills, A., Davies, R.H., Worsley, D., 1993. Water purification by semiconductor photocatalysis. Chem. Soc. Rev. 22, 417–425.

Mills, A., Wang, J., Ollis, D.F., 2006. Dependence of the kinetics of liquid-phase photocatalyzed reactions on oxygen concentration and light intensity. J. Catal. 243, 1–6.

Mir, N.A., Khan, A., Muneer, M., Vijayalakhsmi, S., 2013. Photocatalytic degradation of a widely used insecticide Thiamethoxam in aqueous suspension of TiO2: Adsorption, kinetics, product analysis and toxicity assessment. Sci. Total Environ. 458–460, 388–398.

Musolff, A., Leschik, S., Reinstorf, F., Strauch, G., Schirmer, M., 2010. Micropollutant Loads in the Urban Water Cycle. Environ. Sci. Technol. 44, 4877–4883. doi:10.1021/es903823a

Newcombe, G., 1994. Activated Carbon and Soluble Humic Substances: Adsorption, Desorption, and Surface Charge Effects. J. Colloid Interface Sci. 164, 452–462.

Newcombe, G., Drikas, M., 1997. Adsorption of NOM onto activated carbon: Electrostatic and non-electrostatic effects. Carbon 35, 1239–1250.

Nosaka, Y., 2010. Surface Chemistry of TiO2 Photocatalysis and LIF Detection of OH Radicals, in: Anpo, M., Kamat, P.V. (Eds.), Environmentally Benign Photocatalysts, Nanostructure Science and Technology. Springer New York, pp. 205–215.

Nosaka, Y., Nosaka, A.Y., 2013. Identification and Roles of the Active Species Generated on Various Photocatalysts, in: Pichat, P. (Ed.), Photocatalysis and Water Purification. Wiley-VCH Verlag GmbH & Co. KGaA, pp. 1–24.

Ollis, D., 2013. Photocatalytic Treatment of Water: Irradiance Influences, in: Pichat, P. (Ed.), Photocatalysis and Water Purification. Wiley-VCH Verlag GmbH & Co. KGaA, pp. 311–333.

Ollis, D.F., 2005. Kinetics of Liquid Phase Photocatalyzed Reactions: An Illuminating Approach†. J. Phys. Chem. B 109, 2439–2444.

O'Shea, K.E., Dionysiou, D.D., 2012. Advanced Oxidation Processes for Water Treatment. J. Phys. Chem. Lett. 3, 2112–2113.

Pang, C.L., Lindsay, R., Thornton, G., 2008. Chemical reactions on rutile TiO2(110). Chem. Soc. Rev. 37, 2328–2353.

Park, H., Park, Y., Kim, W., Choi, W., 2013. Surface modification of TiO2 photocatalyst for environmental applications. J. Photochem. Photobiol. C Photochem. Rev., Next Generation Photochemistry from Asia 15, 1–20. doi:10.1016/j.jphotochemrev.2012.10.001

Parsons, S., 2004. Advanced Oxidation Processes for Water and Wastewater Treatment. IWA Publishing.

Pelaez, M., de la Cruz, A.A., O'Shea, K., Falaras, P., Dionysiou, D.D., 2011. Effects of water parameters on the degradation of microcystin-LR under visible light-activated TiO2 photocatalyst. Water Res. 45, 3787–3796.

Pelekani, C., Snoeyink, V.L., 1999. Competitive Adsorption in Natural Water: Role of Activated Carbon Pore Size. Water Res. 33, 1209–1219.

Pichat, P., 2007. A brief overview of photocatalytic mechanisms and pathways in water. Water Sci. Technol. 55, 167.

Pozzo, R.L., Brandi, R.J., Giombi, J.L., Baltanás, M.A., Cassano, A.E., 2005. Design of fluidized bed photoreactors: Optical properties of photocatalytic composites of titania CVD-coated

onto quartz sand. Chem. Eng. Sci. 60, 2785–2794.

Qiu, W., Zheng, Y., 2007. A comprehensive assessment of supported titania photocatalysts in a fluidized bed photoreactor: Photocatalytic activity and adherence stability. Appl. Catal. B Environ. 71, 151–162.

Rengifo-Herrera, J.A., Rincón, A.G., Pulgarin, C., 2013. Waterborne Escherichia coli Inactivation by TiO2 Photoassisted Processes: A Brief Overview, in: Pichat, P. (Ed.), Photocatalysis and Water Purification. Wiley-VCH Verlag GmbH & Co. KGaA, pp. 295–309.

Rezaei, R., Mohseni, M., 2017a. Impact of pH on the kinetics of photocatalytic oxidation of 2,4-dichlorophenoxy acetic acid in a fluidized bed photocatalytic reactor. Appl. Catal. B Environ. 205, 302–309.

Rezaei, R., Mohseni, M., 2017b. Impact of natural organic matter on the degradation of 2,4-dichlorophenoxy acetic acid in a fluidized bed photocatalytic reactor. Chem. Eng. J., Intensification of Photocatalytic Processes for Niche Applications in the Area of Water, Wastewater and Air Treatment 310, Part 2, 457–463.

Rodríguez, F.J., Núñez, L.A., 2011. Characterization of aquatic humic substances. Water Environ. J. 25, 163–170.

Rothenberger, G., Moser, J., Graetzel, M., Serpone, N., Sharma, D.K., 1985. Charge carrier trapping and recombination dynamics in small semiconductor particles. J. Am. Chem. Soc. 107, 8054–8059.

Sakthivel, S., Neppolian, B., Shankar, M.V., Arabindoo, B., Palanichamy, M., Murugesan, V., 2003. Solar photocatalytic degradation of azo dye: comparison of photocatalytic efficiency of ZnO and TiO2. Sol. Energy Mater. Sol. Cells 77, 65–82.

Salvador, P., 2007. On the Nature of Photogenerated Radical Species Active in the Oxidative

Degradation of Dissolved Pollutants with TiO2 Aqueous Suspensions: A Revision in the Light of the Electronic Structure of Adsorbed Water. J. Phys. Chem. C 111, 17038–17043.

Sandell, E.B., Ōnishi, H., 1978. Photometric determination of traces of metals, 4th ed. ed, Chemical analysis. Wiley, New York.

Sarathy, S.R., 2009. Effects of UV/H_2O_2 advanced oxidation on physical and chemical characteristics of natural organic matter in raw drinking water sources.

Sarathy, S.R., Mohseni, M., 2007. The Impact of UV/H2O2 Advanced Oxidation on Molecular Size Distribution of Chromophoric Natural Organic Matter. Environ. Sci. Technol. 41, 8315–8320.

Satterfield, C.N., 1980. Heterogeneous catalysis in practice. McGraw-Hill chemical engineering series.

Schmidt, M., Steinemann, S.G., 1991. XPS studies of amino acids adsorbed on titanium dioxide surfaces. Fresenius J. Anal. Chem. 341, 412–415.

Schnitzer, M., Kodama, H., 1975. An electron microscopic examination of fulvic acid. Geoderma 13, 279–287.

Schwarzenbach, R.P., Egli, T., Hofstetter, T.B., Gunten, U. von, Wehrli, B., 2010. Global Water Pollution and Human Health. Annu. Rev. Environ. Resour. 35, 109–136.

Schwarzenbach, R.P., Escher, B.I., Fenner, K., Hofstetter, T.B., Johnson, C.A., Gunten, U. von, Wehrli, B., 2006. The Challenge of Micropollutants in Aquatic Systems. Science 313, 1072–1077.

Schwarzenbach, R.P., Gschwend, P.M., Imboden, D.M., 2002. c, in: Environmental Organic Chemistry. John Wiley & Sons, Inc., pp. 275–330.

Selli, E., Baglio, D., Montanarella, L., Bidoglio, G., 1999. Role of humic acids in the TiO2-

photocatalyzed degradation of tetrachloroethene in water. Water Res. 33, 1827–1836.

Serrano, B., de Lasa, H., 1997. Photocatalytic Degradation of Water Organic Pollutants. Kinetic Modeling and Energy Efficiency. Ind. Eng. Chem. Res. 36, 4705–4711.

Shaham-Waldmann, N., Paz, Y., 2013. Modified Photocatalysts, in: Pichat, P.(Ed.), Photocatalysis and Water Purification. Wiley-VCH Verlag GmbH & Co. KGaA, pp. 103-143.

Sips, R., 1948. On the Structure of a Catalyst Surface. J. Chem. Phys. 16, 490–495.

Snoeyink, V.L., Summers, R.S., 1990. Chapter 13: Adsorption of Organic Compounds | Water quality and treatment.

Šojić, D.V., Anderluh, V.B., Orčić, D.Z., Abramović, B.F., 2009. Photodegradation of clopyralid in TiO2 suspensions: Identification of intermediates and reaction pathways. J. Hazard. Mater. 168, 94–101.

Ternes, T.A., Meisenheimer, M., McDowell, D., Sacher, F., Brauch, H.-J., Haist-Gulde, B., Preuss, G., Wilme, U., Zulei-Seibert, N., 2002. Removal of Pharmaceuticals during Drinking Water Treatment. Environ. Sci. Technol. 36, 3855–3863.

Thiruvenkatachari, R., Vigneswaran, S., Moon, I.S., 2008. A review on UV/TiO2 photocatalytic oxidation process (Journal Review). Korean J. Chem. Eng. 25, 64–72.

Thomas, A.G., Flavell, W.R., Chatwin, C.P., Kumarasinghe, A.R., Rayner, S.M., Kirkham, P.F., Tsoutsou, D., Johal, T.K., Patel, S., 2007. Adsorption of phenylalanine on single crystal rutile TiO2(1 1 0) surface. Surf. Sci., ECOSS-24Proceedings of the 24th European Conference on Surface Science 601, 3828–3832.

Thurman, E.M., 1985a. Functional Groups of Dissolved Organic Carbon, in: Organic Geochemistry of Natural Waters, Developments in Biogeochemistry. Springer Netherlands, pp. 87–101.

Thurman, E.M., 1985b. Classification of Dissolved Organic Carbon, in: Organic Geochemistry of Natural Waters, Developments in Biogeochemistry. Springer Netherlands, pp. 103–110.

Thurman, E.M., Malcolm, R.L., 1981. Preparative isolation of aquatic humic substances. Environ. Sci. Technol. 15, 463–466.

Tipping, E., Reddy, M.M., Hurley, M.A., 1990. Modeling electrostatic and heterogeneity effects on proton dissociation from humic substances. Environ. Sci. Technol. 24, 1700–1705.

Tournié, P., Laguerie, C., Couderc, J.P., 1979. Correlations for mass transfer between fluidized spheres and a liquid. Chem. Eng. Sci. 34, 1247–1255.

Trillas, M., Peral, J., Domènech, X., 1995. Redox photodegradation of 2,4-dichlorophenoxyacetic acid over TiO2. Appl. Catal. B Environ. 5, 377–387.

Tunesi, S., Anderson, M., 1991. Influence of chemisorption on the photodecomposition of salicylic acid and related compounds using suspended titania ceramic membranes. J. Phys. Chem. 95, 3399–3405.

Turchi, C.S., Ollis, D.F., 1990. Photocatalytic degradation of organic water contaminants: Mechanisms involving hydroxyl radical attack. J. Catal. 122, 178–192.

University of Liverpool, n.d. Chem Tube 3D.

Vega, A., 2009. Development and evaluation of a composite photocatalyst for water treatmment processes. UBC, Canada.

Vega, A., Keshmiri, M., Mohseni, M., 2011. Composite template-free TiO2 photocatalyst: Synthesis, characteristics and photocatalytic activity. Appl. Catal. B Environ. 104, 127–135.

Wang, Y., Combe, C., Clark, M.M., 2001. The effects of pH and calcium on the diffusion coefficient of humic acid. J. Membr. Sci. 183, 49–60.

Wang, Z., Ma, W., Chen, C., Ji, H., Zhao, J., 2011. Probing paramagnetic species in titania-based heterogeneous photocatalysis by electron spin resonance (ESR) spectroscopy—A mini review. Chem. Eng. J., Environmental Nanotechnology 170, 353–362.

Weber, W.J., Morris, J.C., 1963. Kinetics of Adsorption on Carbon from Solution. J. Sanit. Eng.Div. 89, 31–60.

Wetchakun, N., Phanichphant, S., 2008. Effect of temperature on the degree of anatase–rutile transformation in titanium dioxide nanoparticles synthesized by the modified sol–gel method. Curr. Appl. Phys., AMN-3 (Third International Conference on Advanced Materials and Nanotechnology)Third International Conference on Advanced Materials and Nanotechnology 8, 343–346.

Wojcicka, L., Edwards, E., Crosina, Q., 2009. Advanced Oxidation Processes. Can. Consult. Eng. 50, 27–28,30.

Xiang, Q., Yu, J., Wong, P.K., 2011. Quantitative characterization of hydroxyl radicals produced by various photocatalysts. J. Colloid Interface Sci. 357, 163–167.

Yamazaki, S., Matsunaga, S., Hori, K., 2001. Photocatalytic degradation of trichloroethylene in water using TiO2 pellets. Water Res. 35, 1022–1028.

Yang, J.-K., Lee, S.-M., 2006. Removal of Cr(VI) and humic acid by using TiO2 photocatalysis. Chemosphere 63, 1677–1684.

Yang, W.-C., 2003. Handbook of Fluidization and Fluid-Particle Systems. CRC Press.

Yoon, S.-H., Oh, S.-E., Yang, J.E., Lee, J.H., Lee, M., Yu, S., Pak, D., 2009. TiO2 Photocatalytic Oxidation Mechanism of As(III). Environ. Sci. Technol. 43, 864–869.

Zhang, J., Xu, Q., Feng, Z., Li, M., Li, C., 2008. Importance of the Relationship between Surface Phases and Photocatalytic Activity of TiO2. Angew. Chem. Int. Ed. 47, 1766–1769.

Zhang, T.C., Emary, S.C., 1999. Jar Tests for Evaluation of Atrazine Removal at Drinking Water Treatment Plants. Environ. Eng. Sci. 16, 417–432.

Appendices

Appendix A

A.1 2,4-D adsorption mass transfer assessment

Adsorption of an organic compound involves a number of steps, initiated by film diffusion or external mass transfer and followed by intraparticle diffusion and sorption via physiochemical interactions (Snoeyink and Summers, 1990). Film diffusion, 2,4-D transportation by molecular diffusion through the stationary boundary layer, is a function of particle size, hydrodynamic conditions, system physical properties and etc. (Akasu and Kabasakal, 2005). The mass transfer can be defined by equation (A-1).

$$\frac{dC}{dt} = -K_{ma}S(C - C_s) \qquad \text{(A-1)}$$

where K_{ma} is the external mass transfer coefficient and S is specific surface area. C and C_s also represent the concentration of 2,4-D in liquid phase and on the surface of photocatalyst spheres at time t, respectively. It can be assumed that at t=0, the adsorption is governed by film diffusion (Akasu and Kabasakal, 2005). It means, at t=0 the concentration of 2,4-D is equal to the initial concentration ($C=C_0$) and C_s is negligible. With this assumption Eq (A-1) can be simplified as

$$\frac{d(C/C_o)}{dt} = -K_{ma}S \qquad \text{(A-2)}$$

By plotting C/C_0 vs. time the value of K_{ma} can be determined from the slope at t=0. Figure 4-6 shows that the C/C_0 of 2,4-D falls very fast at t=0 (before intraparticle diffusion) and the external mass transfer coefficient is 0.244 $g.m^{-2}.min^{-1}$, irrespective to 2,4-D initial concentrations.

Appendix B

B.1 Hydrogen peroxide contribution in photocatalytic oxidation

This experiment was performed to assess the contribution of hydrogen peroxide generating during the photocatalytic process in producing hydroxyl radicals.

It has been suggested that an alternative mechanism for generating free hydroxyl radical is the reduction of adsorbed hydrogen peroxide and the photooxidation of dissolved H_2O_2 (Salvador, 2007).

$$H_2O_2 \overset{h\nu}{\rightarrow} 2OH^{\bullet}_{aq} \qquad (k_{A1}) \qquad \text{(B-1)}$$

$$Ti^{3+} + H_2O_2 \rightarrow Ti^{4+}OH^{\bullet} + OH^{-} \qquad (k_{A2}) \qquad \text{(B-2)}$$

$$H_2O_2 + O_2^{-\bullet} \rightarrow Ti^{4+} + OH^{\bullet}_{aq} + OH^{-} + O_2 \qquad (k_{A3}) \qquad \text{(B-3)}$$

The contribution of H_2O_2 in photocatalytic oxidation was tested by adding H_2O_2 and the results showed that the effect of H_2O_2 on oxidation of the micropollutant in FBPR is not considerable. No difference between the rate of photocatalytic oxidation of 1 mgL^{-1} 2,4-D in the absence of H_2O_2 and in the presence of 0.2 mM H_2O_2 was observed. It means the additional amount of H_2O_2 did not change the photocatalytic oxidation rate (Figure A-1). It asserts that H_2O_2 does not contribute in generating $^{\bullet}OH_{aq}$. It was the reason that Eqs A-1 to A-3 were not considered in the kinetics analysis.

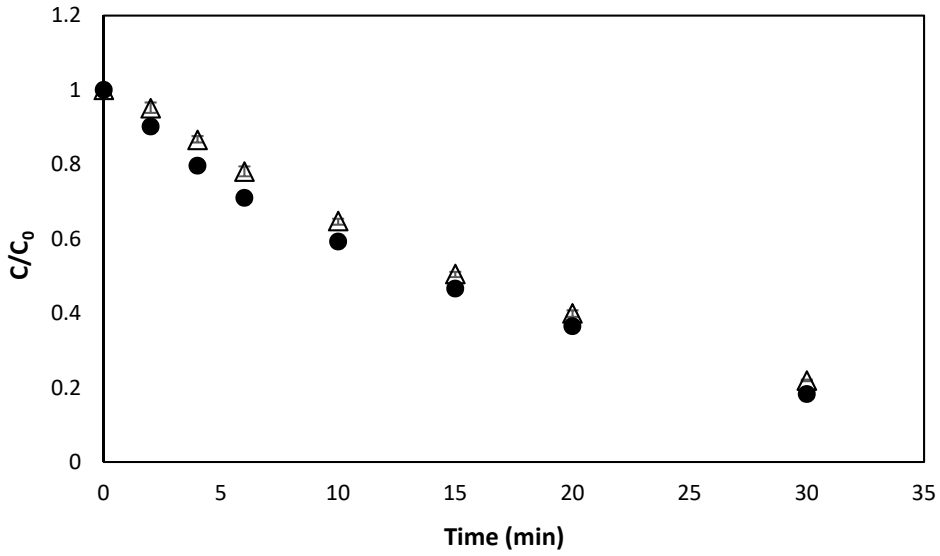

Figure B-1. Photocatalytic oxidation of 2,4-D with the initial concentration of 1 mgL^{-1} in a fluidized photocatalytic reactor at pH 7, (Δ) in the absence of additional H_2O_2, (●) in the presence of 0.2 mM H_2O_2.

B.2 Kinetic parameters estimation using Matlab least-squares optimization technique

```
clear all
clc
ydata = ...%time
 [0 2 4 6 10 15 20 30];
xdata = ... %Experimental concentration
[2.924583333 2.676366667 2.376633333 2.07605 1.584083333 1.145483333
0.784166667 0.3718];
x1=7;
z=xdata(1);
format shorteng
fun = @(x,xdata)-
1/(x(1)*(x(2)*x(3)*x1+x(1)*x1+x(2)))*(((x(2)*x(3)*x1+x(2))*log(x(1)*x(3)*x1*x
data+x(2)*x(3)*x1+x(1)*x1+x(2)))+x(1)*x1*log(xdata))+...

1/(x(1)*(x(2)*x(3)*x1+x(1)*x1+x(2)))*(((x(2)*x(3)*x1+x(2))*log(x(1)*x(3)*x1*z
+x(2)*x(3)*x1+x(1)*x1+x(2)))+x(1)*x1*log(z));
x0 = [0,0,0];
lb = [0.01 0.00001 0.000222];
ub = [1 1 1];
x = lsqcurvefit(fun,x0,xdata,ydata,lb,ub,'levenberg-marquardt')
plot(ydata,xdata, 'O')
hold on
v=1/(x(1)*(x(2)*x(3)*x1+x(1)*x1+x(2)))*(((x(2)*x(3)*x1+x(2))*log(x(1)*x(3)*x1
*xdata(1)+x(2)*x(3)*x1+x(1)*x1+x(2)))+x(1)*x1*log(xdata(1)));
for i=1:8
    ydata1=-
1/(x(1)*(x(2)*x(3)*x1+x(1)*x1+x(2)))*(((x(2)*x(3)*x1+x(2))*log(x(1)*x(3)*x1*x
data+x(2)*x(3)*x1+x(1)*x1+x(2)))+x(1)*x1*log(xdata))+v;
end
```

```
plot(ydata1,xdata,'r')
```

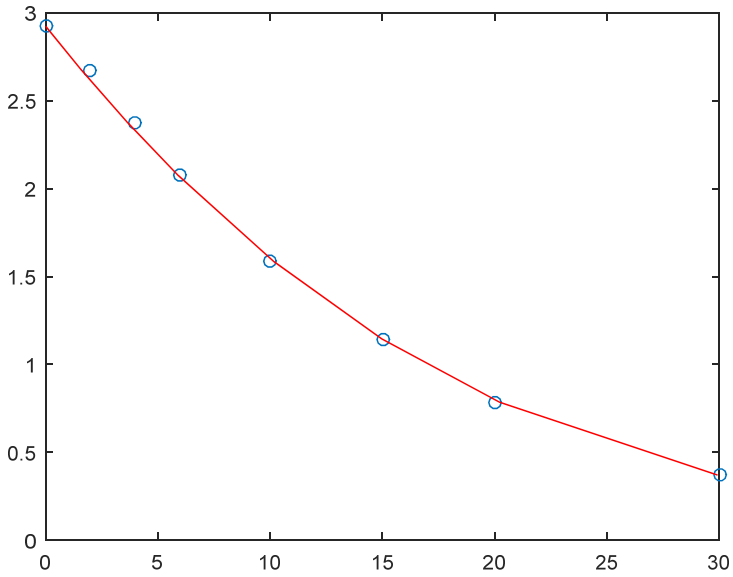


```
x =

   10.0000e-003   201.6036e-003   233.4933e-003
```

B.3 Mass transfer effect evaluation

To understand the mass transfer role as the rate-controlling step in kinetics studies, the effect of mass transfer resistance is evaluated on the overall reaction rate. The external mass transfer occurs between the surface of photocatalytic spheres and surrounding fluid. The physical transport of reactant by either molecular diffusion or convective transport from the bulk makes a concentration gradient between bulk fluid and surface of the photocatalyst.

In the classical example, the first order reaction, the mass transfer is equal to rate of kinetic reaction on surface of catalyst in steady state condition (Chen et al., 2000).

$$K_m(C_b - C_s) = k_r C_s \qquad \text{(B-4)}$$

$$rate = \frac{C_b}{\frac{1}{K_m} + \frac{1}{k_r}} = k_{obs} C_b \quad \text{(B-5)}$$

where $1/K_m$ is mass transfer resistance coefficient which is a function of fluid velocity and physical constants. If mass transfer resistance is very low, it can be assumed only the kinetic controls the reactions.

Several experimental correlations have been proposed to determine the mass transfer influence(Epstein, 2003; McCune and Wilhelm, 1949; Tournié et al., 1979). It can be seen that they are generally expressed in terms of dimensionless group. The mass transfer coefficient is directly related to the Sherwood number. The Sherwood number is defined with independent variables, Reynolds and Schmidt dimensionless numbers (Tournié et al., 1979).

$$Sh=f(Re, Sc) \quad \text{(B-6)}$$

However, Garner et al. (Garner and Suckling, 1958) proposed a correlation for water and solid spheres

$$Sh = 2 + 0.55 Re^{0.5} Sc^{0.33} \quad \text{(B-7)}$$

where

$$Sh = \frac{K_m d_{sph}}{D_{2,4-D}} \quad \text{(B-8)}$$

$$Re = \frac{D_p \rho G}{\mu} \quad \text{(B-9)}$$

$$Sc = \frac{\mu_{H_2O}}{\rho_{H_2O} D_{2,4-D}} \quad \text{(B-10)}$$

By using particle diameters (d_p=0.9 mm), water characteristics, viscosity (μ=0.86 Kg m^{-1} s^{-1}) and density (ρ=997 Kg m^{-3}) (Crittenden et al., 2012), diffusivity of 2,4-D in

water of 6.57×10^{-10} m^2s^{-1} (Duran et al., 2011)), and applying them into equations (A-7) to (A-10), the mass transfer coefficient (K_m) was achieved to 1.16×10^{-4} m s^{-1}.

Mears (1971), proposed Damköhler number, (Eq (A-11)) as a criterion for measuring the effect of bulk mass transfer on surface reaction kinetics

$$\omega = \frac{k_r C_{2,4-D} r_{sp}}{K_m C_{2,4-D}} \leq \frac{0.15}{n} \quad \text{(B-11)}$$

where r_{sp} is sphere radius and n is the integer exponent in power law rate expression and equal to 1 because the degradation followed first order kinetics.

Therefore, Eq (A-11) can be simplified to:

$$\omega = \frac{k_r r_{sp}}{K_m} \leq 0.15 \quad \text{(B-12)}$$

According to observed rate constant (k_r) reported in chapter 6, 0.381×10^{-3} s^{-1} and 1.153×10^{-3} s^{-1} for initial concentration of 7 mgL^{-1} 2,4-D at pH 7 and pH 3 respectively, the Damköhler numbers are:

pH 3, $\omega=4.46\times10^{-3}$ (B-13)

pH 7, $\omega=1.478\times10^{-3}$ (B-14)

As can be seen the Damköhler number for different pH situation is very low. It means the effect of mass transfer is negligible and the overall reaction is driven only by the kinetic.

Appendix C

C.1 The effect of pH on photocatalytic oxidation of initial 2,4-D of 4 mgL^{-1}

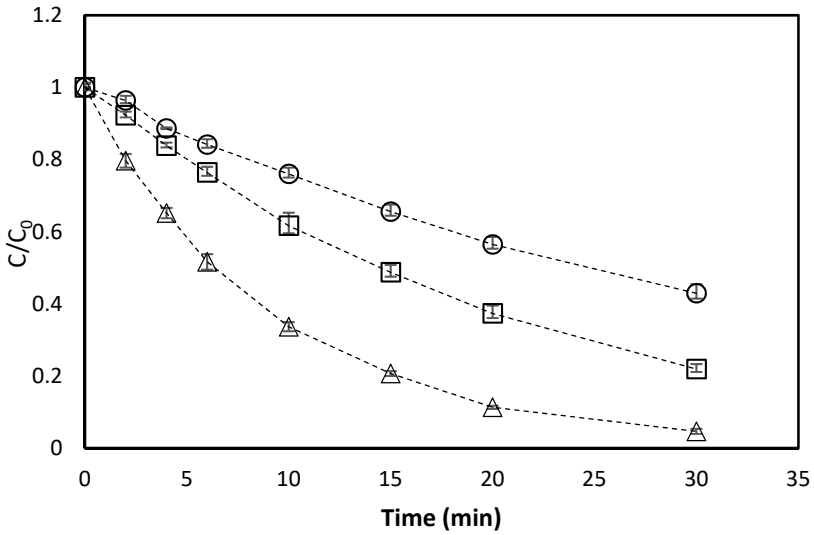

Figure C-1. Photocatalytic oxidation of 2,4-D of 4 mg L^{-1} at pH; (○) 7, (□) 5, (Δ) 3. Error bars represent the standard errors for the triplicate runs.

C.2 The effect of NOM on oxidation of 2,4-D of 4 mg L^{-1} at different pH

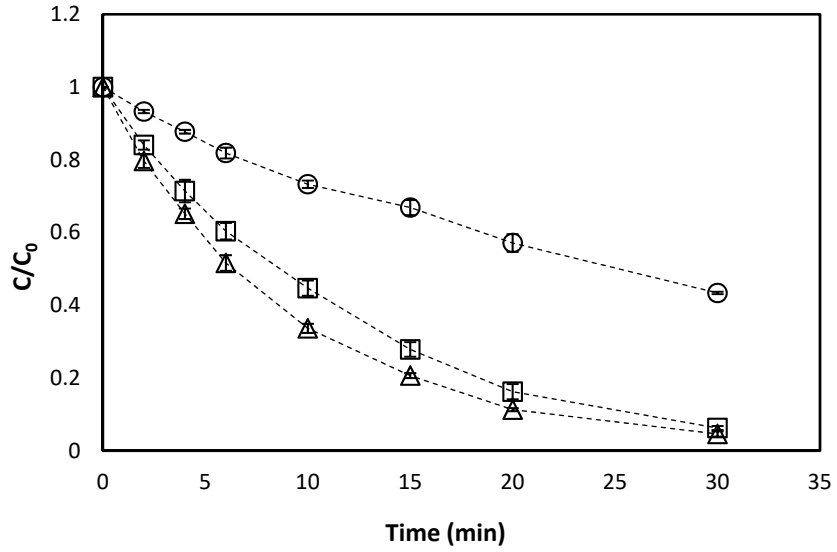

Figure C-2. Photocatalytic oxidation of 2,4-D of 4 mgL^{-1}at pH 3 in the presence of NOM measured as TOC; (○) 5 mgL^{-1}, (□) 1 $mgL^{-1}$and, (Δ) 0 mgL^{-1}. Error bars represent the standard errors for the triplicate runs.

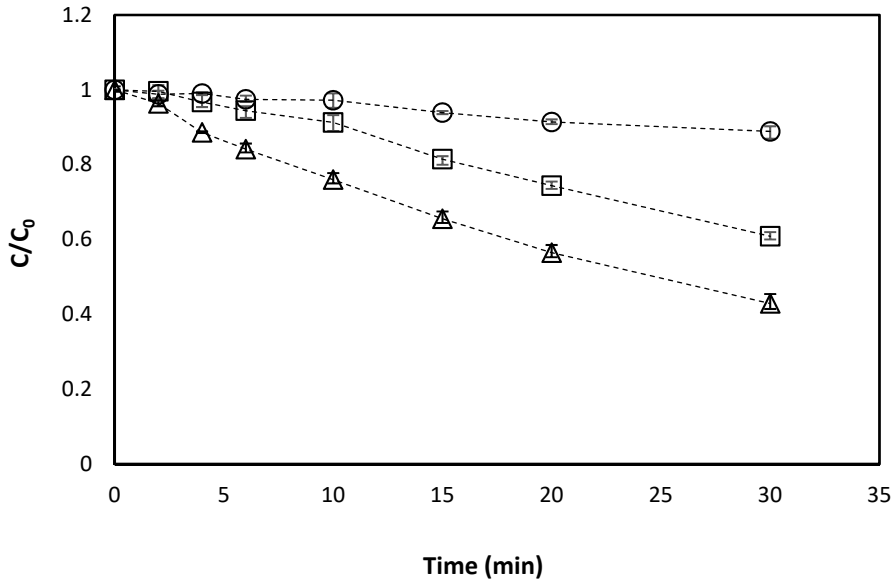

Figure C-3. Photocatalytic oxidation of 2,4-D of 4 mgL^{-1}at pH 7 in the presence of NOM measured as TOC; (○) 5 mgL^{-1}, (□) 1 mgL^{-1} and, (Δ) 0 mgL^{-1}. Error bars represent the standard errors for the triplicate runs.

C.3 The effect of methanol on 2,4-D photocatalytic oxidation rate constant

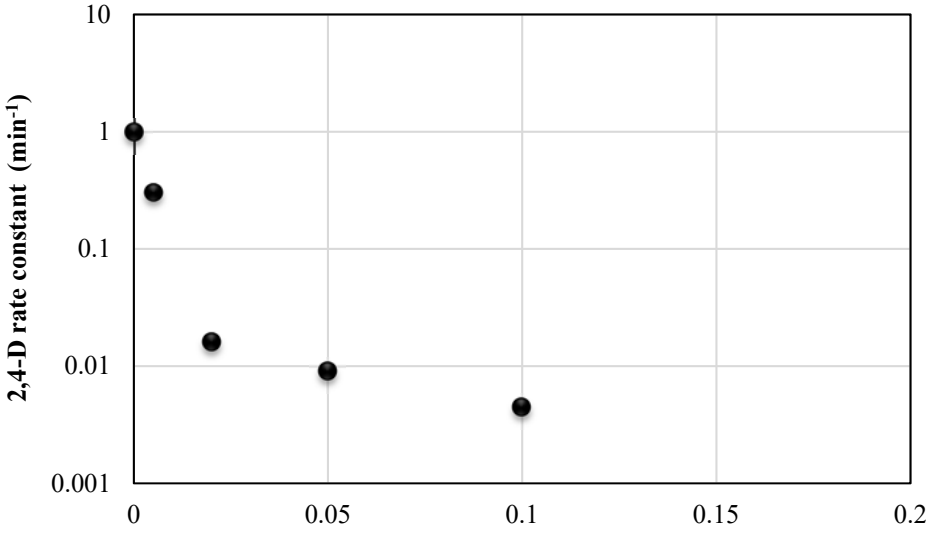

Figure C-4. 2,4-D photocatalytic rate constant in the presence of Methanol different concentrations